GROWTH AND ELECTRO-OPTIC CHARACTERIZATION OF $LiNbO_3$ AND KH_2PO_4 CRYSTALS

A Thesis Submitted
in Partial Fulfilment of the Requirements
for the Degree of
MASTER OF TECHNOLOGY

By
K. SWAMINATHAN

to the
INTERDISCIPLINARY PROGRAMME IN MATERIALS SCIENCE
INDIAN INSTITUTE OF TECHNOLOGY, KANPUR
JULY, 1981

To

my friend K.T. Kembaiyan,

my brother K. Sriram

AND

AT THE FEET OF THE LIGHT

WHO DWELLS WITHIN ALL

MSP-1981-M-SWA-GRD

CERTIFICATE

Certified that the work "Growth and electro-optic characterization of $LiNbO_3$ and KH_2PO_4 crystals" has been carried out under my supervision and the same has not been submitted elsewhere for a degree.

E.C. Subbarao
Professor
Department of Metallurgical Engineering
Indian Institute of Technology
Kanpur.

ACKNOWLEDGEMENTS

I am too soaked in gratitude that to express my thanks for Prof. E.C. Subbarao, I cannot really find words. Here, I fully feel the import of the Zen saying 'The moment you express, you miss the mark'. The patience and kindness Prof. Subbarao has throughout shown towards me has been remarkable. His sympathetic understanding during the difficult periods of this work and his constant encouragement have been mainly responsible for the completion of this work. His pragmatic and open-minded approach to problems and the way of treating all matters with equal importance have shown me an example of ideal carriage and total integration. I am extremely fortunate to have been associated with him, for it has been a very rich and educative experience.

It appears presumptuous for me to express thanks to Dr. K. Veerabhadra Rao, ACMS, considering the amount of help I have received from him and the unflagging spirit of co-operation that accompanied the same. The value of his timely suggestions and advice to instil the necessary enthusiasm and confidence cannot be overestimated. His concern for my welfare has been like that of an elder brother for which I am deeply indebted to him.

It is a pleasure to thank Prof. K.P. Singh of Metallurgical Engineering Department, Prof. P. Venkateswarlu and Dr. G. Chakrapani of Physics Department and Prof. K.V.G.K. Gokhale and Dr. D.M. Rao of Civil Engineering

Department for lending various components at different stages of these studies.

My heartfelt thanks go to Mr. Umesh Kumar for his active help during the last stages of the preparation of the thesis.

The excellent typing of Mr. R.N. Srivastava and the neat copying work of Mr. Vishwanath Singh is greatly appreciated. The nice art work of Mr. V.P. Gupta and Mr. B.B. Srivastava is gratefully acknowledged. I thank all my colleagues and Laboratory staff for their kind co-operation.

Lastly the kindness and affection shown to me by Madam Subbarao, who made me feel like a member of the family cannot be forgotten, and can never be adequately thanked.

K. Swaminathan

CONTENTS

LIST OF TABLES

LIST OF FIGURES

ABSTRACT

After the advent of laser, the electro-optic materials have gained prominence in various laser peripheral devices like modulators, deflectors, second harmonic generators and display devices. The present thesis is divided into two parts: The first part is devoted to $LiNbO_3$ which is the most important material among melt-grown crystals for electro-optic applications. An extensive and upto-date review on the growth and optical properties of $LiNbO_3$ is presented. A crystal pulling apparatus was set up with a resistance furnace which could reach upto a temperature of 1300°C in which a few small crystals were grown. The second part contains a brief review of the literature on KH_2PO_4 (KDP) which is the most extensively used electro-optic crystal. Crystals of KDP were grown from aqueous solution of the salt by slow cooling and slow evaporation methods. These crystals were characterised for refractive index, birefringence and half-wave retardation voltage. The results obtained from these studies are given below along with literature values in brackets (i) refractive index n_o = 1.466 (1.4679) and n_e = 1.507 (1.5090) at λ = 5890 Å (ii) birefringence = 4.155×10^{-2} (4.17×10^{-2}) at 5461 Å (iii) half-wave voltage $V_{\lambda/2}$ = 9.5 kV (9.6 kV) at 6330 Å and (iv) voltage contrast ratio VCR = 25 (200). The general agreement is seen to be good. An electro-optic modulator based on KDP was designed and fabricated and its modulation characteristics were studied. The reasons for the low value of VCR are discussed and methods to improve VCR and modulator performance are suggested.

I. INTRODUCTION

I.1. Historical:

The phenomenon of the change in the refractive indices or other related optical properties of a medium under the influence of an electric field is understood as the electro-optic effect. The modulation of light and electro-optics have had a long and interesting history. Before the turn of the century, Kerr observed a quadratic electro-optic effect (QEO) in liquids like CS_2, where the Kerr birefringence is proportional to the square of the electric field, while Roentgen and Kundt observed a linear electro-optic effect (LEO) in quartz. But Roentgen believed it was only a secondary consequence of the converse piezoelectric deformation acting via the photoelastic effect. It was Pockels,[1] through his classical investigation in 1894, who conclusively proved the existence of a direct effect (independent of piezoelectrically induced strain) of the electric field on the optical behavior. The credit thus goes to Pockels in whose honor the LEO effect is called Pockels' effect. Pockels characterised the LEO effect in crystals of various point groups using either the applied electric field or dielectric polarisation as driving terms. But it was not until 1944 the Pockels' effect came into prominence, when Zwicker and Scherrer[2] reported the synthetic crystals of KH_2PO_4 and KD_2PO_4 to

exhibit a much larger electro-optic effect compared to quartz. In 1949, Billings[3] and later Carpenter[4] demonstrated the usefulness of these crystals for light modulation and as optical shutters. This turned out to be a landmark in the history of the Pockels' effect, along with the advent of laser in 1960. Since the advent of laser and its growing applications in science and technology, the electro-optic materials have acquired a great prominence in various laser peripheral devices like modulator, deflectors, Q-switches, second harmonic generators and display devices. By virtue of the development of such peripheral devices, electro-optic materials have played a crucial role in the development of laser communication systems, optical displays, computer memory devices and non-linear optics. Excellent reviews have appeared on electro-optic single crystals[5,6] and light modulators[7,8,9] A brief description of the electro-optic effect, including both the linear Pockels' and quadratic Kerr effects, follows presently.

I.2. Electro-optic Behavior of Crystals:

It is conventional to consider the change in $1/n^2$ with the application of an electric field, E, where n is the refractive index, rather than a change in n directly.[10] The quantity $1/n^2$ varies with E as

$$\frac{1}{n^2} = \frac{1}{n_o^2} + rE + RE^2 + \ldots \qquad \ldots (I.1)$$

where r and R are the linear and quadratic electro-optic coefficients respectively and n_o is the refractive index in the absence of an electric field. Both the coefficients r and R in equation (I.1) are for a direct (primary) effect which is independent of crystal strain. In addition, if the crystal develops macroscopic strain under the influence of the electric field, there will be a change in index through the elasto-optic effect which is called the secondary or the indirect effect. For the LEO effect, the strain results from the converse piezoelectric deformation and is proportional to the electric field. For the QEO effect, the strain results from electrostriction and is proportional to the square of the field. However, the direct and the secondary effects need not have the same algebraic sign; the overall electro-optic effect in a crystal strained by the field can be larger or smaller than the direct effect alone[11]. Also, if the driving fields are at a frequency corresponding to the acoustic resonance frequency of the material, the secondary effect may be even larger than the direct one because of large strain amplitudes.

Both the direct effect and the secondary effect can be easily shown to be dependent on crystal symmetry. In a centro-symmetric material, reversing the sense of the applied field E does not change the physical situation and so $1/n^2$ will be independent of the sign of E. Terms of odd power in E in equation (I.1) will change sign, however; so the coefficients of these terms must vanish in crystals having

an inversion symmetry. Hence only non-centro-symmetric crystals exhibit the LEO (Pockels) effect (as the piezoelectric effect), there being no such restriction for the quadratic Kerr effect. In the same manner, the secondary effect due to converse piezoelectric strain will be present only in non-centrosymmetric crystals while the secondary effect due to electro-striction will be present in all transparent solids.

I.2.1. Index Ellipsoid:

The optical properties of crystals can be described by the indicatrix or optical index ellipsoid[10] given by

$$\sum_{ij} S_{ij} x_i x_j = 1 \qquad \ldots (I.2)$$

where $S_{ij} \equiv (\frac{1}{\epsilon})_{ij} \equiv (\frac{1}{n^2})_{ij}$ and x_i, x_j refer to the three Cartesian coordinates (x_1, x_2, x_3). Here ϵ is the electronic (relative) dielectric constant and n the refractive index. The indicatrix has the following important property: a plane passing through the center of the ellipsoid perpendicular to the direction of propagation of an electromagnetic wave, will cut the ellipsoid in an ellipse whose semi-axes are the two refractive indices associated with the two components of the wave, plane polarised along those semi-axes. For cubic crystals, the refractive index is isotropic and the index ellipsoid is a sphere of radius n. In the case of uniaxial crystals (hexagonal, tetragonal and trigonal) the index ellipsoid is given by

$$\left(\frac{x_1^2 + x_2^2}{n_o^2}\right) + \frac{x_3^2}{n_e^2} = 1 \qquad \ldots \quad (I.3)$$

where n_o and n_e are the ordinary and extra-ordinary refractive indices along the semi-axes . For the biaxial (orthorhombic, monoclinic and triclinic) crystals the ellipsoid becomes

$$\frac{x_1^2}{n_1^2} + \frac{x_2^2}{n_2^2} + \frac{x_3^2}{n_3^2} = 1 \qquad \ldots \quad (I.4)$$

where n_1, n_2 and n_3 are the principal refractive indices. With the application of an electric field the ellipsoid gets deformed and these distortions are simply related to changes in the coefficients S_{ij} in equation (I.2). Thus the general equation of the indicatrix can be written as

$$\Delta\left(\frac{1}{n^2}\right)_{ij} = \sum_k r_{ij,k}E_k + \sum_{kl} R_{ij,kl}E_kE_l + \ldots \qquad \ldots \quad (I.5)$$

Here the first term on the right hand side represents the LEO effect and $r_{ij,k}$ (third rank tensor components) are called the Pockels or LEO constants. The second term represents the QEO effect and $R_{ij,kl}$ (fourth rank tensor components) are called the Kerr or QEO constants.

I.2.2. Characterisation Techniques:

It is clear from the above discussion that in the final analysis, the determination of EO constants reduces to the determination of changes in optical parameters S_{ij} under

the influence of an electric field. There are three parameters to determine these changes:

(i) the field induces birefringence

(ii) the angle of rotation of the optical indicatrix, and

(iii) the absolute changes in index.

Different methods are usually employed depending on the nature of change in the optical index ellipsoid which in turn depends on the point group symmetry. For example, the first method is used for $\bar{4}3$ m point group, second for $\bar{4}2$ m and third for 4 mm for some typical configurations. Field induced birefringence measurements are made by standard techniques involving a calibrated compensator [4] placed along with the crystal between polarisers in an optical path. The total field induced phase shift difference $\Delta\phi$ associated with the birefringence Δn is given by

$$\Delta\phi = \frac{2\pi}{\lambda} \cdot l \cdot \Delta n \qquad \ldots \quad (I.6)$$

where l is the length of the crystal and λ the vacuum wavelength of the light. The phase difference $\Delta\phi$ is measured directly by the compensator and Δn can be related to EO coefficients. In the third case the birefringence measurements alone cannot be determined separately for some coefficients and the absolute changes in n (or ϕ) are required. Such measurements can be made either using an interferometer [7] or through the use of a prism in a light deflection experiment. [12] Apart from these standard methods, it is also possible to determine the half-wave voltage straight away from which the

electro-optic coefficient can be evaluated. In the present thesis, this method has been employed for the electro-optic characterisation which is described in detail in Chapter III.

I.3. Materials Selection for Electro-optic Devices:

For the selection of good electro-optic material and modulator design, the important material properties and parameters which require careful consideration are discussed below. The importance of a suitable property is determined by the particular application of the material in a device.

(i) The electro-optic figure of merit $n^3 r$ (where n is the refractive index and r the relevant electro-optic coefficient) must be as large as possible. This would mean that modulation can be done at lower half-wave voltages which is desirable.

(ii) The crystals should be transparent at the frequency at which they are to be used. Alternatively the transmission regime of the crystal determines the spectral region available for modulation.

(iii) The crystal growing technique determines the laboratory and commercial availability of large and good optical quality single crystals.

(iv) The relative dielectric constant must be as low as possible because the reactive power required to drive the lumped modulator becomes large with increased dielectric constant. But this requirement is conflicting with the previous requirement since r_{ij} is

directly proportional to the dielectric constant. Hence one has to arrive at a compromise between the two, depending on which parameter is more important for the device intended to be made.

(v) The crystal must have a very low loss tangent of the device ($\tan\delta$) because this determines the electrical loss or modulation power in the crystal.

(vi) The material must belong to a crystal class which has no center of inversion.

(vii) The electrical resistivity of the crystal is related to the space charge effects and causes heating of the crystal by the field. Lower passage of currents will minimise crystal heating.

(viii) The crystal must be sufficiently hard to resist the strains during machining and polishing.

(ix) The crystal should not be hygroscopic to facilitate simpler operations.

(x) The piezoelectric and photoelastic coefficients determine the contribution of the clamped and unclamped electro-optic coefficients.

(xi) The thermal conductivity of the crystal determines the deleterious birefringence due to thermal gradients in the crystal heated by electrical or optical sources. Hence the thermal conductivity of the crystal must be as high as possible.

(xii) If the crystal is a ferroelectric, it is desirable to operate the device near its Curie temperature since

the electro-optic coefficients assume maximum values at that temperature. However, the temperature stability requirements are very stringent for Curie temperature operation of the device.

(xiii) The radiation damage determines the suitability of the material for high laser powers.

(xiv) Natural birefringence is undesirable for modulation because firstly, it is a direct function of the temperature of the device and secondly, the emerging rays must be collinear on the same axes to properly recombine. It is however possible to compensate for the natural birefringence by placing another crystal of identical length, at the same temperature along the optical path such that the natural birefringence of one crystal cancels that produced by the other. The crystal should have as large an induced birefringence as possible.

(xv) The crystal should not be optically active.

It must be stated that there are no materials at the present time which will satisfy all the above requirements. Some of the requirements are mutually contradictory. In such cases, one tries to achieve an optimum

I.4. Aim and Statement of the Problem:

In the present work, it is proposed to systematically investigate the electro-optic behaviour of some typical crystals. For this purpose, two important candidate crystals

$LiNbO_3$ (which is grown from melts) and KDP (grown from solution) are selected. For $LiNbO_3$, an exhaustive survey of literature will be undertaken covering crystal growth and its optical and electro-optical behavior. For crystal growth of $LiNbO_3$ a suitable furnace is proposed to be designed, fabricated, along with a crystal pulling set up. An experimental set up will be developed to grow the crystals of KDP from solution. These crystals of KDP will be subjected to various investigations of interest in electro-optics. These include refractive index, birefringence and electro-optic characterization. Finally, a KDP based electro-optic modulator is intended to be designed, fabricated and tested. The results obtained will be compared with values available in literature.

REFERENCES

(1) F. Pockels, Lehrbuch der Kristalloptik, Leipzig, Teubner, (1906).

(2) Zwicker, B. and Scherrer, P., Electro-optical properties of the ferroelectric crystals KH_2PO_4 (In German), Helv. Phys. Acta, 17 (1944) 346.

(3) B.H. Billings, The electro-optic effect in uniaxial crystals of the dihydrogen phosphate (XH_2PO_4) type. Parts I, II, IV, J. Opt. Soc. Am., 39 (1949) 797.

(4) R. O'B. Carpenter, The electro-optic effect in crystals of the dihydrogen phosphate type, Part III, Measurements of Coefficients, J. Opt. Soc. Am., 40 (1950) 225.

(5) S.H. Wemple and M. DiDomenico, Jr., in Appl. Solid State Sci. (Ed. Wolfe, R.), 3, Ch. 4, p. 263, Academic Press, N.Y. (1972).

(6) I.P. Kaminow, An Introduction to Electro-optic Devices, Academic Press, N.Y. (1974).

(7) I.P. Kaminow and E.H. Turner, Electro-optic light modulators, Proc. IEEE, 54 (1966) 1374.

(8) I.P. Kaminow and E.H. Turner, Linear electro-optical materials in "Handbook of Laser" (R.J. Pressley Ltd.), p. 447, Chemical Rubber Co., Cleveland, Ohio, 1971.

(9) F.S. Chen, Modulation for optical communications, Proc. IEEE, 58 (1970) 1440.

(10) J.F. Nye, Physical properties of crystals, Oxford: England: Oxford University Press, 1960.

(11) P.V. Lenzo, E.H. Turner, E.G. Spencer and A.A. Ballman, Electro-optic coefficients and elastic wave propagation in single domain ferroelectric lithium tantalate, Appl. Phys. Lett., 8 (1966) 81.

(12) E.P. Ippen, Electro-optic deflection with $BaTiO_3$ prisms, IEEE J. Quant. Electron., QE-2 (1966) 152.

II. LITHIUM NIOBATE ($LiNbO_3$)

II.1. Review of Literature:

II.1.1. Introduction:

Crystals like KDP and those belonging to the KDP type, together with their deuterated versions have been studied most extensively for their electro-optic properties and used as modulator materials in the optical communication and laser systems for a long time. In the recent years, $LiNbO_3$ has come to share this important place along with KDP by virtue of its better combination of optical and piezoelectric properties together with its highly advantageous physical and chemical stability. Excelent reviews[1,2] have appeared on the history, properties and applications of $LiNbO_3$.

The ferroelectric properties of $LiNbO_3$ were first discovered by Mathias and Remeika[3]. The crystals studied by them were grown from a flux of LiF. Growth of optically high quality of crystals of $LiNbO_3$ was possible only through the Czochralski pulling method after Ballman[4] first achieved success with this technique a decade and a half back. The major applications with $LiNbO_3$ have been (i) acoustic wave propagation (ii) electro-optic light modulation (iii) optical second harmonic generation (SHG) (iv) optical parametric oscillation and (v) holographic storage (which makes use of the photorefractive effect). In view of the fact that most of these applications require crystals of high optical

quality it is not surprising that intense work on $LiNbO_3$ started only with the advent of Czochralski grown crystals.

In this review it is intended to briefly summarise the work done in the single crystal growth of $LiNbO_3$ and its related aspects with emphasis on the optical properties. $LiNbO_3$ is an excellent example of the interrelation between chemical, structural and physical properties. So we start with a brief description of the crystal structure, the chemistry of $LiNbO_3$, dealing with the phase diagram, considerations of stoichiometry, purity, doping etc.

II.1.1.1. Crystal Structure:

Lithium niobate was first described by Zachariasen[5] as belonging to the centrosymmetric ilmenite ($FeTiO_3$) structure because of a close similarity of the lattice constants. But the discovery of its ferroelectric properties necessitated a re-investigation of its crystal structure. Bailey[6], from his X-ray study, reported the space group of $LiNbO_3$ to be $R3C(C_{3v}^{b})$, and established that the structure of $LiNbO_3$ is not isomorphous with ilmenite whose space group is $R\bar{3}(C_{3i}^{2})$. But Bailey could not determine the position of the Nb ion relative to that of Li and O. Megaw[7] suggested a distorted perovskite structure but this could not be justified because the required atomic displacement between the paraelectric and ferroelectric phases are too large. The structure analysis by X-ray and neutron diffraction methods by Abrahams et al.[8,9,10] represent the most accurate atomic arrangement

in $LiNbO_3$. The position coordinates of the atoms in $LiNbO_3$ have been established beyond any ambiguity (except at very high temperatures). Figure II.1 gives a three-dimensional view of the atomic positions in the $LiNbO_3$ crystal lattice. Figure II.1(a) presents the top view of a unit cell illustrating the ions seen along the direction of the polar axis. Negatively charged oxygen ions occupy the corners of an octahedron. The smaller, positively charged lithium and niobium ions occupy the space within the octahedrons in an ordered fashion, as illustrated in Figure II.1(b). When the temperature is above the Curie point, the lithium ions lie within the plane of the oxygen ions; the niobium ions are midway between planes. Hence, the crystal is in the paraelectric state without any charge. With the temperature below the Curie point, both the lithium and niobium ions move in the same direction, resulting in a positive dipole at one end. When a crystal is initially grown, however, the positive dipole ends in half of the domains point in one direction; dipoles in the remaining domains are oriented in the opposite direction. To switch all of the dipoles into the same direction, the crystal is placed in a dc field at temperatures approaching the Curie point.

$LiNbO_3$ crystallises in the trigonal structure with a rhombhohedral unit cell containing two formula weights. The point group is 3 m. Above 1200°C where the ferroelectric transition takes place, the point group changes to $\bar{3}$ m which is nonpolar.

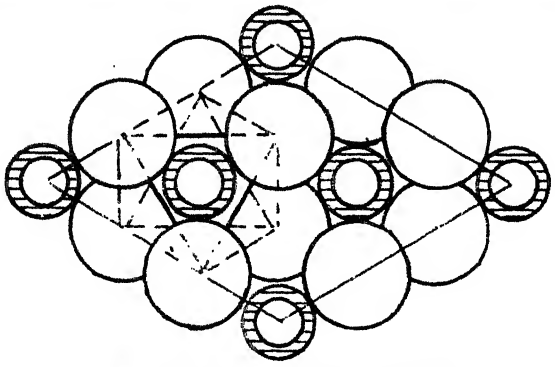

UNIT CELL TOP VIEW

POSITIVE DIPOLE END

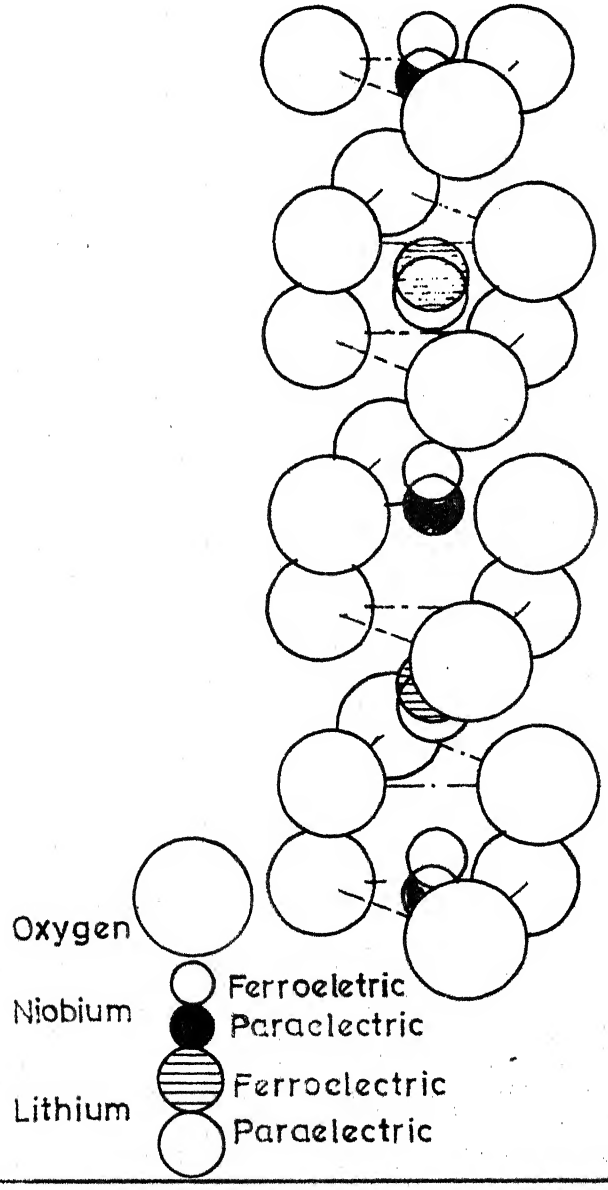

Fig.II.1 A three dimensional view of the stacking sequence of atoms in $LiNbO_3$ crystal (Ref.2)

II.1.1.2. Phase Diagram:

$LiNbO_3$ belong to the Li_2O-Nb_2O_5 system which consists of three more compounds. These three viz. $Li_2O.14Nb_2O_5$, $Li_2O.3Nb_2O_5$ and $3Li_2O.Nb_2O_5$ are of little practical importance.

Reisman and Holtzberg[11] gave the first phase diagram of the Li_2O-Nb_2O_5 system. They investigated the heterogeneous equilibria in the Li_2O-, Ag_2O-Nb_2O_5 systems using differential thermal analysis, X-ray and density techniques. Their phase diagram for the Li_2O-Nb_2O_5 system revealed a congruently melting $LiNbO_3$ at the stoichiometric composition of 50 mole % of Li_2O with zero solid solubility and a maximum melting point of 1253°C. Lerner et al.[12] reexamined the system and contributed to a more accurate version of the phase diagram showing a fairly large solid solution range for $LiNbO_3$. Also the congruent melting point was found to occur at the Li_2O deficient side between 48 to 49 mole % Li_2O and not at the stoichiometric composition. Peterson and Carruthers[13] studied the system using NMR technique and inferred the congruent composition to be 48.6 mole % Li_2O. In 1974, Chow et al.[14] employed a controlled crystal growth program and the measurement of the phase matching temperature at 1.06 μ wavelength radiation, to enable a precise location of the congruently melting composition of $LiNbO_3$. The accepted value, as a result of their experiments, is between 48.50 to 48.60 mole % of Li_2O. Figure II.2 shows the phase diagram of the Li_2O-Nb_2O_5 system as given by Svassand et al.[15]. Figure II.3 shows an

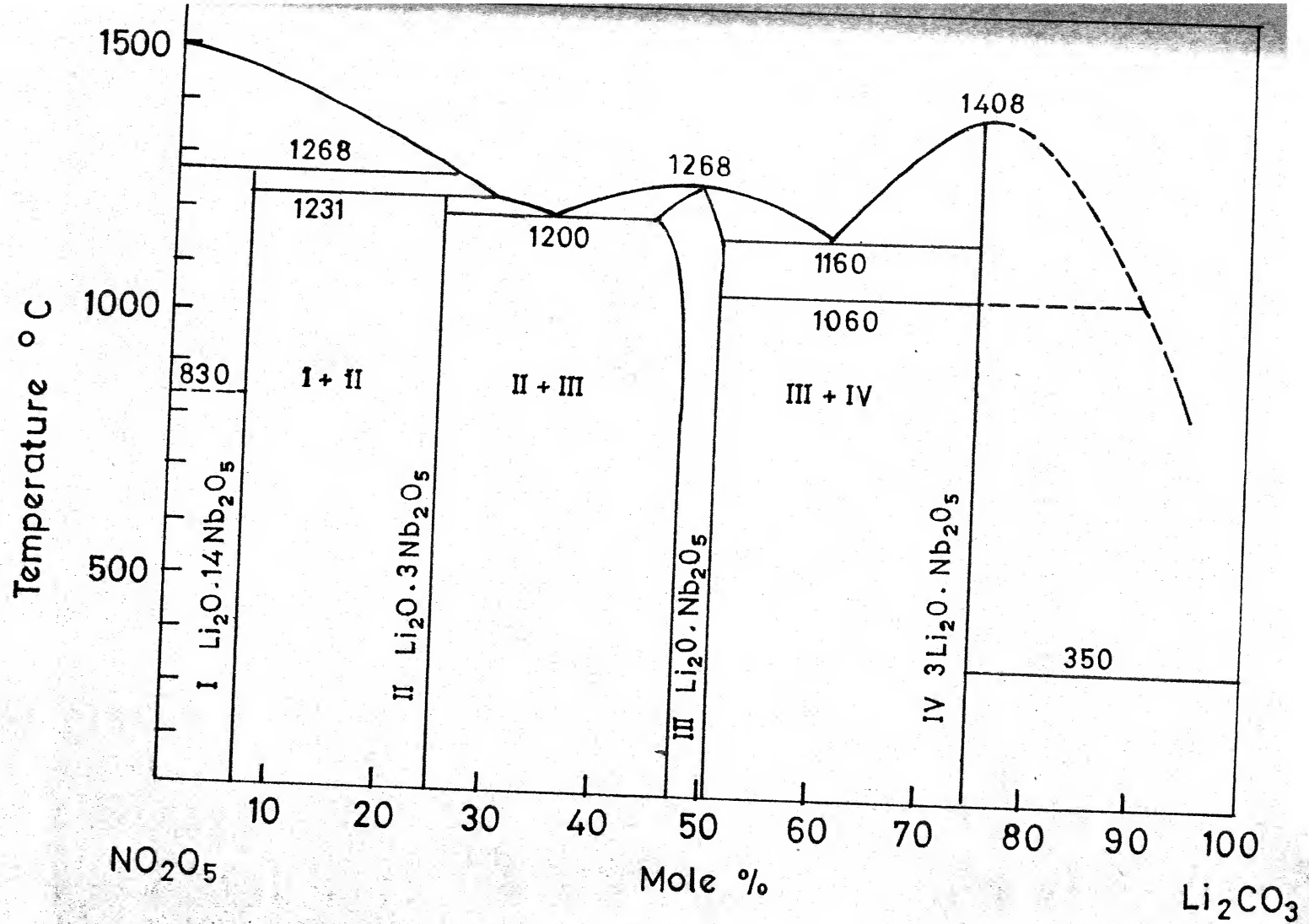

Fig. II.2 Phase diagram of the $Li_2O-Nb_2O_5$ system (Ref. 15)

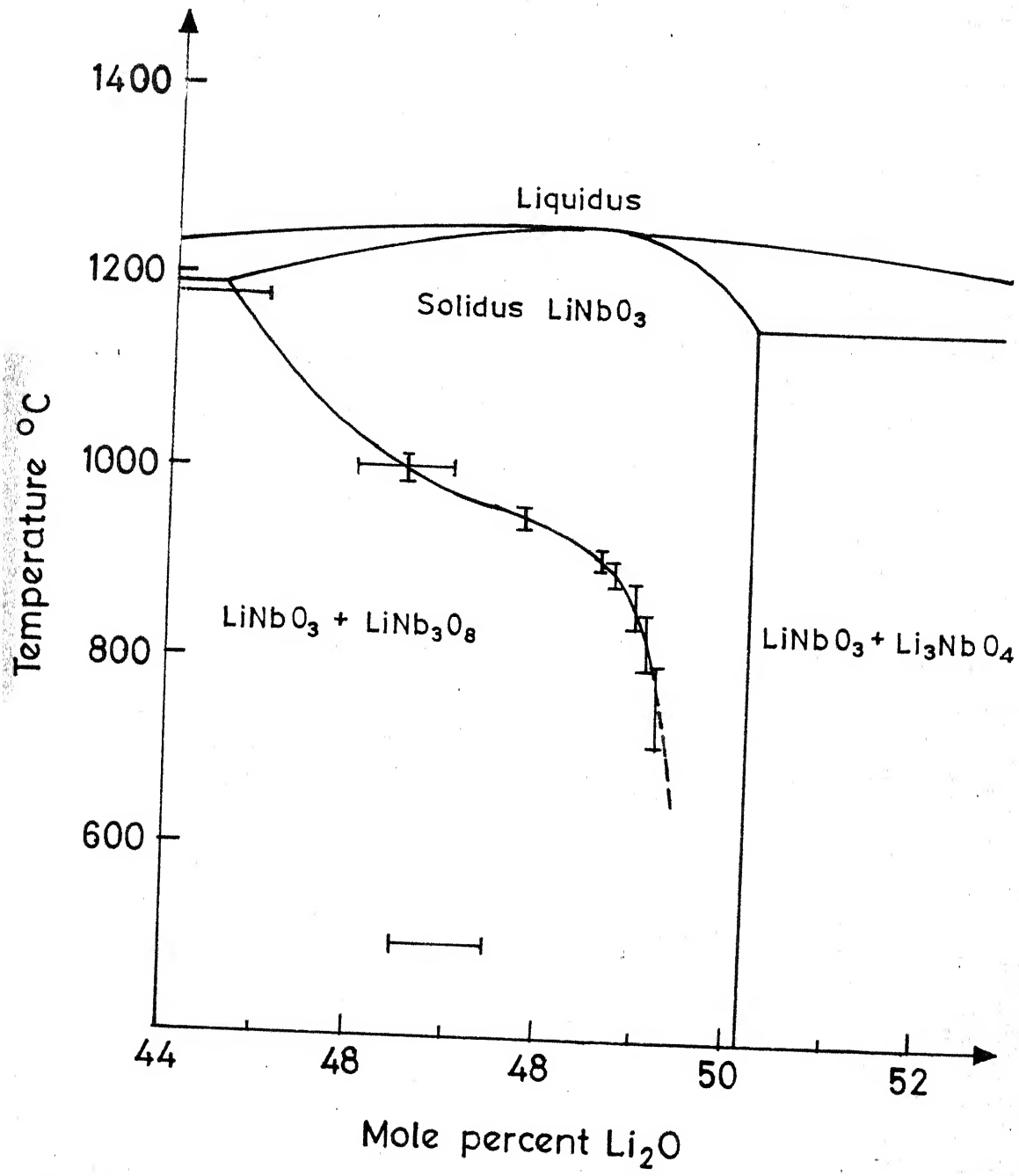

Fig.II.3 An extended view of the solid solution regime of $LiNbO_3$ (Ref. 16)

enlarged view of the solid solution range of $LiNbO_3$, given by Svassand et al.[16]. The solid solution range is seem to be fairly large above 900°C and narrowing down at lower temperatures. As Svassand et al.[16] reported, crystals with congruent compositions showed a strong increase in optical scattering after annealing at 700°C to 900°C for 170 hours and the Guinier X-ray diffraction patterns indicated that these congruent crystals decomposed into $LiNbO_3$ and $LiNb_3O_8$. Subsequent heating above 910°C removed all optical scattering, resulting in clear transparent crystals. The X-ray diffraction patterns now showed only $LiNbO_3$. This led to the conclusion that crystals of congruent composition are inherentlly matastable at room temperature.

II.1.1.3. Stoichiometry and Composition-Dependence of Properties:

The deviations from the stoichiometric composition are described by either the Lithium to Niobium ratio or the ratio of the sum of the metals to oxygen. The latter has an influence only on the electrical properties. The Li/Nb ratio, on the other hand, has a direct and a pronounced bearing on several of the properties and therefore considered very important. Among the strongly dependent properties are the Curie temperature, birefringence, the phase matching temperature for SHG and the NMR line width. The weakly-dependent properties include the lattice parameters, density, dielectric constant, ordinary refractive index, the electrooptic coefficients and the nonlinear optical coefficients. In

fact, the composition of the crystals has come to be characterised by the measurements of these properties, so much so that this effective feedback makes it possible to grow tailor-made crystals to suit the requirements of specific applications. Generally such property measurements relate to the composition of the starting melt and not to the composition of the crystal itself. Carruthers et al.[17] calibrated the crystal composition with respect to the composition of the melt through Curie temperature measurements on ceramic and single crystal samples. Chow et al.[14] redetermined the distribution coefficient, based on a theoretical fit of the phase-matching temperature vs. solid composition and obtained a slightly lower curve. Figure II.4 shows their data superimposed.

The Li/Nb ratio is usually expressed in the following two ways:

$$x = [Li]/[Li] + [Nb] \; ; \quad y = [Li]/[Nb] \qquad \ldots \text{(II.1)}$$

the quantity of the ions being given in moles, as indicated by the brackets. Now x and y are related as

$$x = \frac{y}{1+y} \quad \text{and} \quad y = \frac{x}{1-x} \qquad \ldots \text{(II.2)}$$

Multiplication of x by a factor of 100 directly gives the mole % Li_2O. The congruently melting composition is given by

$$x = 0.486 \quad \text{or} \quad 48.6 \text{ mole \% } Li_2O; \quad y = 0.945 \qquad \ldots \text{(II.3)}$$

Direct measurement of x turns out to be impractical because the large difference in the atomic masses of Li and Nb and

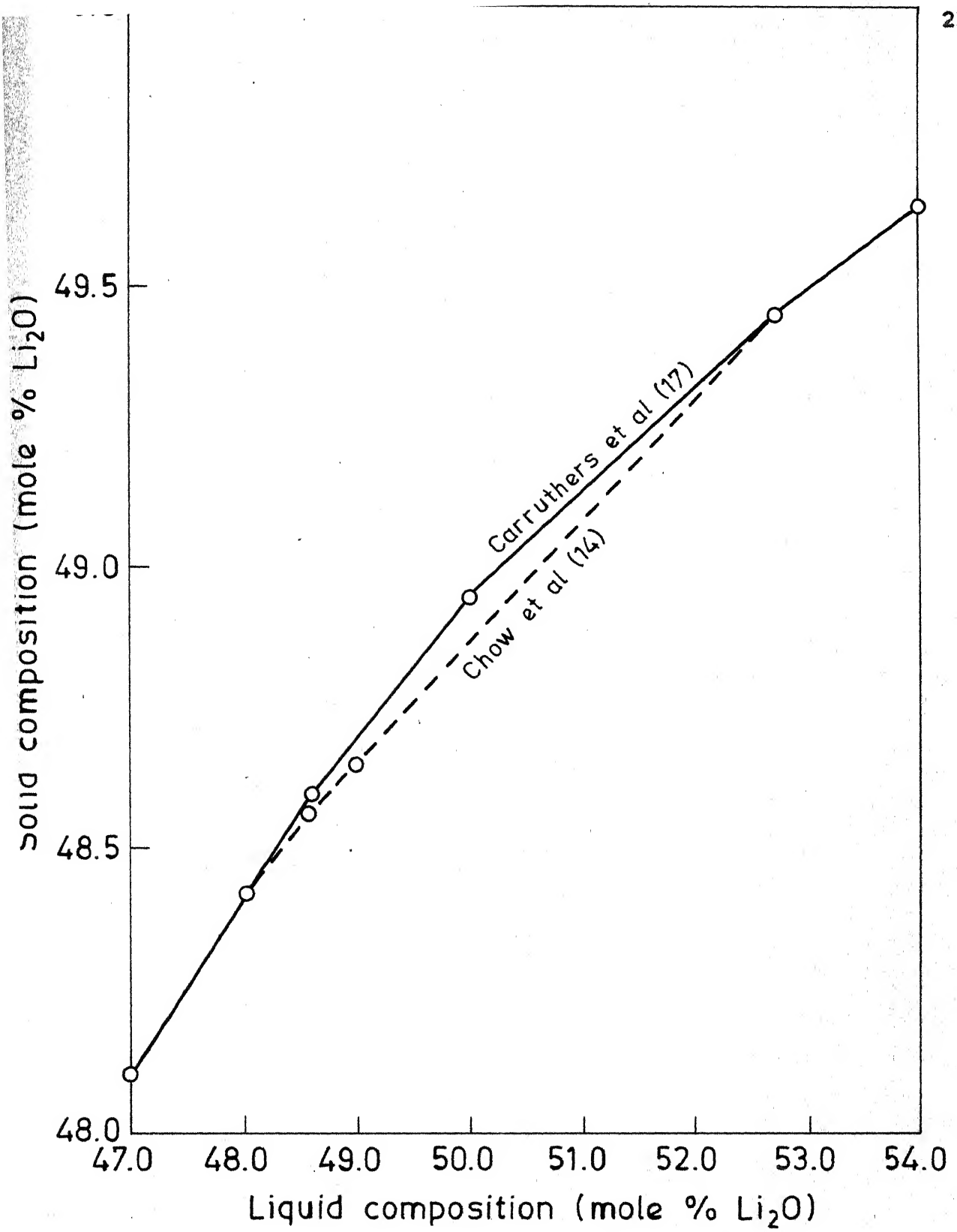

II.4- Variation of the crystal composition as a function of composition of the starting melt of $LiNbO_3$. (Ref. 14)

the difficulties of dissolving $LiNbO_3$ quantitatively for chemical separation preclude a precise chemical analysis.

The Li/Nb stoichiometry affects the homogeneity of the crystals markedly. Byer et al.[18] reported the growth of highly homogeneous crystals using melt of congruent composition. The effect of Li/Nb stoichiometry on the properties will be discussed in detail in a later section.

Several models[19,12,20] have been proposed for the defect structures which cause the deviations in the Li/Nb stoichiometry towards the Li-deficient side. Any defect model has to provide a charge compensating mechanism for the Li deficiency and account for the easy exchange of oxygen, at high temperatures, with the ambient atmosphere. Glass et al.[21] reported a strong discoloration of the crystals when annealed in a reducing atmosphere at 1000°C for a few months. This is considered as being due to the Nb ions changing their valence state from +5 to +4. Annealing in oxygen bleaches the crystals to clear transparency. Till to date, none of the defect models proposed has been established as conclusive for want of precise experimental data on well-characterised crystals.

II.1.1.4. Effect of Impurities and Dopants:

The optical quality of the $LiNbO_3$ crystals is largely influenced by the extent of purity. Impurities that get incorporated into the crystals during growth of undoped $LiNbO_3$ lead to reduced transparency and very often color the

crystals strongly. An after-growth oxygen-anneal to invariably resorted to, for obtaining clear crystals. Use of extremely pure starting materials (viz. Li_2CO_3 and Nb_2O_5) and a crucible of very pure platinum facilitates growth of good optical quality crystals.

Apart from affecting the optical quality, the impurities exercise a marked influence on other properties as well. Recently Blistanov et al.[22] investigated the influence of impurities like Cu, Mg, Mn, Mo, W on the residual light flux (optical transmission) through $LiNbO_3$ crystals kept between crossed polarisers. They reported that the presence of the impurities considerably affected the residual light flux via their influence on the electrical conductivity.

The effect of impurities on properties has been exploited effectively by intentional doping, to produce crystals suitable for different applications. Doping with rare earth ions upto 1 mole %, by additions of the rare earth oxides to the melt, has been performed successfully for converting $LiNbO_3$ into an efficient laser host material. Doping with transition metal ions has been most extensively studied for holographic storage applications. Much of the interest has centered around Fe ion doping[23] because it results in a large photorefractive effect. But for other applications, transition metal impurities are to be strictly avoided, for they result in large, refractive index inhomogeneities under laser illumination. This is known as 'Optical damage' and will be dealt in detail at a later section.

Among other additives studied, MgO stands out as a very popular dopant as it eliminates any cracking tendency of the crystals after growth or during machining. Moreover a small addition of MgO considerably increases the temperature of phase matching for SHG. Bridenbaugh et al.[24] utilised the addition of MgO to raise the phase matching temperature above the index damage anneal temperature. Addition of MgO also causes an increase in the Curie temperature.

In the fabrication of optical waveguides, diffusion of impurity metals like Ti, V has been extensively studied[25]. Boyd et al.[26] could fabricate high quality acoustic surface wave guides through Ti diffusion. They also reported an increase in acoustic velocity for diffusion of metals like Ni, Cu and Cr.

II.1.2. Crystal Growth:

The successful growth of large single crystals through Czochralski technique by Ballman[4] and independently by Fedulov et al.[27] has been the turning point in the history of $LiNbO_3$ because it spurred an intense activity on the material. Since then the technique has been improved to yield high quality crystals weighing upto 1300 g[14]. However attempts have been made to grow $LiNbO_3$ through other methods as well.

Matthias and Remeika[3] grew their first crystals from a flux of LiF. Smolenskii et al.[28] synthesised $LiNbO_3$ crystals from a solution in a LiCl melt. Interest in

the solution-melt method has recently increased because it enables thin single crystal films to be obtained. Kondo et al.[29] used $LiVO_3$ as flux. Ballman et al.[30] determined the phase stability region for the crystallisation of $LiNbO_3$ in several flux systems. They demonstrated the suitability of these flux systems for growth of $LiNbO_3$ thin films by liquid phase epitaxial techniques. Voronkova et al.[31] could obtain 5 to 10 mm size of $LiNbO_3$ crystals from borate, vanadate and tungstate melts. The lattice parameters of these crystals were found to be less than those of the Czochralski grown crystals and was attributable to incorporation of flux material in the $LiNbO_3$ lattice. Kolb and Laudise[32] reported the growth of thin layers of $LiNbO_3$ by the hydrothermal method. Hill and Zimmermann[33] grew monodomain and high quality $LiNbO_3$ crystals of size 1 mm by the hydrothermal method.

In the following section the crystal growth aspects pertaining to the Czochralski method such as the preparation of the charge material, the pulling apparatus and the poling procedures are discussed.

II.1.2.1. Preparation of the Charge Material:

The starting compounds are Li_2CO_3 and Nb_2O_5. To get good quality crystals the compounds used should have a purity exceeding 99.5%. The Li/Nb stoichiometry is usually fixed at the congruent composition in order to avoid inhomogeneities of composition during growth. Calcination of the starting compounds taken in the appropriate amounts gives

$LiNbO_3$ as per the following solid state reaction,

$$Li_2CO_3 + Nb_2O_5 \longrightarrow 2LiNbO_3 + CO_2 \quad \ldots \quad (II.4)$$

The usual calcination procedure is as follows. The starting compounds are first dried at 150°C and appropriate amounts of each of them are carefully weighed to make up the required ratio. They are mixed thoroughly in a medium of acetone to avoid any loss of Li_2O which is volatile. The mixture is taken in a platinum crucible and heated upto 850°C slowly in about 8 hours. At 850°C the mixture is held for another 8 hours to allow the reaction to be completed and then cooled back to room temperature slowly. The calcined product is ground to a fine powder to give the charge material.

II.1.2.2. Czochralski Pulling Technique:

The growth parameters for $LiNbO_3$ are fairly well-established now and crystals several centimeters long and weighing well over 1000 grams have been successfully grown. The best value of T_c for $LiNbO_3$ is considered to be 1195±15°C and that of the melting point to be 1267±5°C. This temperature can be reached by RF heating or by resistance furnace. RF heating is preferred for melts of non-congruent composition to avoid constitutional supercooling. Platinum is the only crucible material which is not attacked by the $LiNbO_3$ melt, although it is wetted by it. Wetting of the crucible leads to a concave meniscus of the melt surface but a flat growth interface can be achieved by growing at a low level in the

crucible or by use of after heaters. The crucible has to be sufficiently thick-walled to withstand the large stresses produced during the solidification of the remaining melt after growth is terminated. This is especially so since platinum-hardening alloy elements like Ir or Rh cannot be used as they lead to crystal discoloration.

A schematic diagram of a Czochralski pulling apparatus, showing all its essential features, is given in Figure II.5. The melt temperature requires a very accurate temperature control to an accuracy of $\pm 0.5^{\circ}C$, to enable a very stable temperature gradient to be obtained at the melt-growth interface. Fluctuations in the temperature produce inhomogeneities in the crystal shape and composition and can also enhance the cracking tendency. $LiNbO_3$ crystals are especially very much susceptible to cracking during cooling after growth or during machining. Brice[34] examined the thermal strains in crystals during growth and cooling, and could correlate the crystal diameter with the allowable axial temperature gradient and the maximum rate of cooling, to prevent cracking. He showed that during growth of a crystal with radius R, the maximum acceptable axial gradient is roughly proportional to $R^{-3/2}$ and that to prevent cracking after growth, there is a maximum rate of cooling proportional to R^{-2}. Thus for $LiNbO_3$ crystals of 6 mm radius, a temperature gradient exceeding $100^{\circ}C\ cm^{-1}$ could cause cracking, whereas for crystals of 10 mm radius, an axial gradient of $50^{\circ}C\ cm^{-1}$ was large enough to cause cracking.

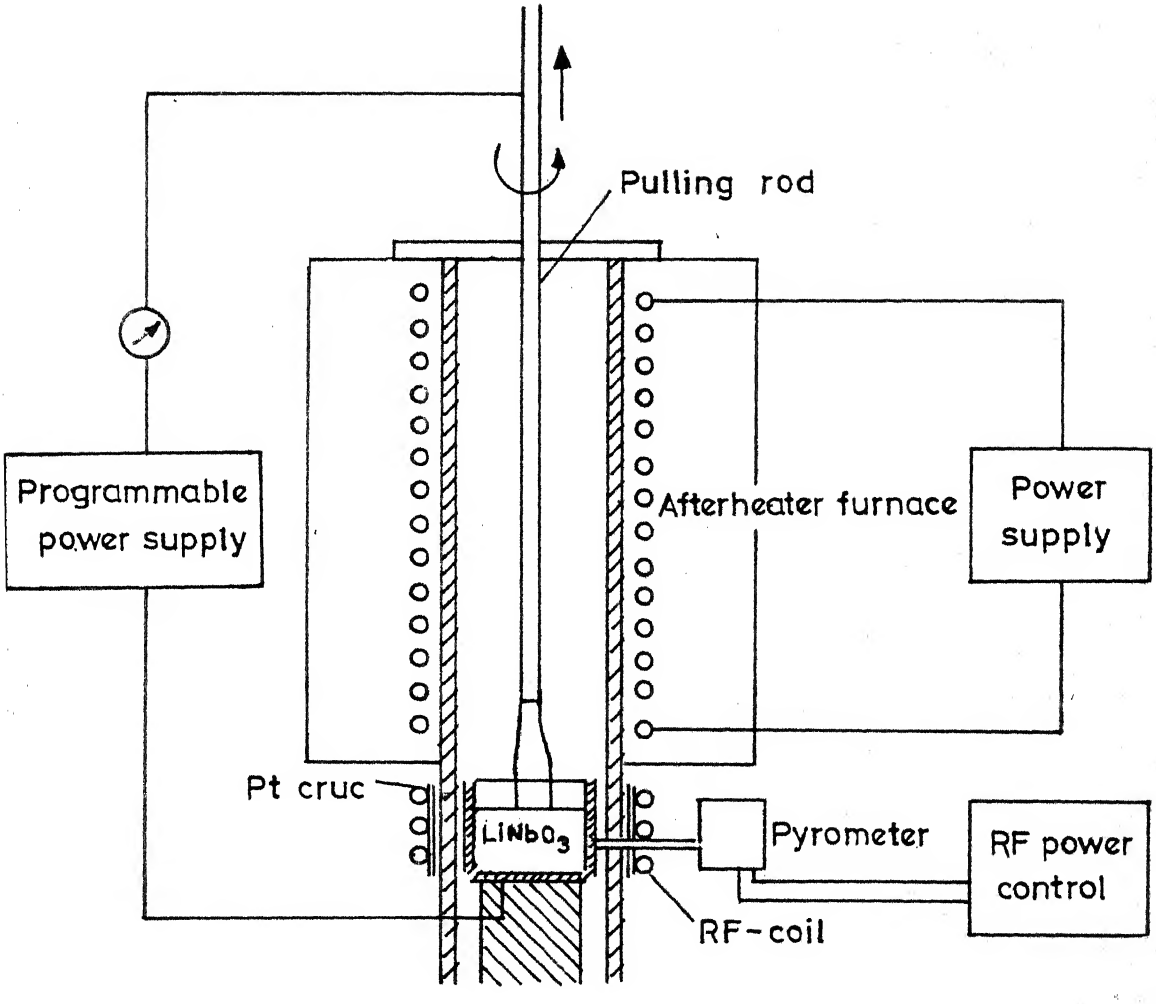

Fig. II.5 Schematic of a crystal pulling apparatus for growth of $LiNbO_3$ crystals (Ref. 1)

This analysis was reported to be valid for a large range of radius extending from 4 mm to 23 mm.

For RF induction heating of the crucible, use of after-heaters and heatshields are indispensable in order to reduce the temperature gradients. The after-heater is generally maintained at a temperature of 1000 to 1100°C during growth and the after-growth annealing period. This is followed by a very slow cooling to room temperature over a period of 15 hours.

Use of tubular resistance heated furnaces results in low axial and radial gradients, thus enabling growth of crack-free material. But this can give rise to problems of constitutional supercooling and diameter control. The pulling rate and the rotation rates are largely fixed by the diameter of the crystal but are affected by several other parameters of the growth system as well. For growing a crystal of 10 mm radius, pulling rates of 4 to 8 mm/h and a rotation rate of 30 rpm are found to be satisfactory.

For most optical applications, Z-axis growth is preferred but crystals are grown in the x and y directions also. Byer et al.[35] reported that x-axis grown boules have much less residual strain than Z-axis grown boules. He also discussed other growth directions and reported growth of high optical quality crystals along $01\bar{1}.4$ direction.

The very significant advances made in controlling the crystal shape have been those where weight sensing has been used to control the crystal diameter automatically during Czochralski growth; the general aim being to produce

a smooth, parallel-sided cylinder once the required diameter is attained. Zydzik[36] reported the successful application of this technique with $LiNbO_3$ and found an improvement in the general quality of the crystals along with a marked decrease in the cracking tendency.

Plate crystals of $LiNbO_3$ were grown by Fukuda and Hirano[37] through the edge-defined, film-fed growth (EFG) technique using a Czochralski pulling aparatus. Crystals of size 20 x 1.5 x 40 mm could be pulled at a typical speed of 3 mm/min, about 40 times as fast as that of conventional Czochralski technique. The technique is economically attractive in that plate crystals with several crystallographic orientations (such as 35° rotated Y-plate) could be grown while such plates have to be cut from boules if Czochralski technique is used. Unpoled crystals revealed, through etching experiments, a domain structure lying parallel to the surface of the plates unlike the Czochralski grown boules where the domain structure is perpendicular to the growth direction.

II.1.2.3. Preparation of Single Domain Crystals:

The existence of a ferroelectric domain structure in the as-grown crystals of $LiNbO_3$ was first reported by Nassau et al.[38] through etching experiments. These domains affect the crystal perfection very seriously, rendering the crystals unfit for many applications. Nassau et al. developed a few poling procedures in 1966, at least one of which has since become a standard technique to

obtain single domain material. These are briefly described below.

(i) Molybdenum addition: An addition of 0.5 at. % MoO_3 to the melt is believed to cause a replacement of Nb by Mo, forming a Li vacancy for charge-compensation:

$$(1-x)LiNbO_3 + x\,MoO_3 \longrightarrow (Li_{1-x}\emptyset_x)(Nb^{5+}_{1-x}Mo^{6+}_x)O_3$$

where $\emptyset$ denote a vacancy in lithium site.
The crystal grown from this Mo doped melt is completely a single domain crystal and contains only one-twentieth of the amount of the dopant added to the melt. Under very good growth conditions like a flat melt-crystal interface, high quality seed etc., single domain crystal growth occurs for a growth direction 20-40° from the c-axis with the negative dipole end of the crystal facing the melt.

An addition of WO_3 has a similar effect though not to the same extent. A possible mechanism can be an accumulation of Mo^{6+} ions near the growth interface thus producing a small electric field and simulating the second technique described below.

(ii) Growth in an electric field: This technique basically makes use of the conductivity of the melt at high temperatures. The application of an electric current to the growing crystal necessitates the incorporation of the following arrangements to the conventional pulling apparatus. The seed-holder and the crucible should be completely insulated from the rest of

the apparatus so as to avoid alternate paths for the electric current to be applied. Electrical contacts are provided for the seed-holder through a rotating friction contact and for the crucible through a welded platinum wire. The resistance of the crystal increases markedly as growth proceeds. Therefore a programmable power supply which can maintain a steady current throughout the growth process should be used. Application of a current as low as 2 mA/cm^2 can result in single domain crystals. The voltage drop across the crystal and the melt is of the order of a few hundreds of volts. More current is required for increasing off-axiality. The method is, however, not suitable for large diameter crystals because of seed decomposition by passage of high currents. Figure II.5 shows schematically the electrical connections required for the application of the poling current.

The temperature profile of the growing crystal, required for poling during growth, is shown in Figure II.6. The after-heater surrounding the growth region should be maintained at a high temperature of more than 1000°C to keep the crystal conductive but it should be considerably lower than the Curie temperature. The Curie boundary lies at a small height above the melt as the temperature of the crystal decreases along the pull direction. The poling current is expected to be effective only for the part of the crystal above the Curie boundary with reference to Figure II.6, where the temperature of the crystal is below T_c. After the growth is stopped, when the poling current cannot be

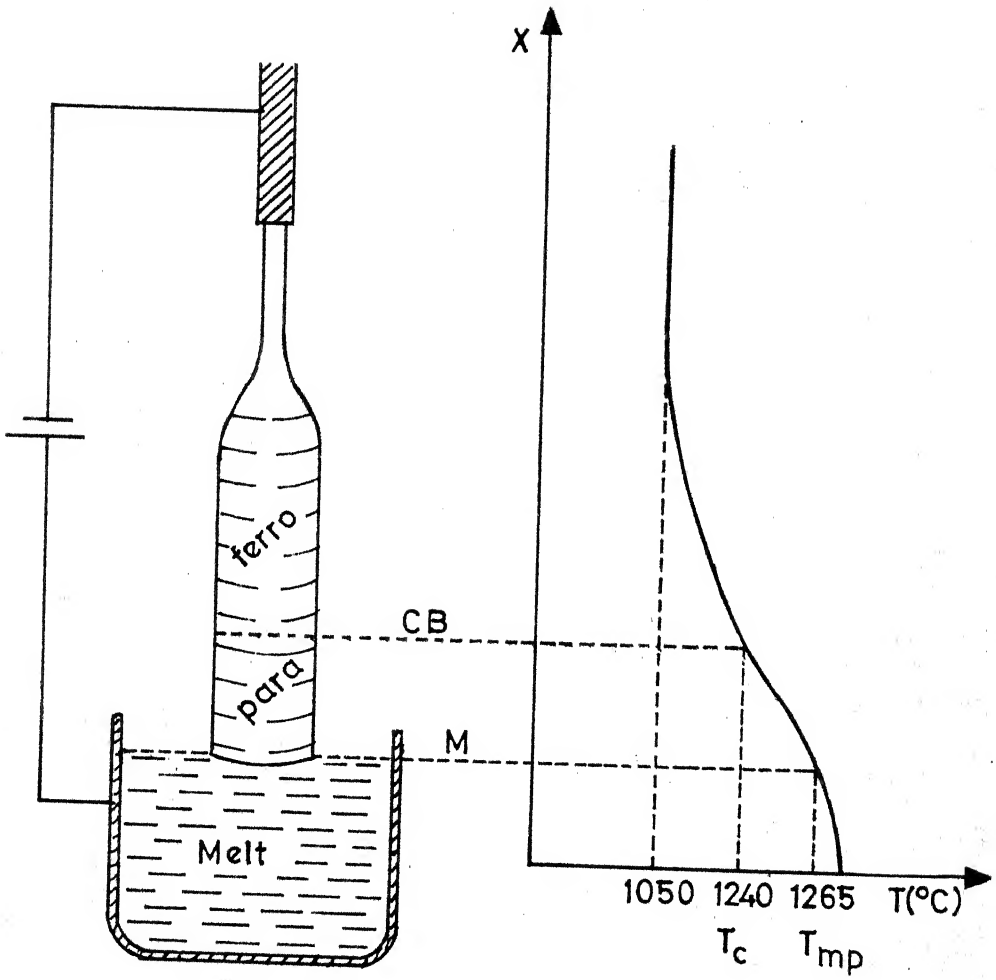

Fig. II.6 Temperature profile for poling during crystal growth of $LiNbO_3$ (Ref. 1)

maintained any more, the part of the crystal below the Curie boundary in the paraelectric state is expected to crystallise with a poly-domain structure as it cools down through the Curie temperature. But it is observed that the single domain structure is extended upto the growth interface, surviving through the paraelectric region and is attributed to an electrolytic action. Some interesting results of Tasson et al.[40] on poling by electric field will be discussed shortly.

(iii) Poling after growth: $LiNbO_3$ has been considered as a 'frozen' ferroelectric[7] because polarisation reversal was not possible near room temperature even at very high fields. But in the region of Curie temperature application of very low fields resulted in single domain crystals. Platinum electrodes are applied to the end faces of a Z-cut crystal by sputtering. The crystal is then heated in a resistance furnace very slowly at a rate of about 200°C/hr. to about 20°C above the Curie temperature. Now a steady poling current of 2 mA/cm^2 is applied to the crystal for about 30 min. while the crystal is cooled to about 10°C below the Curie temperature at the rate of 1°C/min. The current is switched off and the crystal is cooled to room temperature at 100°C/hr. The furnace is supplied with a slow purge of O_2 to prevent any discoloration. Poling results in a single domain material and also serves as an annealing cycle which relieves crystal strain. The method can be used for crystals of any growth direction and remains the most popular method to obtain single domain crystals.

Not much work has been done towards the understanding of poling mechanisms. In 1976, Tasson et al.[40] conducted a study of polarisation reversal using a piezoelectric technique in $LiNbO_3$ crystals. In addition to the effect of an applied electric field, they reported the effect of a thermal gradient and a composition gradient. Their experimental technique consisted in preparing small Z-cut disc samples of congruent composition (0.5 mm thick and 3 mm diameter) with platinum electrodes and stressing the crystals by a mechanical transducer via alumina rods at a frequency of 5 KHz along Z axis. The piezoelectric response, proportional to the average polarisation $\langle P \rangle$ was recorded vs. temperature while applying an electric field or a thermal gradient along Z-axis.

Application of an electric field ($\sim$1 V/cm) during cooling through T_c resulted in the usual effect of poling the crystal. An indirect effect was obtained when the field was switched off before passing T_c resulting in a crystal poled in a sense opposite to that obtained in the direct effect where the field was maintained until T_c was crossed. By quickly heating the sample above T_c and cooling it again without any applied field, the crystal was observed to be spontaneously repoled in the same direction, revealing thereby a memory effect. A half-hour anneal above T_c erased this memory effect. Similar results were obtained for the use of a temperature gradient (100°C/cm).

Tasson et al. also qualitatively established the effect of a composition gradient on the orientation of spontaneous polarisation, through domain structure studies of doped crystals.

In the following section the problems besetting $LiNbO_3$ affecting its utility for Non-Linear Optical (NLO) applications and the methods that can be adopted at the growth stage to overcome them are briefly discussed.

II.1.2.4. Crystal Growth Considerations for NLO Applications:

Two serious drawbacks characterise $LiNbO_3$ for all optical applications. The first of these is a large spatial variation of the birefringence arising from a strong composition dependence of the extraordinary index. This makes it impossible to satisfy the phase-matching conditions, required for efficient SHG at all points within the crystal for a given temperature. Thus the effective phase-matchable lengths of these crystals are much less than the physical length of the crystals. But growth from congruent melts preserves the spatial uniformity of birefringence because the composition variations along the length of the crystal are very much reduced. Even so, it is very much advisable not to grow several boules from a single melt-charge and not to replenish the melt after growth instead of completely replacing it. But congruent melt-grown crystals suffer from a more severe drawback which relates to the refractive index inhomogeneities

at moderate doses of laser beam irradiation. This is termed as 'optical damage'[42] and severely limits the use of $LiNbO_3$ for electro-optical and laser applications. The damage can be completely annealed at 250°C but the phase-matching requirements stipulate that the temperature must be maintained below 200°C. The best way to circumvent this problem is to raise the phase-matching temperature above the index-damage anneal temperature without violating the spatial uniformity of birefringence. Doping with MgO proved to be successful in this regard. MgO has the proper distribution coefficient value and was also known to raise T_c. So it was suspected[42] that it would probably raise T_{p-m} (temperature of phase-matching) also. Bridenbaugh et al.[43] did find an increase of T_{p-m} from 46°C to 87°C for an addition of 1% MgO for crystals of congruent composition at 1.08 μm wavelength for the fundamental wave in SHG. They could grow several centimeters long X-axis crystals with a small MgO addition resulting in a high T_{p-m}. Also Mg^{+2} was found to substitute for Li^+ at the congruent Li/Nb ratio in such a way as to keep the T_{p-m} virtually uniform over the crystal length. MgO addition serves another very useful purpose also viz. the cracking tendency is completely eliminated.

II.1.2.5. Growth of Stoichiometric Crystals:

Growth of stoichiometric crystals is of interest, since the T_{p-m} for these crystals at the operational wavelengths

is considerably higher than the temperature of the refractive index damage anneal. These high T_{p-m} crystals grown from near-eutectic melts and having a stoichiometric composition are called 'hot $LiNbO_3$'. These have very large birefringence variations and short (~3 mm) phase-matchable lengths. Carruthers et al.[17] reviewed the growth of stoichiometric crystals. In stoichiometric crystal growth, under good growth conditions, the following composition variations are observed:

(a) the normal freeze variation over the length of the crystal, as warranted by the phase diagram,

(b) growth striations due to fluctuations in growth rates arising from liquid convection and rotation of the crystal through an asymmetrical temperature gradient.

The intensity of the growth striations can be reduced by using small melt depths and low temperature gradients compatible with good diameter control which minimise the convectional instability within the melt. But in order to prevent constitutional supercooling under low temperature gradients, the growth rates have to be very low.

Growth striations can represent a useful built-in record of the interface shape at any point along the length of the crystal and can be employed in studying defect and morphology changes related to the topology of the solid-liquid interface. In congruently grown crystals of $LiNbO_3$, introduction of dopants with a distribution coefficient not equal to unity can lead to striations. Rauber[44] could obtain well-defined striations with Cr doping by applying

periodic currents to the crystal during growth. The marking of the growth interface by these dopant striations was used to study the growth process and the influence of growth parameters like the temperature gradient, speed of rotation and withdrawal and temperature fluctuations for $LiNbO_3$. Very low currents of the order of 5 mA/cm^2 to 50 mA/cm^2 could substantially change the content of the Cr^{3+} ions. Pulsed currents resulted in a periodic structure. Such doping structures cause changes in the refractive index and the acoustic velocity and hence the method can be used for the growth of light-guiding structures and for the fabrication of acoustic wave guides.

In the following sections the properties of importance of $LiNbO_3$ will be dealt with. The dependence of the properties on composition, temperature etc. will be treated in greater detail.

II.1.3. Optical Properties:

II.1.3.1. Transmission:

Well-oxidised and homogeneous $LiNbO_3$ crystals of high chemical purity possess a water-clear transparency. The transmission range extends from 0.35 m to 5 m where lattice phonon absorption sets in. The optical transmission of single domain $LiNbO_3$, first reported by Nassau et al.[39] is shown in Figure II.7. Transmission is 100% between 0.5 to 4.5 m in the bulk of the crystal but surface reflection

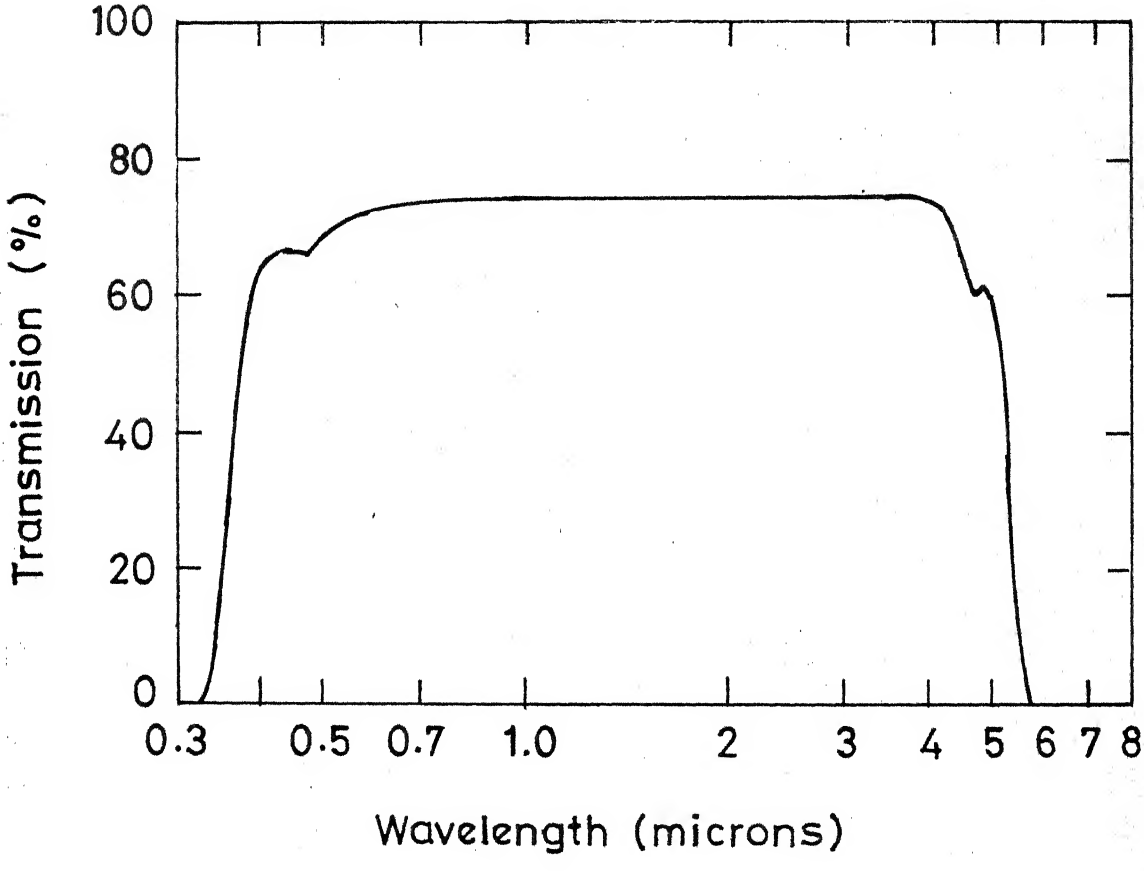

Fig. II.7 Optical transmission of single domain $LiNbO_3$ (uncorrected for deflection losses) [Ref. 39]

is appreciable because of the large refractive indices of $LiNbO_3$. Guseva et al.[45] used a monolayer coating of quartz (n = 1.46) and MgF_2 (n = 1.38) to reduce reflection losses. Figure II.8 shows the effect of a MgF_2 coating on the transmission of $LiNbO_3$ in the visible region. They also reported the effect of crystal thickness on transmission in the near infra-red region and the effect of crystal coloration on the visible transmission. Larger specimen thicknesses and stronger coloration led to a decrease in the transmission values.

II.1.3.2. Refractive Index and Birefringence:

$LiNbO_3$ is a uniaxially negative crystal showing a large negative birefringence = 0.0919 (n_o = 2.3002 and n_e = 2.2083 at 6000 Å and 25°C). The values quoted here are from the measurements of Boyd et al.[48] for unpoled material. Their work first showed that $LiNbO_3$ was a promising material for nonlinear optical applications and prompted extensive studies on the refractive indices and their dependence on temperature, composition, wavelength etc. Boyd et al.[49] subsequently made precise refractive index measurements on single-domain high purity $LiNbO_3$ with 0.5 weight % MgO (to prevent cracking) at 25°C and 80°C, between 0.42 μ and 4.0 μ. No mention is made of the composition of the $LiNbO_3$ crystals on which the measurements were made. Their results are shown in Table II.1. Barker and London[50] made use of these values and showed that the refractive indices in the transparent region of $LiNbO_3$ can be explained in terms of one oscillation

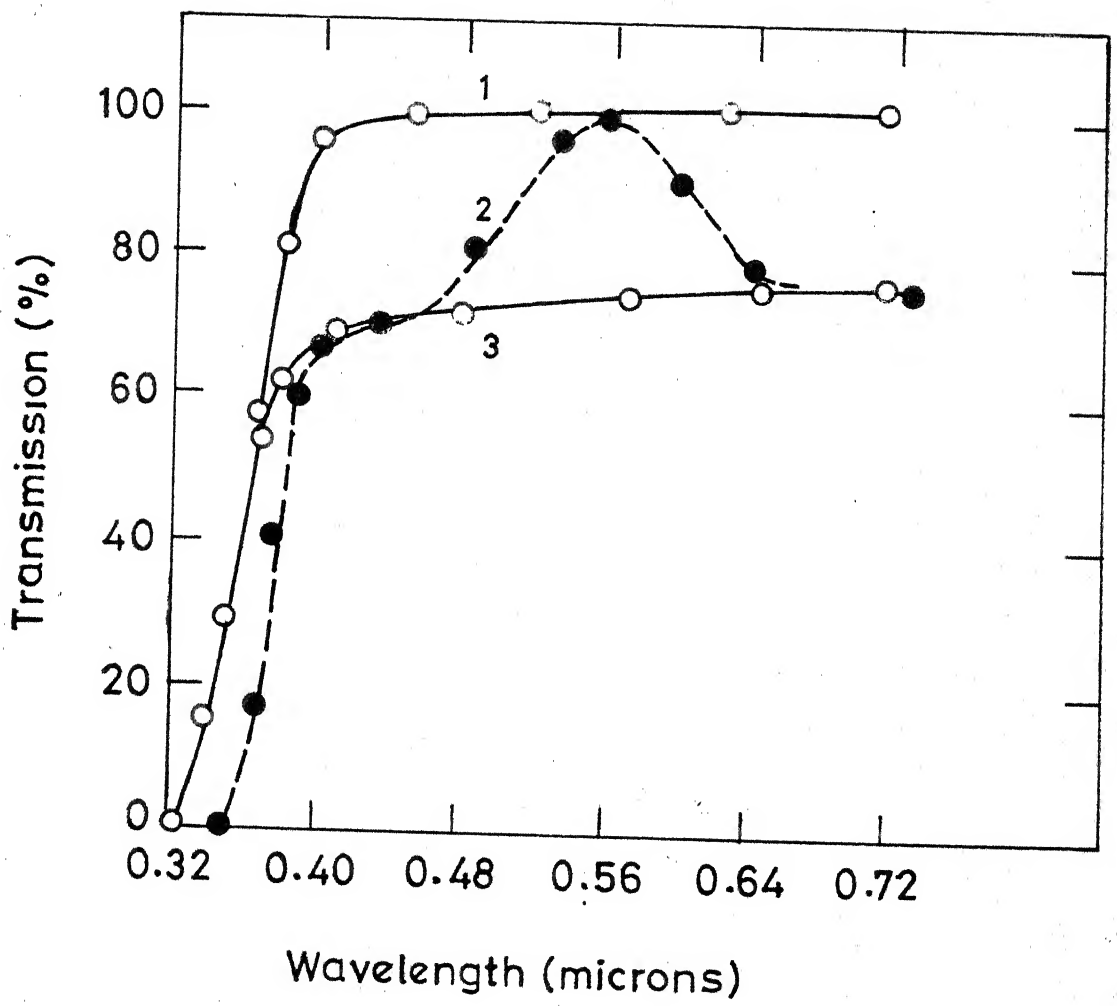

Fig.II.8 λ vs transmission of polydomain $LiNbO_3$ when reflection losses are accounted for (curve 1) and not accounted for (curve 3) and when coated with MgF_2 (curve 2) [ref. 45]

Table II.1. Refractive Indices of $LiNbO_3$ Between 0.42 and 4.0 (Ref.)

Wavelength (μ)	T = 25°C		T = 80°C	
	n_o	n_e	n_o	n_e
0.42	2.4144	2.3038	2.4170	2.3090
0.45	2.3814	2.2765	2.3836	2.2814
0.50	2.3444	2.2446	2.3462	2.2498
0.60	2.3002	2.2083	2.3013	2.2118
0.70	2.2756	2.1874	2.2758	2.1900
0.80	2.2598	2.1741	2.2600	2.1766
1.00	2.2407	2.1580	2.2407	2.1601
1.40	2.2208	2.1410	2.2208	2.1426
1.80	2.2074	2.1297	2.2074	2.1318
2.20	2.1948	2.1187	2.1947	2.1211
2.60	2.1814	2.1080	2.1812	2.1099
3.00	2.1663	2.0955	2.1660	2.0972
3.40	2.1493	2.0814	2.1490	2.0830
3.80	2.1299	2.0652	2.1298	2.0669
4.00	2.1193	2.0564	2.1193	2.0582

term in the UV and several infra-red terms (Figure II.9) and have explained the temperature dependence in these terms.

Measurement of the far infra-red refractive indices as a function of wave number at 300°K and 80°K were reported by Bosomworth.[51] The temperature dependence of the refractive indices becomes very important for SHG phase matching by temperature tuning and has been studied extensively by several workers over a wide range of temperatures for several wavelengths. The results of Iwasaki et al.[52] are shown in Figures II.10 and II.11. The increase in n_e with increasing temperature is much higher than that of n_o, thereby leading to reduced birefringence values for higher temperatures. Miller and Savage[53] carried out measurements of the changes in the refractive indices of $LiNbO_3$ and its birefringence from room temperature upto Curie temperature at 0.6328 . All the optical data were seen to exhibit distinct changes at the Curie temperature, $T_c = 1195 \pm 15°C$. Their results are shown in Figure II.12. Hobden and Warner[54] derived two temperature dependent Sellmeier equations to give the refractive indices of undoped $LiNbO_3$ between 0.4 μm to 4 μm, valid upto 500°C, from measurements of the refractive indices between 19°C and 374°C for wavelengths between 0.4 μm to 0.7 μm.

Warner et al.[55] measured the optical birefringence of $LiNbO_3$ at 0.6328 μ and 1.152 μ from room temperature upto the ferroelectric Curie temperature and was found to fall by a factor of 8 between room temperature and T_c, as temperature was increased. The variation of birefringence with temperature

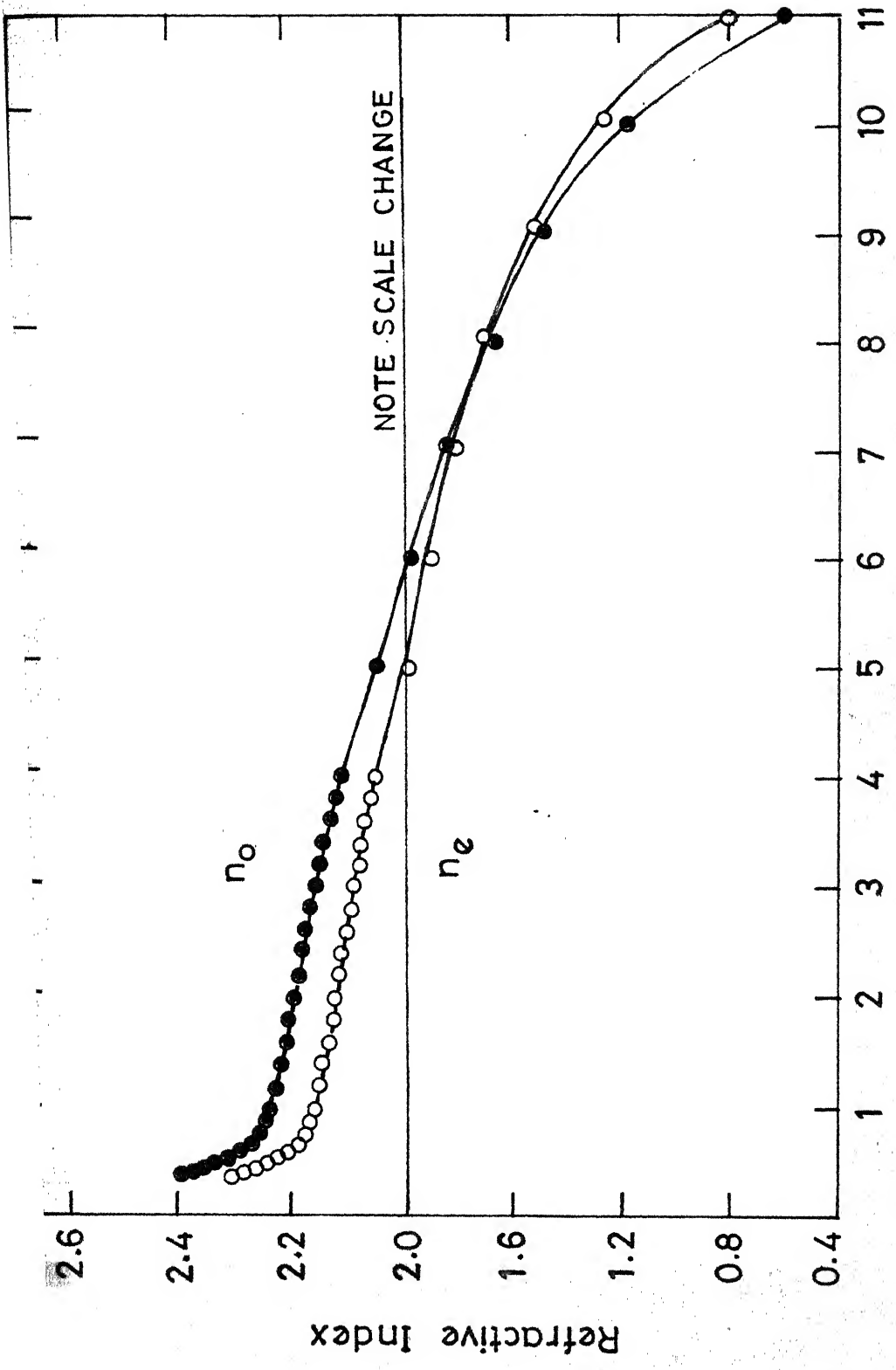

Fig.II.9 Refractive indexes of $LiNbO_3$ as a function of wavelength at 300° k (Ref. 48)

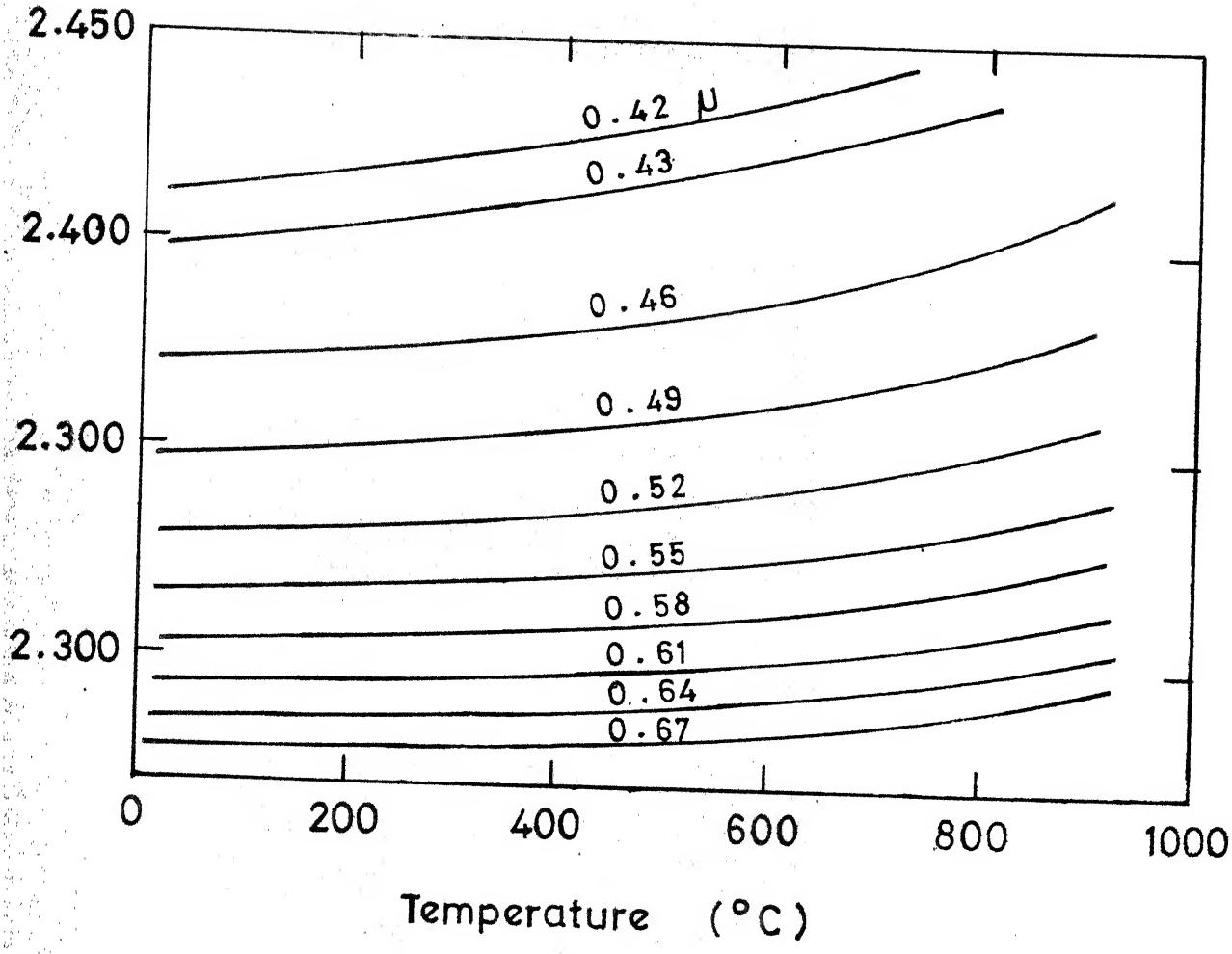

g.II.10 Variation of ordinary refraction index of $LiNbO_3$ with temperature for several wavelengths(Ref. 50)

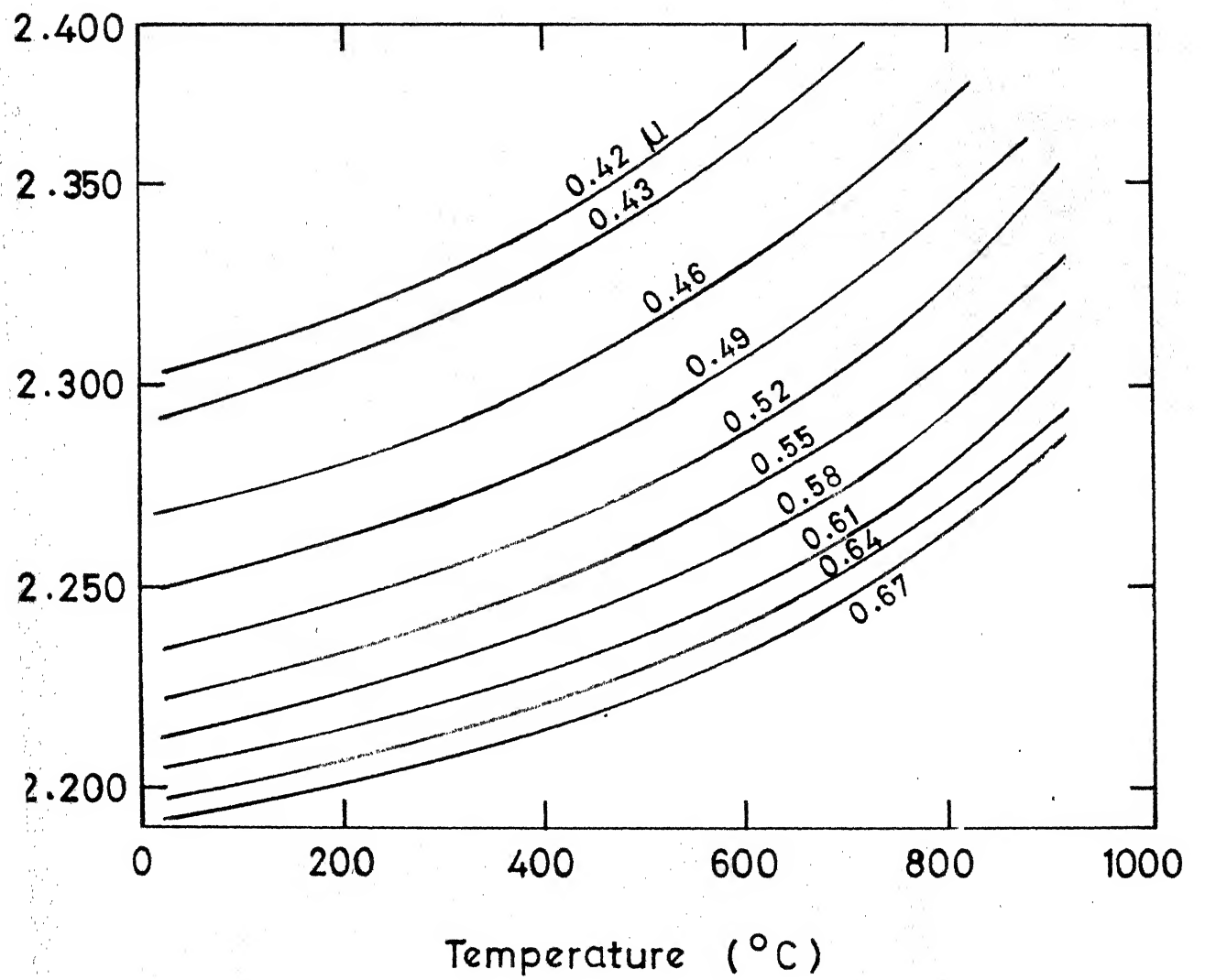

Fig II.11 Variation of extraordinary refractive index of $LiNbO_3$ with temperature for several wavelengths (ref. 50)

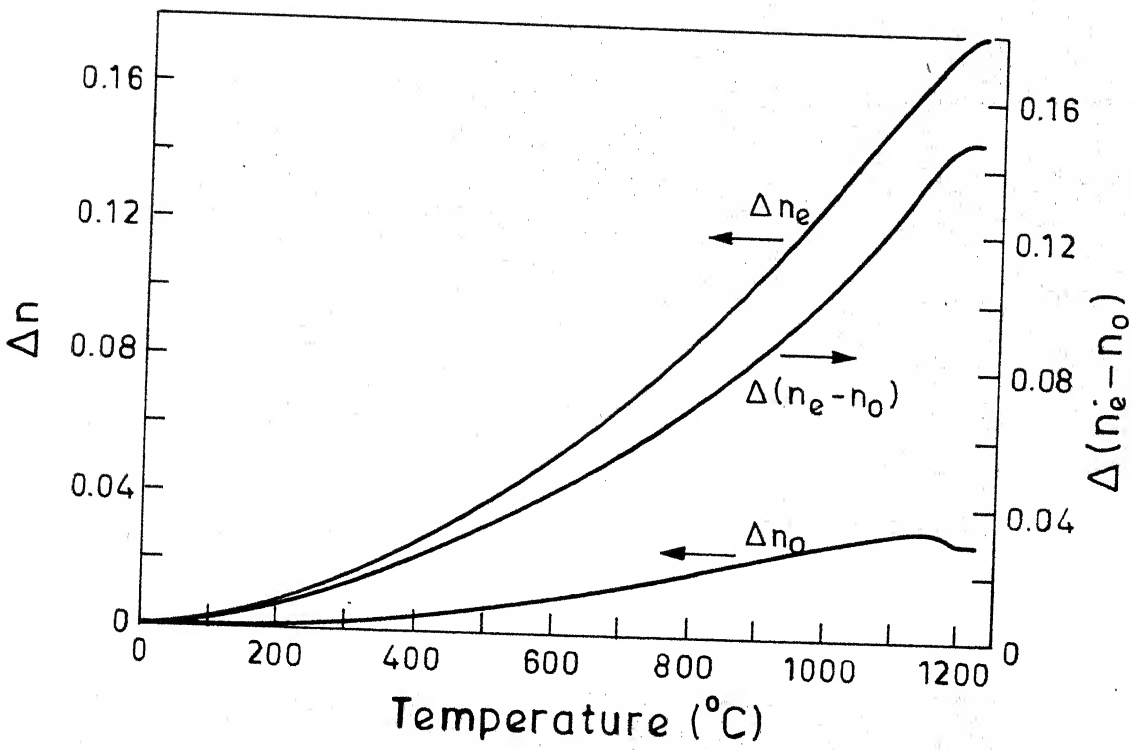

ig. II.12 Change in the refractive indices and birefringence of $LiNbO_3$ vs temperature at $\lambda = 6328$ Å. (Ref. 51)

is shown in Figure II.13. At 0.6328 μ, the slope of the graph $\frac{d(\Delta n)}{dT}$ varies from -2.7×10^{-5}/°C at 100°C to -9.5×10^{-5}/°C at 1000°C.

Virogradov et al.[56] evaluated the ordinary refractive index n_o from the measured transmission of a Z-cut $LiNbO_3$ crystal in the frequency range of 120 to 150 GHz and reported a value of 7.2 ± 0.2 for n_o. Irisova and Kozlov[57] measured the dependence of the phase shift $\Delta\phi$ between the ordinary and the extraordinary waves, in a Y-cut $LiNbO_3$ crystal, on the frequency of the electromagnetic radiation in the range of 100 to 150 GHz
At points for which the following relation holds:

$$\Delta n.d.2\pi\nu/c = \pi m \qquad \text{(II.5)}$$

where m is a positive integer, d is the crystal thickness, c the velocity of light in vacuum, ν the frequency of the electromagnetic radiation and Δn is the birefringence, the amplitude of the interference oscillations decreases to zero enabling the value of Δn to be determined with maximum accuracy. For $LiNbO_3$, a birefringence of 1.57 ± 0.01, with no dispersion in the range 100-150 GHz was reported.

The variation of the refractive indices of $LiNbO_3$ with hydrostatic pressure upto 7 k.bars was measured by Vedam and Davis[58] through an interferometric method. Both the indices for $\lambda = 5893$ Å showed a linear increase with pressure with slopes of 0.32×10^{-3}/k.bar and 0.69×10^{-3}/k.bar respectively for the ordinary and the extraordinary

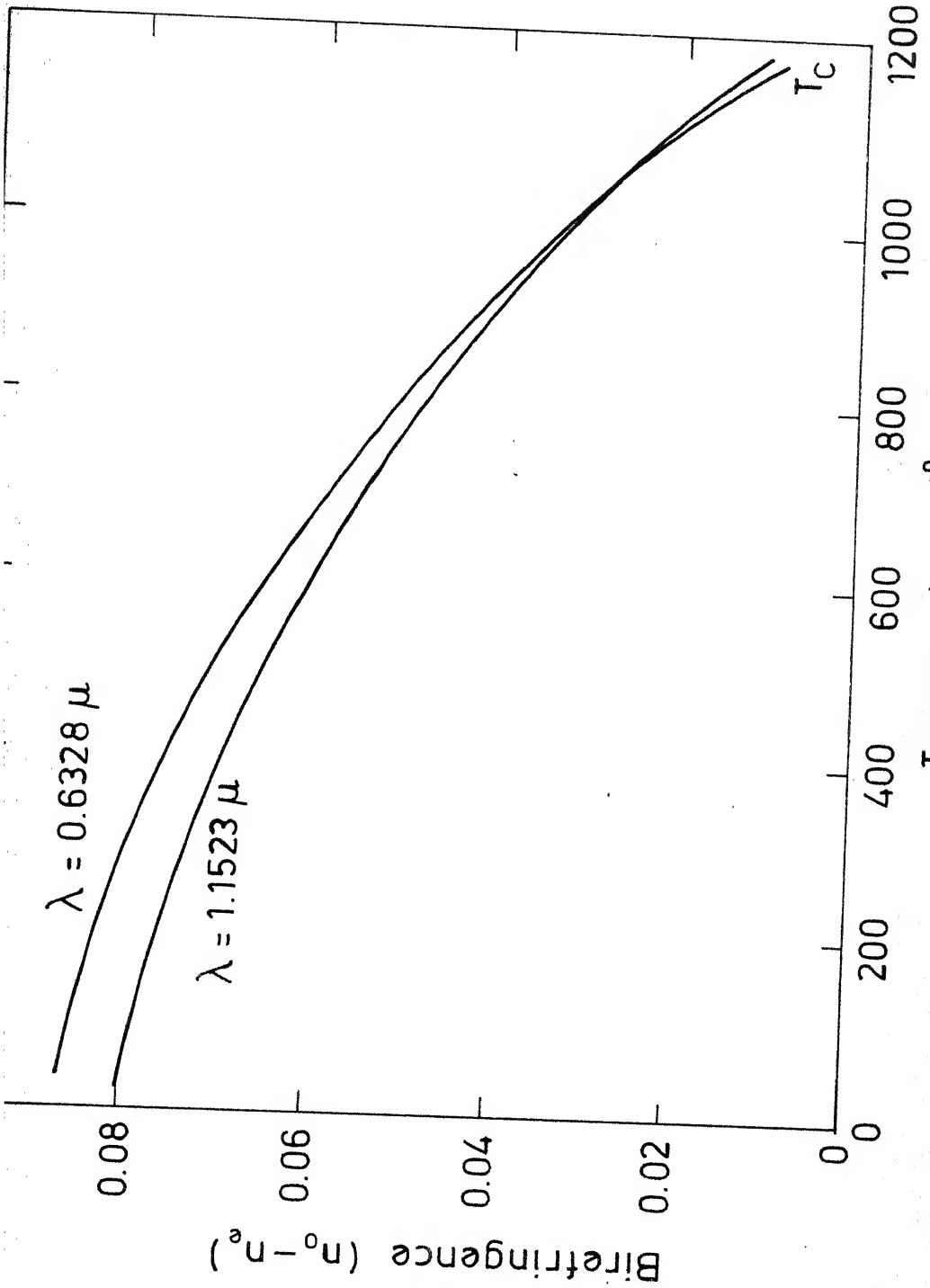

Fig. II.13- Variation of birefringence of $LiNbO_3$ as a function of temperature. (Ref. 53)

rays, as is evident from Figure II.14, where the volume strain induced by the applied hydrostatic pressure is also indicated. These values agree well with the calculated values of $\frac{dn_o}{dP} = 0.29 \times 10^{-3}$/k.bar and $\frac{dn_e}{dP} = 0.61 \times 10^{-3}$/k.bar at $\lambda = 6328$ Å obtained from the following relations[59]

$$\Delta n_o = \frac{-n_o^3}{2}\left[(p_{11} + p_{12})\eta_1 + p_{13}\eta_3\right] \qquad \text{(II.6)}$$

and

$$\Delta n_e = \frac{-n_e^3}{2}\left[2p_{31}\eta_1 + p_{33}\eta_3\right] \qquad \text{(II.7)}$$

where η_i are the Lagrangian strains and p_{ij} are the strain-optic coefficients and have been determined by Dixon and Cohen[60] from measurements of the intensities of the light scattered by sound waves in $LiNbO_3$. Vedam and Davis also determined the proportional change of the refractive index with density $\rho(dn_o/d\rho)$ and $\rho(dn_e/d\rho)$ to be 0.35 and 0.79 respectively, from the slope of Δn vs. volume strain, in Figure II.16 using the relation

$$\rho(dn/d\rho) = -\Delta n/\frac{\Delta V}{V_o} \qquad \text{(II.8)}$$

ρ and V being the density and volume of the sample respectively.

That the composition dependence of the optical birefriengence in $LiNbO_3$ has strong implications for the use of $LiNbO_3$ in nonlinear optical applications, was briefly indicated previously in Section II.1.2.4. The spatial [illegible] of birefringence due to composition inhomogeneities was

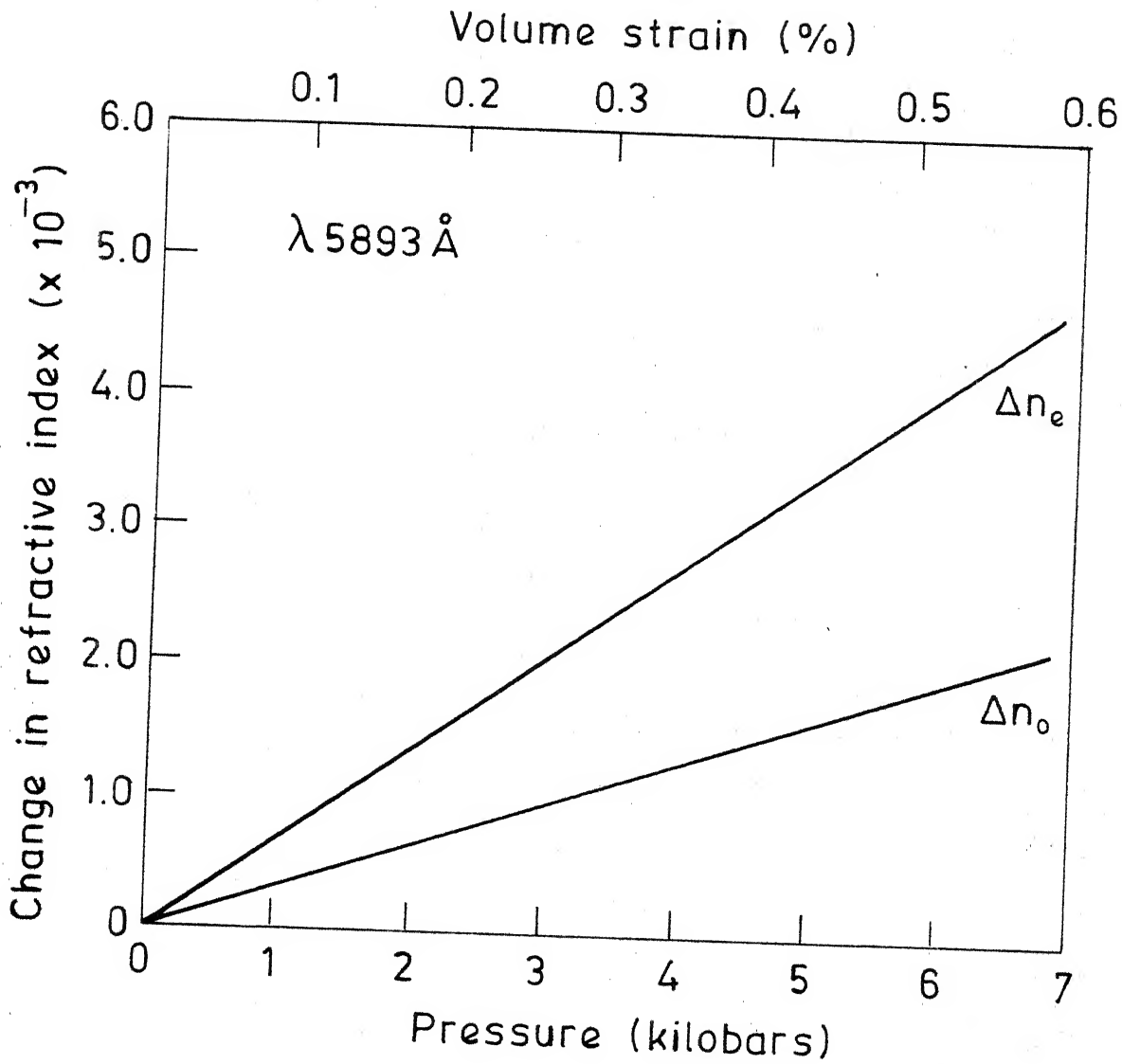

II.14 - Change in refractive indices of $LiNbO_3$ vs hydrostatic pressure and volume strain at 20°C. (Ref. 56)

overcome by growing crystals of $LiNbO_3$ from congruent melt. Nelson and Mikulyak[61] determined the refractive indices of congruent composition $LiNbO_3$ crystals between 0.4 μm and 3.0 μm at 24.5°C to an accuracy of two parts in 10^4. Bergman et al.[62] first reported the variation of the refractive indices of $LiNbO_3$ at 0.6328 μm as a function of the melt stoichiometry. Their results, shown in Figure II.15, reveal a strong dependence of the extraordinary refractive index on the Li/Nb mole ratio whereas the ordinary refractive index is seen to be practically independent of the composition variations. This makes it convenient to characterise the composition of the material through birefringence measurements rather than the absolute indices. Interferometric methods[63] have been used to measure birefringence directly but a very sensitive technique for birefringence measurement has been the use of SHG phase-matching temperature. Midwinter[43] also studied the effect of composition on the refractive indices by growing crystals from melts of stoichiometric composition, doped with 0.5 wt % of Li_2CO_3, Nb_2O_5 and also MgO. In all the three cases, doping resulted in a decrease of the extraordinary refractive index leading to increased birefringence.

II.1.3.3. Nonlinear Optical Behavior and Second Harmonic Phase Matching:

If a light wave of frequency ω_1 enters a nonlinear crystal, the output will contain higher harmonics in addition to the fundamental, like $2\omega_1$, $3\omega_1$ ... etc.

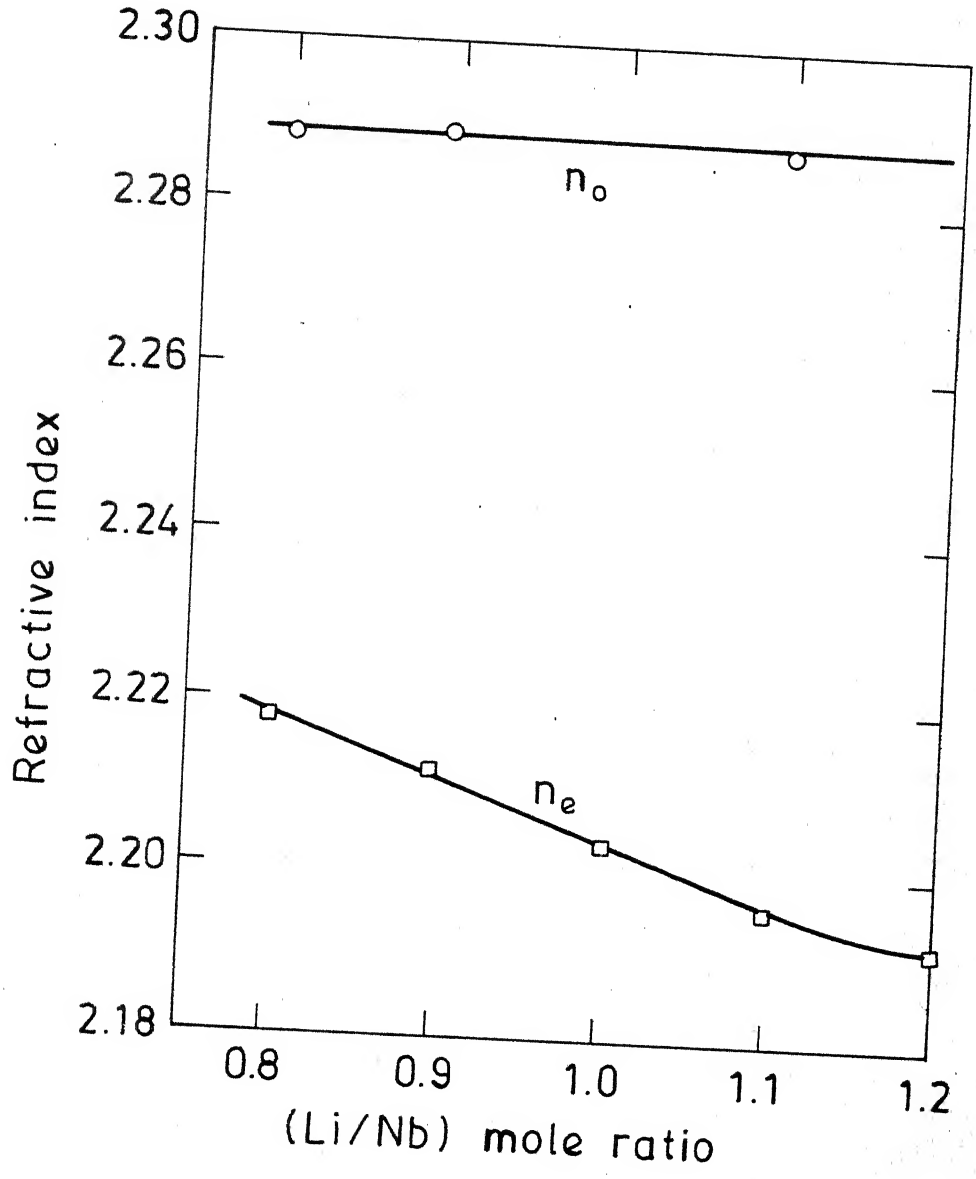

Fig. II.15 - Variation of the refractive indices of $LiNbO_3$ as a function of melt stoichiometry. (Ref. 60)

Boyd et al.[48] first observed large amounts of second harmonic generation (SHG) in $LiNbO_3$ and its nonlinear coefficient d_{31} was found to be about 11 times the d_{36} value of KDP. Since then $LiNbO_3$ has played a crucial role in the development of nonlinear optics. Power conversion from the polarisation wave to the second harmonic wave will be most effective if the two waves can be phase matched i.e. the two waves must see the same refractive index. For two waves of different frequencies ω and 2ω, phase-matching would be possible only with a birefringent crystal which can compensate for the refractive index dispersion in the medium. By virtue of its large negative birefringence, $LiNbO_3$ offers easy phase-matching and hence an efficient SHG. Because $LiNbO_3$ is negative uniaxial ($n_e < n_o$), the polarising wave of frequency ω should be used as the ordinary ray while the second harmonic ray has to be polarised in the extraordinary direction. When phase-matching is achieved $n^e_{2\omega} = n^o_{\omega}$. This can be accomplished by two methods, viz. (i) angle tuning where a proper choice of the angle of incidence with respect to the optic axis is made use of to achieve exact phase-matching of the two rays and (ii) temperature tuning where the temperature dependence of the refractive indices $n^e_{2\omega}$ and n^o_{ω} is exploited to locate a particular temperature called the phase-matching temperature T_{p-m} where the indices become equal for the fundamental wave and the second harmonic wave. Boyd et al.[48] obtained phase-matching of the fundamental beam with the extraordinary second harmonic

due to d_{31} by using a phase-matching angle of 68° with the 1.152 μm gas laser. Miller et al.[64] first made use of the thermally tunable refractive indices in $LiNbO_3$ to obtain noncritical phase-matching in the plane perpendicular to the optic axis. It was Midwinter[43,63] who first employed optical means to evaluate the quality of single crystals of $LiNbO_3$ by birefringence variation measurements and made a direct correlation between the SHG performance and the compositional inhomogeneities. He also demonstrated the effect of a temperature gradient in cancelling a gradient of birefringence in crystals having a uniform composition gradient, leading to an appreciable improvement in SHG performance.

Since the concept of phase-matching temperature is based on the thermal dependence of the refractive indices, it follows quickly that the compositional inhomogeneities, which strongly affect the extraordinary refractive index, should exert a corresponding influence on the phase-matching temperature. This was experimentally verified by Fay et al.[19] and Bergman et al.[62] whose results are shown in Figures II.16 and II.17. The data of the latter, as in Figure II.17, includes the variation of the ferroelectric Curie temperature with Li/Nb stoichiometry. The phase-matching temperature T_{p-m} was also found to be considerably enhanced by MgO addition to the $LiNbO_3$ melt during crystal growth. Bridenbaugh et al.[44] utilised this effect to obtain a spatially uniform T_{p-m} which was higher than the optical damage anneal temperature, in congruent melt grown crystals of $LiNbO_3$.

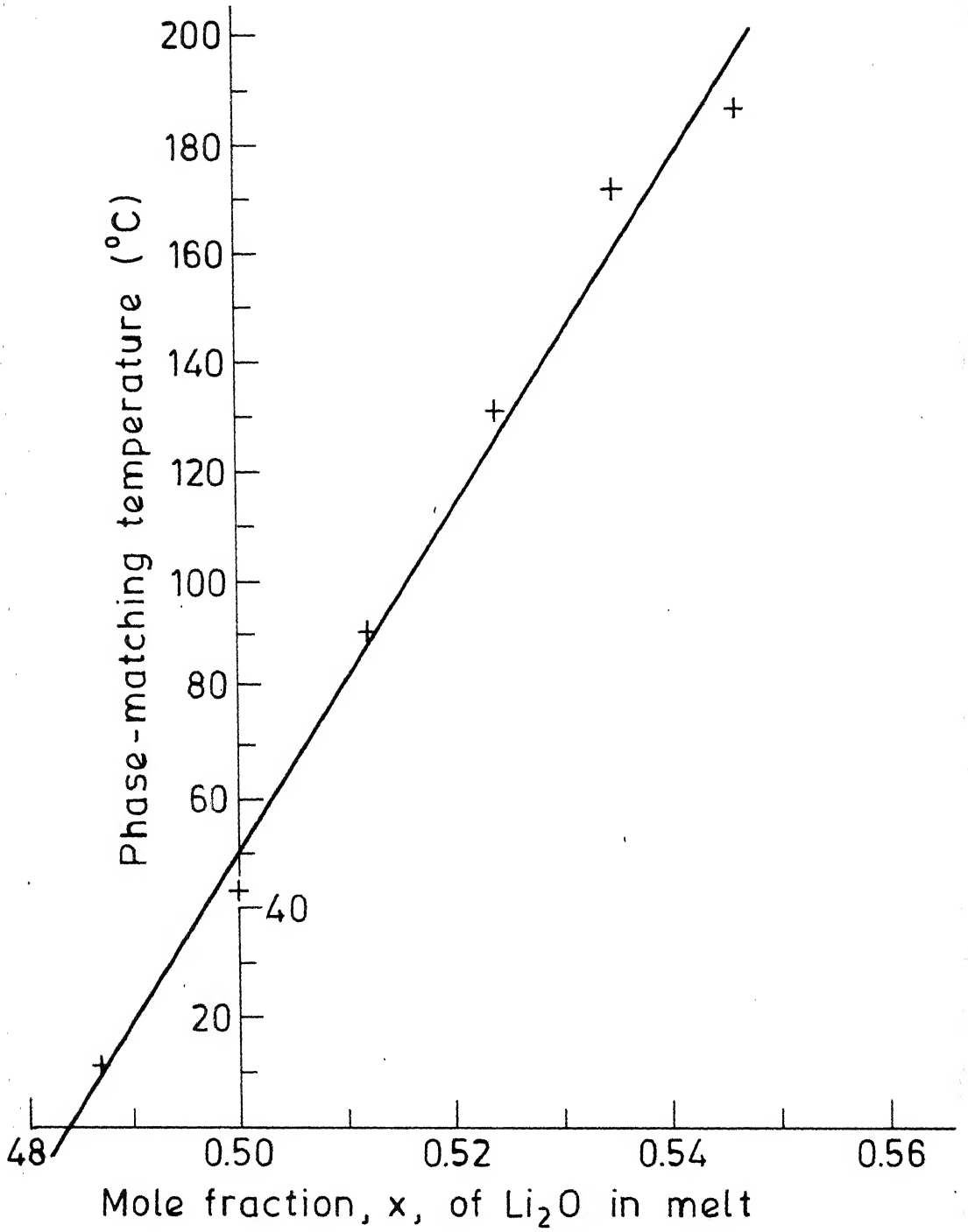

II.16 - Variation of phase-matching temperature as a function of melt composition. (Ref. 19)

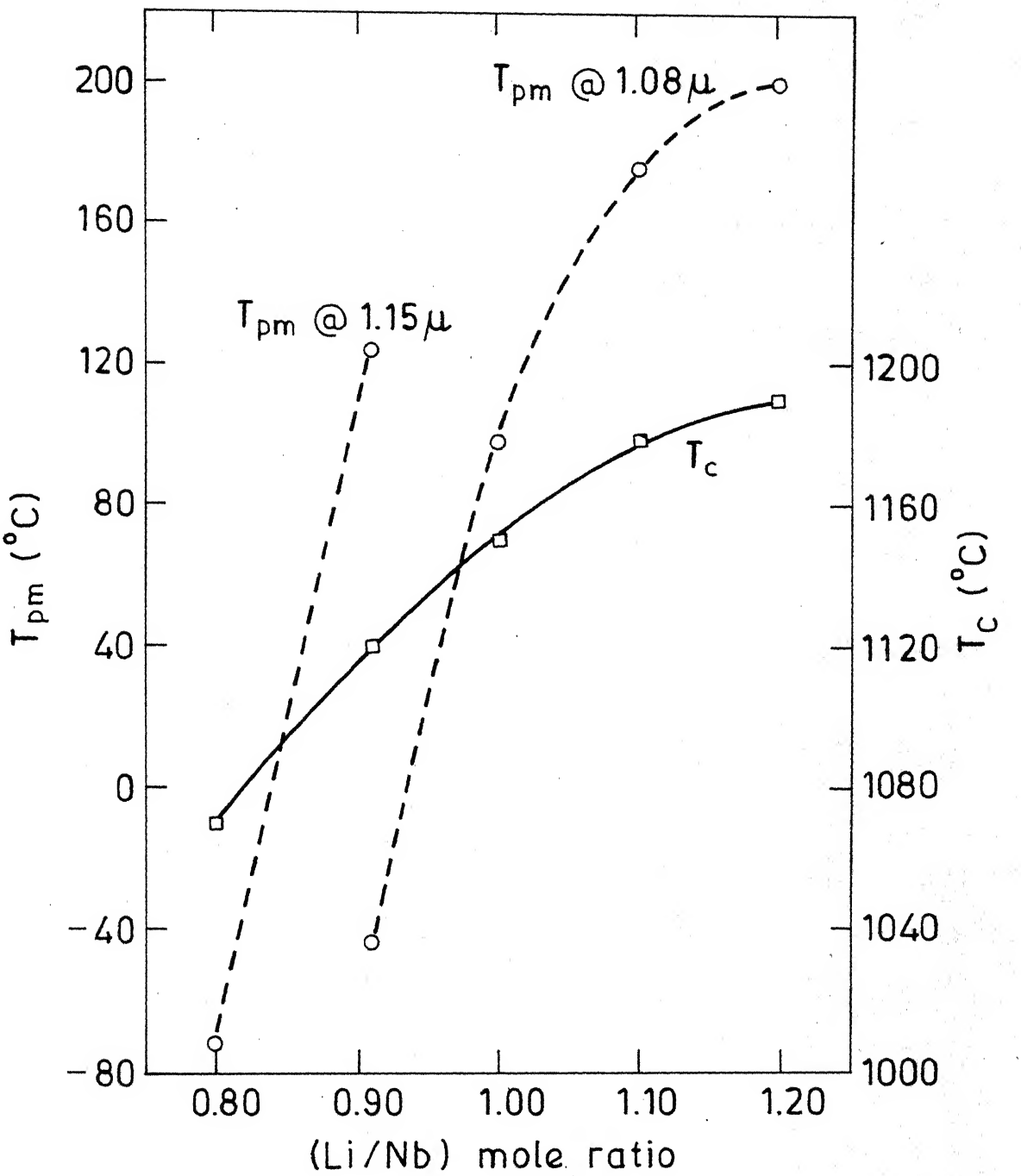

Fig. II.17 - Variation of phase-matching temperature and Curie temperature as a function of melt stoichiometry. (Ref. 60)

The effect of optical inhomogeneities due to long-range and local composition variations, on phase-matching and the second harmonic generation performance have been treated in detail by Byer et al.[18], Nash et al.[65] and Smith[66]. In the plot of SHG gain vs. temperature, a sharp peak occurs at the T_{p-m}. This peak is adversely affected by local index inhomogeneities in the laser beam interaction volume of the crystal. The half-width of the peak $\Delta T°C$ or the area under the gain plot divided by the peak height[65] offers an easy quality criterion of the crystal for the nonlinear optical applications. Byer et al.[18] published these data along with the phase-matching temperatures for both stoichiometric and congruent crystals of $LiNbO_3$ for different pump wavelengths. This is presented in Table II.2. Since the T_{p-m} of $LiNbO_3$ is a strong function of its composition, with approximately 150°C variation for each mole % Li_2O difference in the solid, and the half-width of the SHG peak is less than 1°C, as seen from Table II.2, SHG measurements constitute the most sensitive checks in evaluating the quality of the crystals with respect to composition. Chow et al.[14] describe a SHG coding cavity to measure the T_{p-m} and used it as a very sensitive probe to determine the congruent composition of $LiNbO_3$ correct to 0.01 mole %. Thus the SHG measurements, by virtue of the attendant high precision, permit a very accurate control of stoichiometry in $LiNbO_3$ and constitute a very powerful tool in monitoring the growth of crystals with desired properties for specific applications.

In addition to SHG, $LiNbO_3$ has been extensively investigated for other nonlinear optical applications like parametric oscillation, frequency mixing and frequency up-conversion etc. Using a Nd-laser (1.06μ) to observe SHG in $LiNbO_3$ Boyd et al.[48] followed by Miller and Savage[53] first determined the values for the following nonlinear optical coefficients on a scale where d_{36} for KDP is unity:

$$d_{22} = 6.3 \pm 0.6, \quad d_{31} = 11.9 \pm 1.7 \quad \text{and} \quad d_{33} = 83 \pm 21$$

The temperature dependence of the coefficient $d_{33}^{2\omega}$ is shown in Figure II.18. Miller et al.[67] determined the values of these coefficients for different Li/Nb stoichiometric ratios. This is given in Table II.3. Bjorkholm[68] reported that the coefficients d_{22} and d_{31} have opposite sign in $LiNbO_3$. Miller and Nordland[69] made a determination of the relative signs of the nonlinear optical coefficients giving rise to SHG in polar materials and reported that d_{33} and d_{31} have the same signs in $LiNbO_3$. In 1976, Choy and Byer[70] used a wedge technique to compare the nonlinear coefficients of infra-red and visible nonlinear crystals. Also they accurately redetermined the absolute nonlinear susceptibility of $LiIO_3$ and $LiNbO_3$ by a parametric fluorescence method and could establish a uniform absolute scale of nonlinear susceptibility values relative to d_{31} of $LiIO_3$ extending from 0.488μm in the visible range upto 10.6μm in the infra-red.

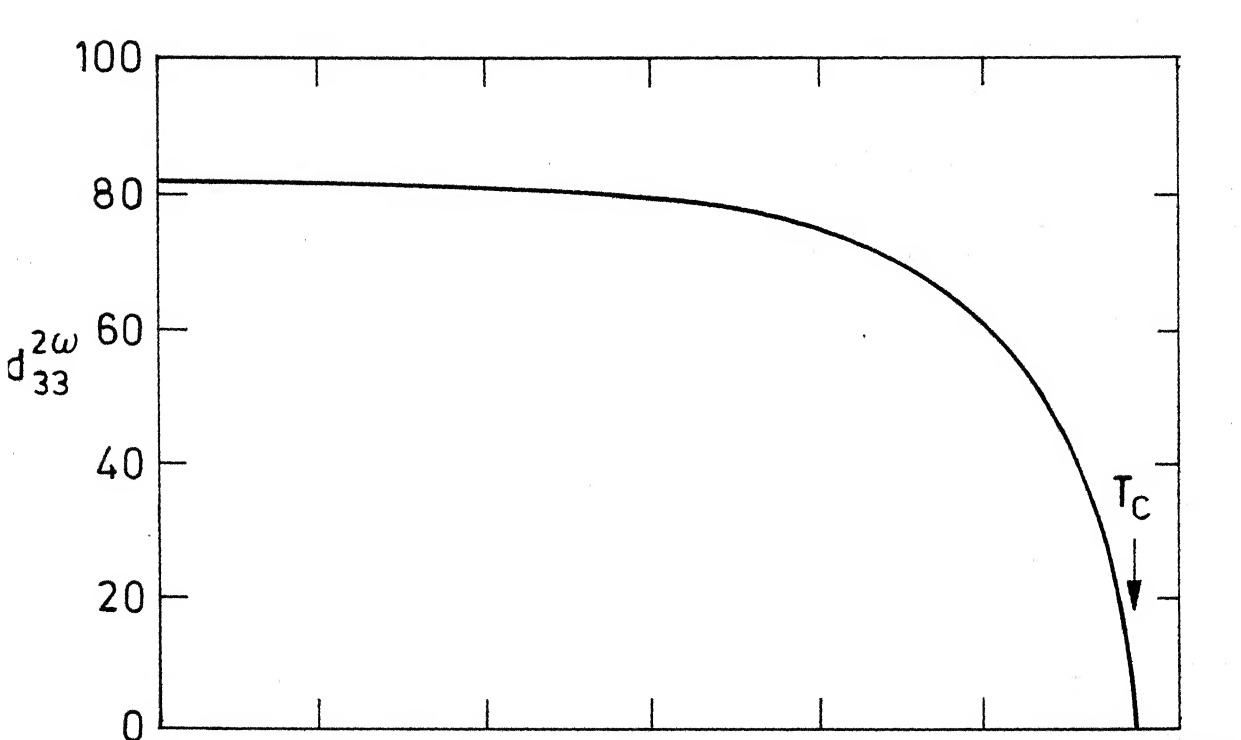

II.18 - Non-linear coefficient $d_{33}^{2\omega}$ for $LiNbO_3$ as a function of temperature. (Ref. 60)

II.1.3.4. Optical Damage or the Photorefractive Effect:

The most serious disadvantage of $LiNbO_3$ in many optical applications has been its large susceptibility to changes in the refractive index due to laser irradiation of moderate power. This is called 'optical damage' and should be overcome for many optical applications except holographic information storage where the same effect becomes indispensable and takes on the name 'photorefractive effect'. The effect was first reported by Ashkin et al.[41] in 1966 for laser power densities as low as 2 mw in a 4 mil-diameter beam. Since then much attention has been focussed on this aspect of $LiNbO_3$ and papers continue to be published regarding the mechanisms and the extent of damage in pure and doped $LiNbO_3$.

The refractive index damage is permanent at room temperature but above 170°C it relaxes faster than it is generated. Above 250°C the index damage does not arise at all. Levinstein et al.[69] reported that the index inhomogeneity was minimised by field annealing at 250 V/cm at 700°C with gold electrodes. For use in nonlinear optical applications, the temperature of phase-matching was raised above the index damage anneal temperature by the use of Li-rich melts for growth but this led to large spatial variation of birefringence and very short phase-matchable lengths. The problem was satisfactorily overcome by MgO doping to congruent melts, resulting in very homogeneous crystals with high phase-matching temperatures. This was

discussed earlier in Section II.1.2.4.

The study of Chen[70] strongly supported the theory that the refractive index is modulated via the electro-optic effect by a space charge field produced by the redistribution of electrons among traps after excitation by light. The origin of these traps was believed to arise from defects associated with non-stoichiometry but other sources were looked for because the optical damage was found to occur in crystals of stoichiometric composition also. Peterson et al.[71], for the first time through EPR studies identified iron impurities present in 10 ppm level in pure $LiNbO_3$ crystals as the origin of laser radiation damage. Intentional doping of $\simeq$ 500 ppm Fe_2O_3 to the $LiNbO_3$ melt resulted in a hundred-fold increase in the laser induced index change. Not only the Fe impurity content but the valence state of the impurity also was found to have a strong influence on the extent of damage. Engelmann and Gouser[72] confirmed that Fe^{3+} ions acted as traps under UV irradiation and Fe^{2+} ions as sources of photoelectrons under visible radiation through Mossbauer spectroscopy studies. Vladimirstev et al.[73] evaluated the optimum parameters of Fe doped $LiNbO_3$ crystals for obtaining the highest optical damage sensitivity to be 25-35% Fe^{2+} concentration at a total iron concentration of 0.06 and 0.08 at %. Annealing treatments in oxidising and reducing atmospheres altered the ratio of the Fe^{2+} and Fe^{3+} ions and thus altered the extent of optical damage. The photorefractive sensitivity dependence on the ratio

Fe^{2+}/Fe^{3+} was established[74] to be due to the migration of electrons from Fe^{+2} ions in the illuminated zone to empty traps (Fe^{+3} ions) by measurements of Fe^{3+} ion concentration through ESR studies before and after laser illumination. Before illumination the Fe^{3+} ions were distributed uniformly throughout the sample but after illumination the number of the Fe^{2+} ions in the illuminated zone increased by over 30%.

Other transition element impurities like Mn, Cu have also been found to enhance the photorefractive sensitivity considerably though not to the same extent as for Fe doping, while other elements like Cr, Co, Ni were not effective due to weak ion-lattice interactions in $LiNbO_3$. Optical absorption spectra have been obtained for all transition metal ion dopings in $LiNbO_3$ but there still exists some controversy about the preference of site of these ions in the $LiNbO_3$ lattice.

As was indicated briefly earlier, optical damage in $LiNbO_3$ is presently believed to arise from photo-excited electrons, from such substitutional donor impurity centers like iron, which are redistributed among electron-traps in the lattice. This causes a macroscopic charge separation, verified through detection of electrostatic potentials[75], which modulates the refractive index of the crystal via the Pockels linear electro-optic effect. Several mechanisms have been proposed and confirmed experimentally for different conditions of the $LiNbO_3$ crystal, for this electron redistribution.

Chen[70] first accounted for the photorefractive process in $LiNbO_3$ by attributing it to the presence of internal fields like a net spontaneous polarisation field within the crystal. Glass et al.[76] reported that a bulk photovoltaic effect with saturation voltages of the order of 10^5 V/cm is responsible for the photocurrents in $LiNbO_3$ crystals doped with Fe and Cu impurities. Amodei[77] proposed a diffusion mechanism, which can generate strong electric fields sufficient to cause significant refractive index changes of the order of 10^{-4} in $LiNbO_3$. Belabaev et al.[78] made a study of the influence of chemical reduction of $LiNbO_3$ crystals, pure and doped, on the mechanisms responsible for the photorefractive effect. Their results indicated that the photovoltaic effect is predominant in the case of doped unreduced samples while diffusion fields ($\sim$1600 V/cm) take over in the case of reduced samples of very light doping or no doping. Belinicher et al.[79] reported that a change in the sample temperature of a few degrees resulted in internal electric fields of the order of 10^4 V/cm due to the pyroelectric effect in undoped $LiNbO_3$ crystals. Schein and Cressman[80] subsequently confirmed the effect of pyroelectric fields produced by the heating of the sample in the vicinity of the laser beam, in causing optically induced refractive index changes. The most widely held opinion is that a 'volume photovoltaic effect' is primarily responsible for optical damage in $LiNbO_3$ containing an iron impurity[79,81]. A large number of papers have appeared on the photovoltaic effect-induced

photorefractivity in $LiNbO_3$ doped with iron impurity. von der Linde et al.[82], for the first time, obtained large index variations in high purity undoped $LiNbO_3$ with high intensity laser pulses at a second harmonic wavelength of 0.53μm, thereby revealing a nonlinear mechanism for the modulation of the refractive index. The effect was attributed to a multi-photon absorption, which obviates the need for impurities for the excitation process. Levanyuk and Osipov[83] have given a detailed critical discussion with a theoretical treatment for the different mechanisms responsible for the photorefractive effect in ferroelectric crystals.

As mentioned at the outset of this section, the photorefractive effect is sought to be enhanced, mainly for applications like the development of volume holographic storage devices, phase light correctors and effective volume phase diffraction gratings for use in tunable lasers. The effect has to be suppressed for the development of electro-optic and opto-accustic modulators with improved radiation resistance and for efficient devices for synthesising optical frequencies. Attempts to decrease optical damage in $LiNbO_3$ have been made through crystal purification and by control of impurity valence. Holman et al.[84] developed a new chemical process to improve the optical damage resistance in $LiNbO_3$ crystals through increasing the non-stoichiometry by crucible-out-diffusion technique involving Li_2O transport. The reduced optical damage susceptibility could be due to an increase in charge trapping defects or due to a direct

decrease in the photogenerated carrier density by the altering of the $LiNbO_3$ band structure or the ionisation energy of the crystalline impurities.

In 1977, Ohmori et al.[85] reported a local charge in the refractive index of $LiNbO_3$ by X-ray irradiation. The index damage could be easily erased by a uniform illumination of UV light, thus allowing it to be infra-red that the index change due to X-ray irradiation is not the radiation damage due to lattice disorder or defects but the same phenomenon as the laser induced optical damage. But there was no significant difference in the extent of optical damage between pure $LiNbO_3$ and Fe doped $LiNbO_3$ for the same dosage of X-ray irradiation unlike the laser induced damage which is much more severe for Fe doped $LiNbO_3$ compared to undoped $LiNbO_3$. The results are shown in Figure II.19, with CuK_α line acting as the X-ray source.

Apart from index changes, laser irradiation is reported to cause structural changes in the $LiNbO_3$ lattice. Ohnishi[86] first observed lattice strains in Fe-doped $LiNbO_3$ by X-ray topography, by subjecting the samples to an inhomogeneous light illumination from a Xe arc lamp (140 mW/cm^2) and an Ar laser (0.51μm of 75 mW/cm^2 power). The X-ray topographs revealed a strain image whose intensity increased exponentially with the exposure time(from 30 secs. to 1 hr.) upto a saturation value. The strain could be erased by a 10-minutes anneal at 186°C. Abranov et al.[87] reported changes in the structural parameters accompanying

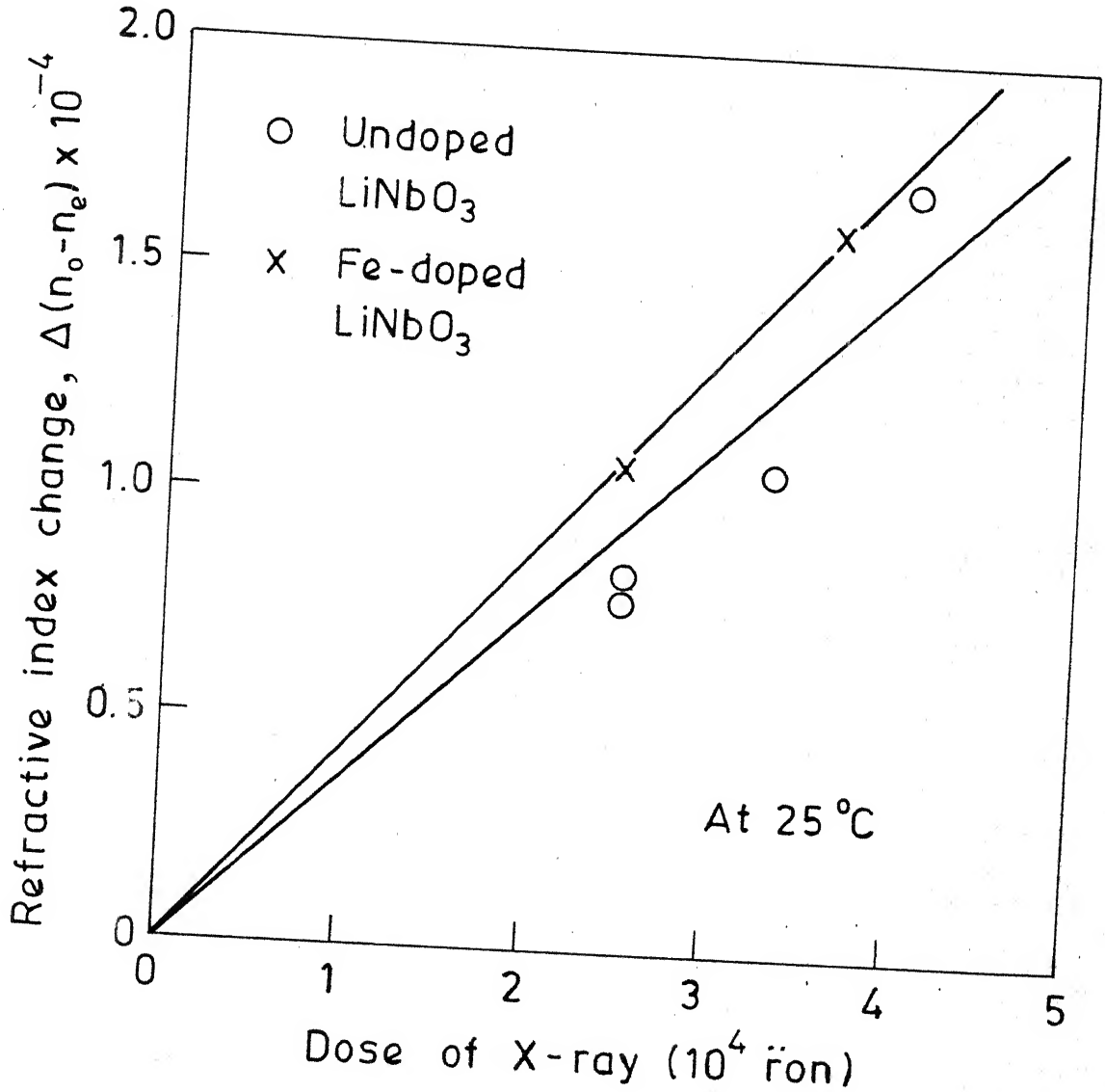

ig. II.19. X-ray induced index change in pure and Fe-doped $LiNbO_3$. X-ray source is Cu-$k\alpha$ line. (Ref. 85)

the photorefraction effect in Fe-doped $LiNbO_3$. The structural changes were revealed by a change of crystal lattice parameters and a broadening of the diffraction maxima. Kudryavtseva et al.[88] conducted a study of the damage in microdefect-free $LiNbO_3$ crystals subjected to pulsed laser irradiation at 1.06μ wavelength and discovered a strong dependence of the damage threshold on the direction of laser irradiation and on its polarisation. The damage was defined as microscopically observable changes in the mechanical continuity of the interior of the sample. This anisotropy of the optical strength of $LiNbO_3$ was found to be due to the second harmonic excitation.

II.1.3.5. Electro-optic Properties:

The electro-optic effect in $LiNbO_3$ was first detected by Peterson et al.[89] Due to the lack of inversion symmetry in the structure, $LiNbO_3$ exhibits a large LEO effect. Because of the symmetry of point group 3 m, to which $LiNbO_3$ belongs, only four coefficients are required to describe the electro-optic behaviour of the crystal. These are, namely, r_{13}, r_{22}, r_{42} and r_{33}.

The d.c. electro-optic coefficients r_{ij}^T, corresponding to a free crystal, have been measured at 0.6328 μ by a number of workers, e.g. Bernal et al.,[91] Lenzo et al.[91] and Iwasaki et al.[92] Smakula and Clasby[93] reported the values of r_{22}^T at different wavelengths. Hulme et al.[94] investigated the signs of the electro-optic coefficients for $LiNbO_3$. Zook et al.[5] studied the temperature dependence of the r_{ij}^T coefficients at 0.6328 μ and proposed a model for the electro-optic effect in $LiNbO_3$. Turner et al.[96] investigated the composition dependence of the r_{ij}^T coefficients in $LiNbO_3$ and showed that the values of the electro-optic coefficients remained unaltered by changes in the melt composition of $LiNbO_3$. The last measurements of the r_{ij}^T coefficients were reported in 1972 by Onuki et al.[97] The high frequency clamped coefficients r_{ij}^S were measured by Turner et al.[98] at 0.6328 μ and 3.39 μ at room temperature. The values of the electro-optic coefficients are given in Table II.3A.[99] From the above table, it is seen that:

TABLE II.3A. Electro-optic Coefficients of Lithium Niobate (in 10^{-12} m/V)

Constant stress (T) Constant strain (S)	r_{13}	r_{22}	r_{42}	r_{33}	λ in μ	T°C	Reference
T		6.7			0.6328	R.T	(91)
T		6.7			0.6328	R.T	(93)
T			32±2		0.6328	R.T	(90)
T	+9.6	+6.6	+32.8	+30.8	0.6328		(94)
T	10.9			34.0	0.6328		(97)
T	+10.0	6.81		+32.2	0.6328	100°C	(95)
T		-6.4			0.6328	R.T	(92)
T		5.4			1.15	R.T	(93)
T		3.1			3.39	R.T	(93)
S	6.5	3.1	23.0	28.0	3.39	R.T	(96)
S	8.6	3.4	28.0	30.8	0.6328	R.T	(96)

(i) There is very good consistency in the values reported by different workers at a particular wavelength,

(ii) The values for the high-frequency clamped coefficients are somewhat lower compared to the values of the 'free' coefficients, and

(iii) There is a decrease in the values of the electro-optic coefficients for higher wavelengths.

Kaminow and Johnston[100] provided a new insight into the electro-optic behaviour of $LiNbO_3$ by correlating the radio-frequency clamped electro-optic coefficient with the corresponding Raman-scattering efficiencies. They reported that the maximum contribution to the electro-optic coefficients r_{33} and r_{13} came from the lowest-frequency optic A_1 mode and to r_{42} and r_{22} from the next lowest E mode, with only a small pure electronic contribution. Wemple and Di Domenico[101] made an important contribution to the understanding of the electro-optic effect in $LiNbO_3$ by showing that the LEO effect can be interpreted as a basically quadratic effect biased by the spontaneous polarisation.

Figure II.19A[92] represents the temperature dependence of r_{22}^T measured at four different wavelengths. The sign of r_{22}^T was determined as negative because the authors so defined the positive y direction in order to keep the piezoelectric constant d_{22} positive. The modulus of r_{22}^T is seen to exhibit a dispersion increasing with decreasing wavelength and increasing temperature. Figure II.19B[95] shows the

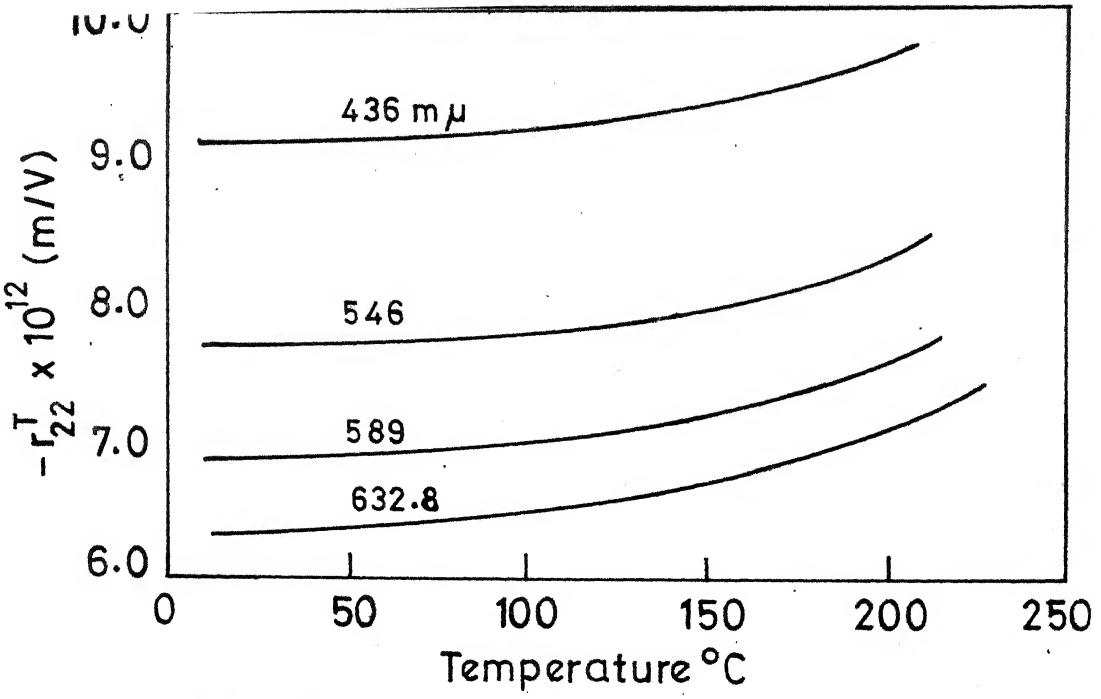

Fig.II.19A r_{22}^{T} vs temperature in $LiNbO_3$ at different wavelengths (Ref.92)

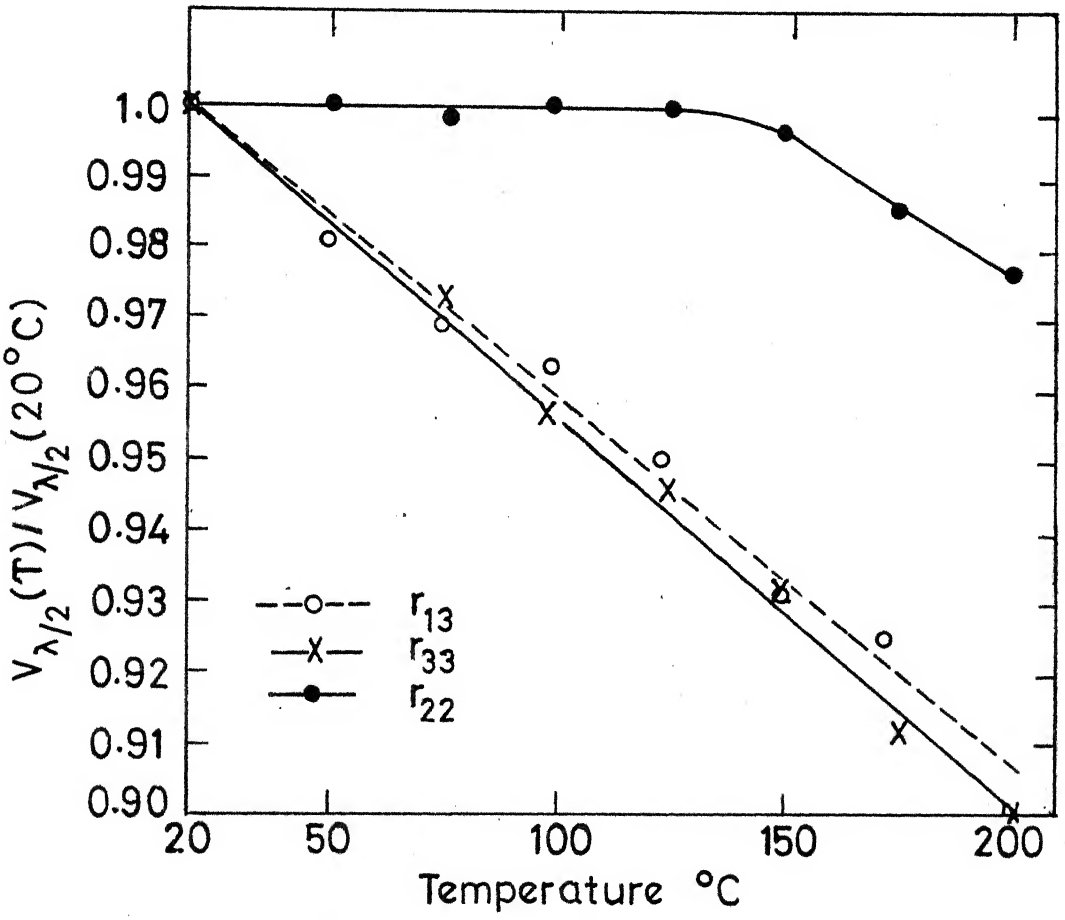

Fig.II.19B. Temperature variation of $V_{\lambda/2}$ corresponding to r_{13}, r_{22} and r_{33} coeffcients in $LiNbO_3$ (Ref.95)

temperature dependence of the half-wave voltage normalised with respect to the room temperature value of half-wave voltage, corresponding to the measurement of r_{13}, r_{22} and r_{33} coefficients in $LiNbO_3$. While the half-wave voltage values for the modes corresponding to r_{13} and r_{33} show a linear decrease with temperature rise, with approximately a 10% reduction between R.T. and 200°C, the temperature dependence of $V_{\lambda/2}$ for the r_{22} coefficient is unusual and has been discussed by the authors.

II.2. Experimental Details:

II.2.1. Description of the Crystal Pulling Apparatus:

A refractory brick furnace (20" in diameter and 20" in height) was fabricated and six globar heating elements were employed. The furnace could reach a temperature of 1300°C in about 8 hours. A power input of 3 kW required to hold it at that temperature. The furnace was coupled with a Honeywell proportional controller with which the heating rate, holding time and the cooling rate of the furnace can be preset and controlled. A Pt-Pt-10%-Rh thermocouple was used as the temperature sensor in the middle portion of the furnace and this is connected to the temperature controller.

The schematic of the crystal pulling apparatus along with the furnace is shown in the Figure (II.20). A Pt-10% Rh pull rod of 8 mm diameter and 8" long with a seed holder of 13 mm diameter at the bottom is connected to a stainless steel rod. This is in turn attached to an aluminum rod over which an aluminium stepped pulley is mounted. This is connected by a suitable O-ring to another stepped pulley fitted on to the shaft of a d.c. motor (30 rpm). The rotation speed of the seed holder can be adjusted by changing the position of the O-ring. The motor is mounted on a movable platform in the vertical direction by a suitable arrangement. The seed rod is passed into the furnace through a hole in the brick plug covering the opening at the top of the furnace. The crucible with the charge material is introduced into the

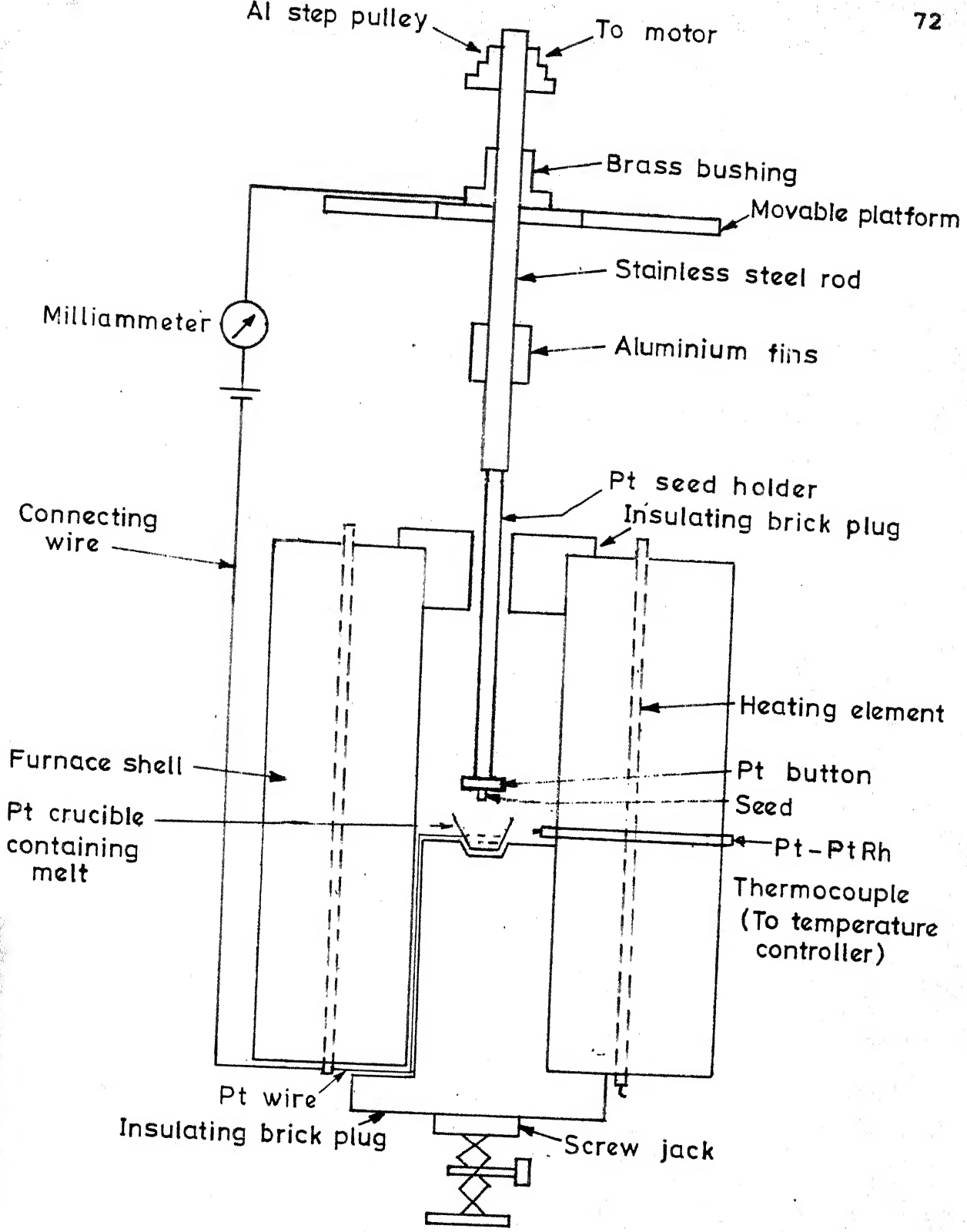

FIG. II.20 Schematic of the crystal growth setup for growing $LiNbO_3$ single crystal

furnace through the bottom hole. The platinum crucible is placed inside an alumina crucible filled with alumina powder, so that the crucible is not deformed because of the large pressures applied to the crucible wall when the melt solidifies during cooling.

When the charge material is melted thoroughly and then held just above the melting temperature, the platinum seed-holder with the seed is lowered inside the furnace. The alignment of the crucible with the seed-holder is previously set ready. The seed-holder is lowered till the seed makes contact with the melt. This contact is detected by passing a few mA battery current through the seed-rod, on to the charge crucible via the melt which is conducting at that temperature. When the seed makes contact with the melt, the electrical circuit is closed and is indicated by the deflection in the milli ammeter connected in the circuit.

II.2.2. Preparation of the Charge Material:

The starting compounds are separately dried overnight in an oven at 150 to 200°C. Appropriate amounts of the starting compounds viz. Li_2CO_3 (99.9% pure) and Nb_2O_5 (99.95% pure) are taken and carefully weighed in the ratio of the congruent composition (48.6 mole % Li_2O). For a typical batch, the amounts of the starting compounds taken were 18 gms of Li_2CO_3 and 68 gms of Nb_2O_5 to give the congruent composition of $LiNbO_3$. Thorough mixing is achieved in a medium of acetone. $LiNbO_3$ is prepared by calcining this

mixture through the reaction given by equation (II.4). Calcination is done in a platinum crucible and the heating procedure for the calcination is as follows. A temperature of 600° C is reached in 3 hours and then it is raised to 850° C in 6 hours where it is held for 4 hours. Then the calcined product is cooled to room temperature slowly and subsequently powdered.

X-ray diffraction data were taken on the calcined material. The interplanar spacings ('d' values) are compared with the standard 'd' spacings values obtained from a computer program obtained with the lattice parameters a_H and c_H of the hexagonal cell. The experimental 'd' values agree very well with the standard values indicating a complete reaction delivering the homogeneous compound of $LiNbO_3$. Table II.4 shows a comparison of the experimental 'd' values with the calculated 'd' values, along with the intensity ratio.

II.2.3. Crystal Growth:

The charge material is taken in a 100 cc platinum crucible. Below the crucible is placed a platinum foil to which a platinum wire is connected and taken out of the furnace. This is for the purpose of checking the seed contact with the melt. Initially to determine the melting point of the $LiNbO_3$ charge prepared in the laboratory, the seed holder is kept within the charge and heating is commenced. When the charge is melted, the meter shows a deflection since the melt is conducting the battery current. The melting point determined by this method is 1270° C and the value quoted in literature[1]

Table II.4. X-ray Diffraction Data for Calcined $LiNbO_3$

hk.l	d_{cal} (Å)	d_{obs} (Å)	Relative intensity I/I_o
01.2	3.7498	3.7666	100.0
10.4	2.7363	2.7444	68.8
11.0	2.5741	2.5829	47.8
00.6	2.3105	2.3132	9.4
11.3	2.2488	2.2521	22.5
20.3	2.1222	2.1281	37.7
02.4	1.8749	1.8768	59.7
11.6	1.7195	1.7172	87.0
12.2	1.6375	1.6385	58.9
01.8	1.6152	1.6140	30.0
21.4	1.5755	1.5154	58.0
30.0	1.4862	1.4869	36.2
20.8	1.3682	1.3668	16.9
-	1.3218	1.3200	15.4
30.6	1.2499	1.2483	18.1
31.2	1.2174	1.2174	28.3
12.8	1.2081	1.2071	30.2
13.4	1.1647	1.1647	13.5
03.9	1.0695	1.0681	15.7

* The calculated d values are obtained from a computer program for the hexagonal cell with $a_H = 5.1483$ Å and $c_H = 13.8631$ Å using the formula

$$d = \left[\frac{4(h^2 + hk + l^2)}{3a^2} + \frac{l^2}{c^2} \right]^{-1/2}$$

is 1265° C. Then the seed rod is lifted out of the melt and the melt was cooled to room temperature.

The solidified melt provides good seed crystals. It was observed that the volume reduction of $LiNbO_3$ charge material on melting, was about two-thirds of the initial volume in the crucible.

Once the melting point is thus ascertained, for the subsequent growth runs, the seed holder is kept 6" above the crucible level. The seed crystal is tied to the seed-holder with a platinum wire. Now the furnace heating is started and in 8 hours the melting temperature is reached. After holding the temperature at 10° C above the melting point for half an hour to ensure complete melting and homogenisation, the temperature is brought down to 1270° C and stabilised there. Now the seed holder is lowered inside the furnace slowly and the contact is made with the melt as indicated by the deflection in the milliammeter. The rotation of the seed is now started. Then the crystal is pulled from the melt at a rate of 1 mm/hr. The rotation rate employed is 4-6 rpm. After pulling for 6 hours, the crystal grown is raised a few inches and then the furnace temperature is reduced at the rate of 60° C/hr till a temperature of 900° C is attained. Now the power to furnace is cut off and the crystal and the crucible are allowed to cool to room temperature.

At this stage, it may be mentioned that the entire growth cycle had to be completed within 18 hours because of stringent power situation during the period of these

investigations. Thus the heating cycle upto the melting temperature were carried out in 8 hours and growth was limited to 6 hours. The remaining period of 4 hours is for slow cooling of the crystal at the rate of 60°C/hr so as to avoid any thermal shock to the crystal.

Thus the entire study of $LiNbO_3$ was constrained by power limitations and hence intensive trials to improve the size and quality of the crystals were not feasible.

II.3. Results and Discussion:

A crystal pulling apparatus with a resistance heating furnace was set up for growing crystals of $LiNbO_3$. The furnace was chosen to be massive to enable the after-growth cooling to proceed at a slow rate when the power to furnace is shut off as the temperature reaches 900°C.

The size of the crystal that could be grown from the growth runs conducted with the crystal pulling set up used in the present work was of 10 x 10 x 5 mm dimensions. The transparency of the crystal obtained varied from region to region. Hence it was not possible to carry out the optical experiments on these crystals for electro-optic investigations.

The difficulties encountered in the growth of $LiNbO_3$ crystals from the crystal pulling apparatus set up in the present work are analysed below, with some possible solutions for overcoming them.

(i) The design of the furnace should be such that a sharp temperature gradient is maintained at the seed-melt

interface. In our experimental set-up this gradient was sought to be attained by appropriate positioning of the melt crucible in the furnace, exploiting the temperature profile existing along the length of the furnace. It is considered advisable if the temperature gradient required at the melt-seed interface is obtained by splitting the furnace into two zones; the lower zone covering the crucible kept at the melting point while the upper zone is maintained at a considerably lower temperature. This arrangement would also provide for a convenient after-growth cooling procedure which is necessary to prevent the cracking of the crystal due to thermal shock. It is also felt that an incorporation of seed-cooling arrangement during growth would give a very stable temperature gradient near the seed-melt interface and thus would improve the system to produce better crystals.

(ii) The facility to view the crystal during growth will greatly help to monitor the growth of the crystal. The lack of such an arrangement in our experimental set-up constituted a severe handicap.

(iii) It also looks worthwhile to arrange for crucible rotation during crystal pulling so that a flat melt interface can be ensured.

(iv) The quality of the crystals grown can be considerably enhanced by using a sealed furnace where provision for an oxidising atmosphere is possible.

REFERENCES

(1) A. Raüber, 'Chemistry and Physics of Lithium Niobate', Current Topics in Materials Science, ed. E. Kaldis, Vol. 1, 481-601, North-Holland, 1978.

(2) J.T. Milek and M. Neuberger, Linear electro-optic modulator materials - Handbook of Electronic Materials, Vol. 8, IFI/Plenum (USA) 1972.

(3) B.T. Matthias and J.P. Remeika, Ferroelectricity in the ilmenite structure, Phys. Rev. 76 (1949) 1886.

(4) A.A. Ballman, Growth of piezoelectric and ferroelectric materials by the Czochralski technique, J. Am. Ceram. Soc. 48 (1965) 112.

(5) W.H. Zachariasen, Skr. Norske Vid.-Ada., Oslo, Mat. Naturv., No. 4 (1928).

(6) P. Bailey, Ph.D. Thesis, Bristal (1952) cited by H.D. Megaw, Acta Cryst. 7 (1954) 187.

(7) H.D. Megaw, Ferroelectricity and crystal structure, Acta Cryst. 7 (1954) 187.

(8) S.C. Abrahams, J.M. Reddy and J.L. Bernstein, Ferroelectric lithium niobate. 3. Single crystal X-ray diffraction study at 24°C, J. Phys. Chem. Solids 27 (1966) 97.

(9) S.C. Abrahams, W.C. Hamilton and J.M. Reddy, Ferroelectric lithium niobate. 4. Single crystal neutron diffraction study at 24°C, J. Phys. Chem. Solids 27 (1966) 1013.

(10) S.C. Abrahams, H.J. Levinstein and J.M. Reddy, Ferroelectric lithium niobate. 5. Polycrystal X-ray diffraction study between 24° and 1200°C, J. Phys. Chem. Solids 27 (1966) 1019.

(11) A. Reisman and F. Holtzberg, Heterogeneous equilibria in the systems Li_2O-, Ag_2O-Nb_2O_3 and oxide models, J. Am. Chem. Soc. 80 (1958) 6503.

(12) P. Lesner, C. Legras and J.P. Dumas, (in French), J. Crystal Growth, 3/4 (1968) 231.

(13) G.E. Peterson and J.R. Carruthers, ^{93}Nb NMR as a sensitive and accurate probe of stoichiometry in $LiNbO_3$ crystals, J. Solid State Chem., 1 (1969) 98.

(14) K. Chow, H.G. McKnight and L.R. Rothrock, The congruently melting composition of $LiNbO_3$, Mats. Res. Bull., 9 (1974) 1067.

(15) L.D. Svassand, M. Eriksrud, A.P. Grande and F. Mo, Crystal growth and properties of $LiNb_3O_8$, J. Crystal Growth, 18 (1973) 179.

(16) L.O. Svassand, M. Eriksrud, G. Nakken and A.P. Grande, Solid solution range of $LiNbO_3$, J. Crystal Growth, 22 (1974) 230.

(17) J.R. Carruthers, G.E. Peterson, M. Grasso and P.M. Bridenbaugh, Non-stoichiometry and crystal growth of lithium niobate, J. Appl. Phys., 42 (1971) 1846.

(18) R.L. Byer, J.F. Young and R.S. Feigelson, Growth of high-quality $LiNbO_3$ crystals from the congruent melt, J. Appl. Phys., 41 (1970) 2320.

(19) H. Fay, W.J. Alford and H.M. Dess, Dependence of second-harmonic phase-matching temperature in $LiNbO_3$ crystals on melt composition, Appl. Phys. Letters, 12 (1968) 89.

(20) K. Nassau and M.E. Lines, Stocking fault model for stoichiometry deviations in $LiNbO_3$ and $LiTaO_3$ and the effect on the Curie temperature, J. Appl. Phys., 41 (1970) 533.

(21) A.M. Glass, G.E. Peterson and T.J. Negran, in: Laser induced damage in optic materials, Ntl. Bur. Std. Special Publication No. 372, ed. A.J. Glass (U.S. GPO, Washington D.C., 1972).

(22) A.A. Blistanov, E.V. Makarevskaya, V.V. Geras'kin, O. Kamalov and M.M. Koblova, Influence of impurities on the optical quality and electrical conductivity of $LiNbO_3$, Sov. Phys. Solid State, 20 (1978) 1489.

(23) J.J. Amodei, W. Phillips and D.L. Staebler, Improved electro-optic materials for holographic storage applications, IEEE J. Quantum Electr. QE-7 (1971) 321.

(24) P.M. Bridenbaugh, Factors affecting the growth of $LiNbO_3$ useful for nonlinear optical applications, J. Crystal Growth, 19 (1973) 45.

(25) R.V. Schmidt and I.P. Kaminow, Metal-diffused optical waveguides in $LiNbO_3$, Appl. Phys. Lett., 25 (1974) 458.

(26) G.D. Boyd, R.V. Schmidt, F.G. Storz, Chemistry of metal-diffused $LiNbO_3$ for acoustic devices, J. Appl. Phys., 48 (1977) 2880.

(27) S.A. Fedulov, Z.I. Shapiro and P.B. Ladyzhinskii, The growth of crystals of $LiNbO_3$, $LiTaO_3$ and $NaNbO_3$ by the Czochralski method, Sov. Phys.-Crystallogr., 10 (1965) 218.

(28) G.A. Smolanskii, N.N. Krainik, N.P. Khuchna, V.V. Zholanova and I.E. Mylnikova, The Curie temperature of $LiNbO_3$, Phys. Stat. Sol., 13 (1966) 309.

(29) S. Kondo, S. Miyazawa, S. Fushimi and K. Sugii, Liquid-phase-epitaxial growth of single-crystal $LiNbO_3$ thin film, Appl. Phys. Lett., 26 (1975) 489.

(30) A.A. Ballman, H. Brown, P.K. Tien and S. Riva-Sanseverino The growth of $LiNbO_3$ thin films by liquid phase epitaxial techniques, J. Crystal Growth, 29 (1975) 289.

(31) V.J. Voronkova, N.F. Evlanova, V.K. Yanovskii, Crystallisation of $LiNbO_3$ from solution in borate, vanadate and tungstate melts, Sov. Phys. Crystallogr., 23 (1978) 129.

(32) E.D. Kolb and R.A. Laudise, The phase diagram LiOH-Ta_2O_5-H_2O and the hydrothermal synthesis of $LiTaO_3$ and $LiNbO_3$, J. Crystal Growth, 33 (1976) 145.

(33) Hill and Zimmermann, The hydrothermal synthesis of single domain $LiNbO_3$ crystals by transport reactions, J. Electrochem. Soc., 115 (1968) 978

(34) J.C. Brice, Cracking of Czochralski grown crystals, J. Crystal Growth, 42 (1977) 427.

(35) R.L. Byer, R.L. Herbst, R.S. Feigelson and W.L. Kway, Growth and application of (01.4) $LiNbO_3$, Optics Comm., 12 (1974) 427.

(36) G. Zydzik, The growth of $LiNbO_3$ crystals using an automated puller, Mats. Res. Bull., 10 (1975) 9.

(37) T. Fukuda and H. Hirano, Growth and characteristics of $LiNbO_3$ plate crystals, Mats. Res. Bull., 10 (1975) 801.

(38) K. Nassau, H.J. Levinstein and G.M. Loiacono, The domain structure and etching of ferroelectric lithium niobate, Appl. Phys. Lett., 6 (1965) 228.

(39) K. Nassau, H.J. Levinstein and G.M. Loiacono, Ferroelectric lithium niobate 2. Preparation of single domain crystals, J. Phys. Chem. Solids, 27 (1966) 989.

(40) M. Tasson, H. Legal, J.C. Gay, J.C. Peuzin and F.C. Lissalde, Piezoelectric study of poling mechanism in lithium niobate crystals at temperature close to the Curie point, Ferroelectrics, 13 (1976) 479.

(41) A. Ashkin, G.D. Boyd, J.M. Dziedzic, R.G. Smith, A.A. Ballman, J.J. Lovinstein and K. Nassau, Optically induced refractive index inhomogeneities in $LiNbO_3$ and $LiTaO_3$, Appl. Phys. Lett., 9 (1966) 72.

(42) J.E. Midwinlar, Lithium niobate: Effects of composition on the refractive indices and optical second-harmonic generation, J. Appl. Phys., 39 (1968) 3033.

(43) P.M. Bridenbaugh, J.R. Carruthers, J.M. Dziedzic and F.R. Nash, Spatially uniform and alterable SHG phase-matching temperature in lithium niobate, Appl. Phys. Lett., 17 (1970) 104.

(44) A. Rauber, Doping modulation by electric currents in lithium niobate during crystal growth, Mats. Res. Bull., 11 (1976) 497.

(45) L.M. Guseva, V.P. Klyuev, I.S. Rez, S.A. Sedulov, A.P. Lyubimov and Z.I. Tatarov, Investigation of some of the optical characteristics of ferroelectric lithium Niobate, Bull. Acad. of Sci. USSR, Phys. Ser., 31 (1967)

(46) G.D. Boyd, R.C. Miller, K. Nassau, W.L. Bond and A. Savage, $LiNbO_3$: An efficient phase matchable non-linear optical material, Appl. Phys. Lett., 5 (1964) 234.

(47) G.D. Boyd, W.L. Bond and H.L. Carter, Refractive index as a function of temperature in $LiNbO_3$, J. Appl. Phys., 38 (1967) 1941.

(48) A.S. Barker and R. Loudon, Dielectric properties and optical phonons in $LiNbO_3$, Phys. Rev., 158 (1967) 433.

(49) D.R. Bosomworth, Far infra red optical properties of $LiNbO_3$, Appl. Phys. Lett., 9 (1966) 330.

(50) H. Iwasaki, H. Toyoda and N. Niczeki, Dispersion of the refractive indices of $LiNbO_3$ crystals between 20° C and 900° C. Japan J. Appl. Phys., 6 (1967) 1101.

(51) R.C. Miller and A. Savage, Temperature dependence of the optical properties of ferroelectric $LiNbO_3$ and $LiTaO_3$, Appl. Phys. Lett., 9 (1966) 169.

(52) M.V. Hobden and J. Warner, The temperature dependence of the refractive indices of pure lithium niobate, Phys. Lett., 22 (1966) 243.

(53) J. Warner, D.S. Robertson and K.F. Hulme, The temperature dependence of optical birefringence in lithium niobate, Phys. Lett., 20 (1966) 163.

(54) E.A. Vinogradov, N.A. Prisova and G.V. Kozlov, Electro-optic effect in $LiNbO_3$ in the millimeter range, Sov. Phys. Sol. State, 12 (1970) 605.

(55) N.A. Irisova and G.V. Kozlov, Birefringence of certain crystals in the millimeter wavelength range, Sov. Phys. Crystall., 15 (1971) 941.

(56) K. Vedam and T.A. Davis, Piezo- and thermo-optic behavior of $LiNbO_3$, Appl. Phys. Lett., 12 (1968) 138.

(57) K. Vedam and S. Ramaseshan, Progress in crystal physics. ed. R.S. Krishnan (Interscience Publishers, Inc., New York), 1960, p. 102.

(58) R.W. Dixon and M.G. Cohen, A new technique for measuring magnitudes of photoelastic tensors and its application to lithium niobate, Appl. Phys. Lett., 8 (1966) 205.

(59) D.F. Nelson and R.M. Mikulyak, Refractive indices of congruently melting lithium niobate, J. Appl. Phys., 45 (1974) 3688.

(60) J.G. Bergman, A. Ashkin, A.A. Ballman, J.M. Dziedzic, H.J. Lavinskin and R.G. Smith, Curie temperature, birefringence and phase matching temperature variations in $LiNbO_3$ as a function of melt stoichiometry, Appl. Phys. Lett., 12 (1968) 92.

(61) J.E. Midwinter, Assessment of lithium meta-niobate for nonlinear optics, Appl. Phys. Lett., 11 (1967) 128.

(62) R.C. Miller, G.D. Boyd and A. Savage, Nonlinear optical interactions in $LiNbO_3$ without double refraction, Appl. Phys. Lett., 6 (1965) 77.

(63) F.R. Nash, G.D. Boyd, M. Sargent III and P.M. Bridenbaugh, Effect of optical inhomogeneities on phase matching in nonlinear crystals, J. Appl. Phys., 41 (1970) 2564.

(64) R.G. Smith, Effects of index inhomogeneities on optical second harmonic generation, J. Appl. Phys., 41 (1970) 3014.

(65) R.C. Miller, W.A. Nordland and P.M. Bridenbaugh, Dependence of second-harmonic generation coefficient of $LiNbO_3$ on melt composition, J. Appl. Phys., 42 (1971) 4145.

(66) J.E. Bjorkholm, Relative signs of the optical nonlinear coefficients d_{31} and d_{22} in $LiNbO_3$, Appl. Phys. Lett., 13 (1968) 36.

(67) R.C. Miller and W.A. Nordland, Relative signs of nonlinear optical coefficients of polar crystals, Appl. Phys. Lett., 16 (1970) 174.

(68) M.M. Choy and R.L. Byer, Accurate second-order susceptibility measurements of visible and infra red nonlinear crystals, Phys. Rev., B14 (1976) 1693.

(69) H.J. Levinstein, A.A. Ballman, R.T. Denton, A.Ashkin and J.M. Dziedzic, Reduction of the susceptibility of optically induced index inhomogeneities in $LiTaO_3$ and $LiNbO_3$, J. Appl. Phys., 38 (1967) 3101.

(70) F.S. Chen, Optically induced change of refractive indices in $LiNbO_3$ and $LiTaO_3$, J. Appl. Phys., 40 (1969) 3389.

(71) O.E. Peterson, A.M. Glass and T.J. Negran, Control of the susceptibility of lithium niobate to laser-induced refractive index changes, Appl. Phys. Lett., 19 (1971) 130.

(72) H. Engelmann and U. Gouser, Fe-doped charge states after irrediation in $LiNbO_3$, Ferroelectrics, 23 (1980) 97.

(73) Y.V. Vladimirstev, V.A. Golenishchev-kutuzov, S.A. Migachev and N.A. Shamukov, Optical damage in transition metal doped ferroelectrics, Ferroelectrics, 22 (1978) 653.

(74) Y.V. Vladinuistev, V.A. Golenischev-kutuzov, S.A. Migachev and N.A. Shamukov, Characteristics of optically induced changes in the refractive index of $LiNbO_3$, Sov. Phys. Sol. State, 20 (1978) 1994.

(75) L.B. Schein, P.J. Cressman and F.M. Tesche, Electrostatic observation of laser-induced optical damage in $LiNbO_3$, J. Appl. Phys., 48 (1977) 4844.

(76) A.M. Glass, D. Von der Linde and T.J. Negran, High-voltage bulk photovoltaic effect and the photorefractive process in $LiNbO_3$, Appl. Phys. Lett., 25 (1974) 233.

(77) J.J. Amodei, RCA Rev., New Jersey, 32 (1971) 185.

(78) K.G. Belabaev, V.B. Markov and S.G. Odulov, Photovoltaic effect in reduced $LiNbO_3$ crystals, Sov. Phys. Sol. State, 20 (1978) 1458.

(79) V.I. Belincher, I.F. Kanaev, V.K. Malinovskii and B.I. Sturman, Mechanisms for the optical damage in $LiNbO_3$ crystals, Bull. Acad. Sci. USSR Phys. Ser., 41, No. 4 (1977) 67.

(80) L.B. Schein and P.J. Cressman, Pyroelectric induced optical damage in $LiNbO_3$, J. Appl. Phys., 49 (1978) 798.

(81) I.B. Barkan, S.I. Marennikov, E.V. Pestryakov and M.V. Entin, Laser-induced optical damage in Fe-doped $LiNbO_3$, Bull. Acad. Sci. USSR Phys. Ser., 41, No. 4 (1977) 82.

(82) D. Von der Linde, A.M. Glass and K.F. Rodgers, Multiphoton photorefractive processes for optical storage in $LiNbO_3$, Appl. Phys. Lett., 25 (1974) 155.

(83) A.P. Levanyuk and V.V. Osipov, Mechanisms for the photorefractive effect, Bull. Acad. Sci. USSR Phys. Ser., 41, No. 4 (1977) 83.

(84) R.L. Holman, P.J. Cressman, J.F. Revelli, Chemical control of optical damage in lithium niobate, Appl. Phys. Lett., 32 (1978) 280.

(85) Y. Ohmori, M. Yamaguchi, K. Yoshino and Y. Ininshi, Optical damage in $LiNbO_3$ induced by X-ray irradiation, Japan J. Appl. Phys., 16 (1977) 181.

(86) N. Ohnishi, Lattice strains induced in Fe-doped $LiNbO_3$ crystals by light, Japan J. Appl. Phys., 16 (1977) 1451.

(87) N.A. Abranov, V.V. Voronov and Yu. S. Kuzminov, Local photodeformation in crystals of $LiNbO_3$: Fe, Ferroelectrics, 22 (1978) 649.

(88) A.P. Kudryavtseva, A.A. Blistanov and V.A. Pashkov, Anisotropy of the optical strength of $LiNbO_3$ crystals, Sov. Phys. Sol. State, 20 (1978) 1457.

(89) G.E. Peterson, A.A. Ballman, P.V. Lenzo and P.M. Bridenbaugh, Electro-optic properties of $LiNbO_3$, Appl. Phys. Lett., 5 (1964) 62.

(90) E. Bernal, G.D. Chen and T.C. Lee, Low-frequency electro-optic and dielectric constants of $LiNbO_3$, Phys. Lett., 21 (1966) 259.

(91) P.V. Lenzo, E.G. Spencer and K. Nassau, Electro-optic coefficients in single-domain ferroelectric $LiNbO_3$, J. Opt. Soc. Am., 56 (1966) 633.

(92) H. Iwasaki, H. Toyoda, N. Niizeki and H. Kubota, Temperature and optical frequency dependence of the d.c. electro-optic constants r_{22}^T of $LiNbO_3$, Japan J. Appl. Phys., 6 (1967) 1419.

(93) P.H. Smakula and P.C. Clasby, The electro-optic effect in LiNbO3 and KTN, AIME Metall. Soc. Trans., 239 (1967) 421.

(94) K.F. Hulme, P.H. Davies and V.M. Cound, Signs of electro-optic coefficients for $LiNbO_3$, J. Phys. C, Ser. 2, 2 (1969) 855.

(95) J.D. Zook, D. Chen and G.N. Otto, Temperature dependence and model of the electro-optic effect in $LiNbO_3$, Appl. Phys. Lett., 11 (1967) 159.

(96) E.H. Turner, F.R. Nash and P.M. Bridenbaugh, Dependence of the linear electro-optic effect and dielectric constant on melt composition in $LiNbO_3$, J. Appl. Phys., 41 (1970) 3278.

(97) K. Onuki, N. Ochida and T. Saku, Interferrometric method for measuring electro-optic coefficients in crystals, J. Opt. Soc. Am., 62 (1972) 1030.

(98) E.H. Turner, High frequency electro-optic coefficients of $LiNbO_3$, Appl. Phys. Lett., 8 (1966) 303.

(99) Landolt-Bornstein Tables, Group III, 16, Springer-Verlag, N.Y. (1981).

(100) I.P. Kaminow and W.D. Johnston, Quantitative determination of sources of the electro-optic effect in $LiNbO_3$ and $LiTaO_3$, Phys. Rev., 160 (1967) 519.

(101) S.H. Wemple and M. Di Domenico, Oxygen-octahedra ferroelectrics. H. Electro-optical and non-linear optical device applications, J. Appl. Phys., 40 (1969) 735.

III. POTASSIUM DIHYDROGEN PHOSPHATE (KH_2PO_4)

III.1. Introduction and Literature Survey:

KH_2PO_4 (KDP) is one of the most widely known and extensively explored electro-optic crystals. Crystals of KDP are easily grown from an aqueous solution in large sizes. Extensive studies were made on KDP because of its attractive properties in piezoelectric and electro-optic applications. The major disadvantage with KDP is that it is hygroscopic which can pose problems of water on the exposed surface leading to arcing or high voltage breakdown. Above T_c (123°K) KDP belongs to the non-centrosymmetric $\bar{4}2$ m group of the tetragonal system and has two linear electro-optic constants r_{41} and r_{63}. It is transparent in the range 0.4 to 1.3 μ.

KDP and isomorphos are grown by slow cooling or slow evaporation of a saturated solution at a constant rate. The method is discussed in detail e.g. by Egli and Johnson[1] Ascoli and Droci[2] and host of other investigators. The size of the crystal grown can be increased by using large volume solution tanks. Any solution growth apparatus would mainly comprise of an accurate temperature control correct to about ±0.1°C and an arrangement for rotation of seed holder. The growth characteristics depend upon the growth parameters like pH, degree of supersaturation, impurity content and cooling rate. Close control of growth variables is essential to grow

strain-free crystals of high optical quality. The effect of pH is to influence the growth habit as well as the ease of growth. The degree of supersaturation influences not only the growth rate but also the habit and the quality of the crystals. Mullin et al.[3] made a thorough investigation on the crystal habit modification in KDP and ADP crystals due to the effect of the level of supersaturation, pH and the presence of foreign ions like Cr^{3+}, Fe^{3+} and Al^{3+}. They reported that low supersaturation at normal pH ($\sim$3.8) tended to give tapered crystals and at a higher pH ($\sim$5) the linear growth rates of both principal axes are considerably increased. The effect of additives like Cr^{3+}, Fe^{3+} and Al^{3+} in low concentrations ($\sim$ 50 ppm level) is reported to cause a tapering habit. Some of the most recent work includes the study of the influence of hydrodynamic environment on the growth of KDP crystals.[4] The crystals grown are usually cut with hacksaw or crystal cutting machines and are polished on wax-soaked clothes. In the present investigations a Metals Research cutter has been used for cutting the crystals of KDP. A fine cloth soaked in rouge and wax has been used as the polishing base.

KDP is a negative uniaxial crystal with the optic axis along the tetragonal Z-axis. Zernicke[5] has made extensive and accurate measurements for the two refractive indices of KDP between 0.2μ and 1.5μ at 25° C. The temperature dependences of the refractive indices of KDP were

reported by Phillips,[6] Yamazoki and Ogawa[7] and Vishnevskii and Stefanskii.[8]

KDP has a birefringence value of 0.041 at 25°C for 5890 Å. The dispersion of birefringence with wavelength has been studied over a wide range of wavelengths. Zwicker and Scherrer[9] first made measurements of the thermal birefringence coefficient for KDP. Above the Curie temperature, KDP remains uniaxial and exhibits a large electric field-dependent birefringence which is linear with the polarisation or strain induced by the field. Below T_c, the crystal becomes biaxial showing a large 'spontaneous' birefringence having a linear dependence on the polarisation or strain. Shamburov and Kucherova[10] investigated the variations in anomalous birefringence (non-zero birefringence along the optic axis) in KDP produced by optical inhomogeneities introduced during crystal growth.

The electro-optic properties of KH_2PO_4 were investigated by Carpenter.[11] He measured both the electro-optic constants viz. r_{41} and r_{63} in KDP and also discussed the percentage contribution of the clamped effect. Rosner et al.[12] studied the clamped electro-optic effect of KDP and reported r_{41} at 6330 Å. Sonin et al.[13] studied the electro-optic properties of KDP single crystals in the region of phase transition. Perfilova and Sonin[14] studied the quadratic effect in KDP crystals at room temperature at 5400 Å by using appropriate orientation of the applied electric field and the direction of the incident light in order to suppress the

linear effect. Perfilova et al.[15] studied the fourth order electro-optic effect in KDP and found that the induced birefringence is proportional to the fourth power of the electric field for fields upto 10 kV/cm. Vlokh et al.[16] reported r_{63} for KDP at high temperature at 4500 Å. Veerabhadra Rao and Narasimhamurty,[17] in a systematic study, determined the dispersion of both the linear electro-optic constants of KDP with wavelength, in the visible region. Pisarevskii et al.[18] measured the clamped electro-optic coefficient r_{63}^{s} of KDP as a function of modulating frequency. Pyle[19] and Ott and Sliker[20] reported a linear wavelength dependence of the longitudinal half-wave voltage of unclamped KDP at room temperature in the visible region. Zwicker and Scherrer[7] first related the d.c. electro-optic properties of KDP and deuterated KDP to the ferroelectric behaviour of these crystals. They observed that the d.c. (unclamped) electro-optic coefficient, based on the electric field, showed a Curie-Weiss behavior as a function of temperature. On the other hand, the electro-optic coefficient based on the dielectric polarisation was found to be practically temperature independent.

Some of the recent work on the electro-optic behavior of KDP includes that of Onako and Ho[21] who studied the electro-optic effect and vacuum UV absorption, and Pockels' effect of KDP in the UV region.[22]

III.2. Growth and Electro-optic Characterisation of KDP Crystals

III.2.1. Crystal Growth:

The solution growth method consists mainly in preparing a saturated solution and providing a stable temperature control. The seed crystal is held in this solution and growth takes place by deposition of salt on the seed from the solution. To maintain growth, the solution should be always kept at supersaturation.

This can be achieved without direct addition of salt by (a) lowering the temperature of the solution slowly and (b) slow evaporation of the solution. For a perfect crystal to be grown, it is necessary that the solution should be kept free from mechanical and thermal shocks. Also the solution should be kept free from impurities, should be at the desired pH value and the solution should be continuously stirred at a suitable rate.

III.2.1.1. Experimental Set Up:

The schematic of the method is shown in Figure III.1. The basic unit in the technique is a thermostat whose temperature can be controlled to an accuracy of about $\pm 0.1^{\circ}C$ which is done by a mercury contact thermometer. The thermostat has a system for drawing out the temperature controlled water. An auxiliary thermometer calibrated to $\pm 0.1^{\circ}C$ measures the actual temperature in the hot water bath. This water from the bath is circulated in a glass jacket which contains the

saturated solution of the salt whose crystal is to be grown. By proper insulation the difference in temperature between the solution and the water being circulated can be minimised to about 0.5°C. A pyrex glass seed holder of the shape shown in Figure III.1 is made of suitable size and placed in the container of the solution. This is made to rotate at a speed of 1 rpm to stir the solution. This rotation can be either clockwise or anticlockwise and can even be made oscillatory.

III.2.1.2. Procedure:

The following procedure is found to be best suited, after a few trials, for making a saturated solution at any temperature. A saturated solution of KDP is made by dissolving a required amount of salt in 1000 cc of distilled water, at the rate of 45 g/100 cc water[23] for saturation at 50°C. Then a few grams of an excess amount of salt is added to make the solution supersaturated at 50°C and left for half an hour. Then the solution is filtered into another conical flask on the heater itself. This flask with solution is transferred into a water bath maintained at 50°C. The auxiliary thermometer which measures the actual temperature of the bath is now used to measure the temperature of the solution in the flask to eliminate errors inherent in the thermometer. The temperature of the water bath is now maintained to show a temperature of 50°C in the solution. At this stage a few milligrams of salt in powder form is added as a check for the saturation state and then the flask is

left covered for about half an hour. In the meantime the seed is pasted onto the seed holder with quickfix and attached to the motor and kept ready in the double walled beaker where the solution is to be poured. Already the water from the thermostat is circulated into the water jacket of the growth beaker so that the surroundings of the seed are made ready for receiving the solution at 50°C. The saturated solution is now filtered as it is, poured into the container. Just one or two drops of water is added to the saturated solution so as to very slightly undersaturate it in order to dissolve away any surface layer imperfection of the seed crystal. The container is suitably closed on the top with petridish made into half moons and thermocole cut suitably to prevent heat losses. The motor is now put onto start seed rotation. Thus in the system there is no risk of undersaturation or heavy deposit on the seed. After attaining equilibrium, the temperature in the water bath is reduced at regular intervals as desired, by 0.1°C in every 6 hours. By this method it was possible to grow crystals of KDP in about 48 hours at 50°C to a size of 25 mm x 12 mm x 12 mm. The crystals were clear and of good quality for optical investigations.

Crystals of KDP were also grown by the slow evaporation method. Saturated solutions were prepared at a temperature slightly above the room temperature and then left in open petri dishes at room temperature. The small crystallites that appeared in a few hours time were taken out and one or two of them were reintroduced to serve as seeds. In

two to three days small crystals of very clear transparency could be obtained. (Plate III.1).

III.2.2. Electro-Optic Characterisation:

The crystals of KDP grown by the method described in Section III.2.1 were characterised for the following parameters viz. (i) Refractive index (ii) Birefringence and (iii) Half-wave retardation voltage and e.o. coefficient r_{63}.

III.2.2.1. Refractive Index Measurement:

For isotropic crystals the simplest method for refractive index determination is to cut a prism out of the crystal and find the angle of minimum deviation with a spectrometer. The refractive index, n, can be calculated from the formula

$$n = \frac{\sin \frac{A + D}{2}}{\sin \frac{A}{2}} \qquad \ldots \quad (III.$$

where A is angle of prism and D is the angle of minimum deviation.

But for birefringent crystals the cutting of the prism becomes very tedious since it involves proper orientation of prism faces with respect to the optic axis and requires crystals of big size. For such crystals the determination of refractive index becomes very simple by using suitable liquids to match the refractive index of the crystal under investigation. The procedure is to keep a set of liquids of known refractive

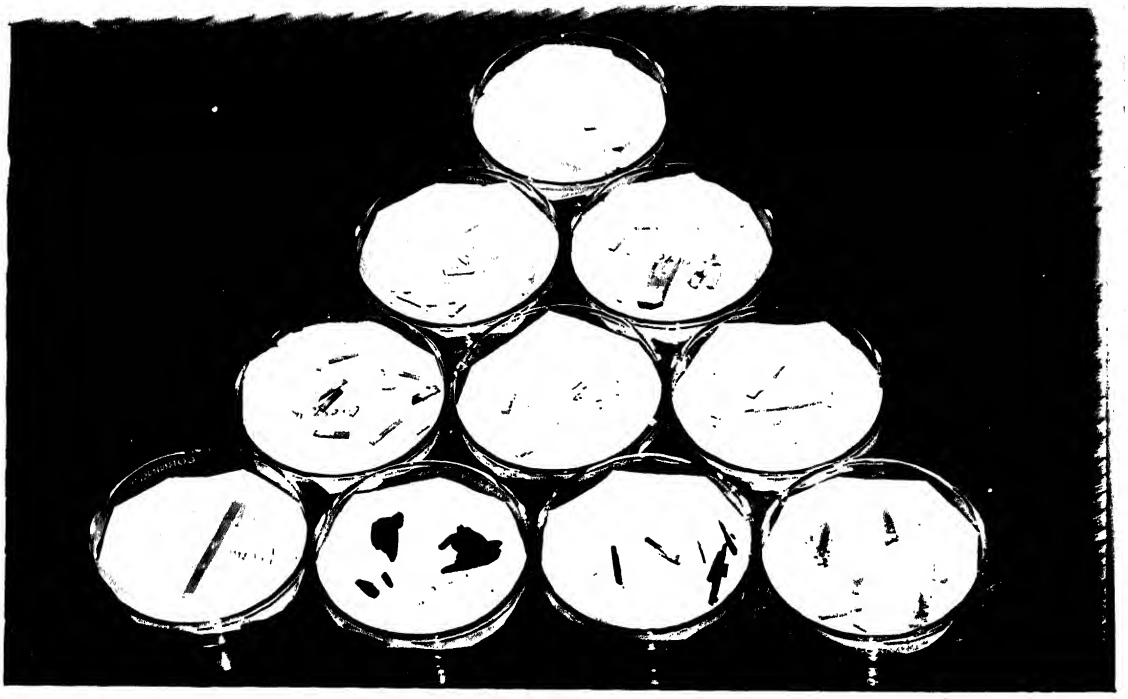

PLATE III.1 KDP crystals, grown in the laboratory. The topmost petridish shows pure KDP crystals. The rest show Cr-, Mn-, Fe-doped KDP crystals.

indices differing by 0.005 and find which liquid has the same refractive index as the crystal immersed in it using polarised light. The crystal would become invisible when the liquid has a refractive index matching that of the crystal. The search for the right liquid is not laborious because using the 'Becke line' effect it is possible to tell whether the refractive index of the liquid is higher or lower than that of the crystal. The crystal is immersed in a drop of liquid of known refractive index on a microscope slide and observed under moderate magnification and parallel light in the polarizing microscope. The crystal is first focussed sharply and then the objective is raised slightly. For liquid of refractive index less than that of the crystal, a line of light (the Becke line) is seen inside the edges of the crystal. As the objective is raised more and more, the line contracts further and further within the boundaries of the crystal. If the liquid has a refractive index higher than that of the crystal, the Becke line appears round the outside of the crystal and expands further as the objective is raised further. The Becke line always follows the outline of the crystal irrespective of the crystal shape. By observing this effect and trying suitable liquids in turn it is possible to find in a few minutes a liquid in which particles are nearly invisible.

Since KDP is a birefringent crystal, in order to observe one refractive index at a time, a polarising microscope, where plane polarised light is obtained by means of a Nicol prism placed between the light source and the microscope slide,

is employed. The plane of vibration of light can be adjusted with respect to the crystal either by rotating the Nicol prism or by rotating the microscope slide through 90°; the two cross-wires in the eye-piece indicate planes parallel and perpendicular to the plane of vibration of the light transmitted by the polariser.

The procedure described above was followed to determine the refractive indices of the KDP crystals grown in our experimental set up described earlier. The liquids used were supplied by R.P. Cargille Laboratories, Inc.; U.S.A. The values obtained for ordinary and extra-ordinary refractive indices of KDP crystal for sodium wavelength are shown in Table III.1. The literature[23] values are given for comparison.

III.2.2.2. Birefringence Measurement:

III.2.2.2.1. Principle: For any technique other than the prism method for determination of natural birefringence $\Delta\mu$, the value of $\Delta\mu$ has to be assumed for at least one wavelength in order to calculate the dispersion of $\Delta\mu$ at other wavelengths. The method adopted here to determine the birefringence is the channelled spectrum method. On passing light from a polariser through a plate cut from a doubly refracting crystal, light travels in the crystal as two beams plane polarised at right angles to one another. Since these beams travel with different velocities a path-difference $t(\mu_1 - \mu_2)$ is introduced, where μ_1 and μ_2 are the refractive indices for this particular direction of travel and t is the thickness

Table III.1. Refractive Indices for KDP at 25°C for λ = 5890 Å

	n_o	n_e	$(n_o - n_e)$
Experimental	1.4660	1.5070	0.0410
Literature	1.4679	1.5090	0.0411

of the plate. If this path difference is equal to an integral number p of wavelengths the two beams on emerging from the crystal will combine to give a beam, plane polarised in the same azimuth, as the incident beam. Thus any wavelength λ_o which satisfies the equation

$$p\lambda_o = t(\mu_1 - \mu_2) = t\Delta\mu \quad \ldots \quad (III.2)$$

will be extinguished if the plate be introduced between crossed nicols or polarisers. If white light is passed through the plate there will be a number of wavelengths λ_o, λ_1, λ_2 such that

$$p\lambda_o = (p + 1)\lambda_1 = (p + 2)\lambda_2 \quad \ldots \quad (III.3)$$

For all these wavelengths the light will be extinguished resulting in dark bands or fringes corresponding to the wavelength λ_o, λ_1 ... etc. By observation of the angle of minimum deviation of the light corresponding to each band and by calibrating the spectrometer, it is possible to obtain the values of λ_o, λ_1, etc. If two bands corresponding to λ_o and λ_n are chosen, we have

$$p\lambda_o = (p + n)\lambda_n \quad \ldots \quad (III.4)$$

Hence $$p = n\lambda_n/(\lambda_o - \lambda_n) \quad \ldots \quad (III.5)$$

This value will not, in general, be integral, partly because of experimental errors in determining the wavelengths and partly because of the effect of dispersion of the double refraction with wavelength. On taking the nearest integral

value of p, the value of $\Delta\mu$ can be determined from equation (III.2).

III.2.2.2.2. Experimental Set-up: The schematic diagram for the determination of birefringence in KDP is shown in Figure III.2. Light from a white lamp passes through a collimating lens L_1 onto a polariser P. The crystal under investigation is placed between the polariser and analyser which are kept crossed. Light emerging from the analyser, after passing through a condenser lens, is incident on the constant deviation spectrometer which is calibrated with sodium lamp. When the optical alignment is ready, the crystal is introduced between the polarisers and a banded spectrum is obtained in the field of view of spectrometer. Starting from one end of the spectrum, the wavelengths corresponding to each of the dark fringes upto the other end of the spectrum are recorded directly from the calibrated spectrometer. The birefringence value obtained from Table III.1 is substituted in equation (III.2) to obtain the value of p. With this value the birefringence value at all other wavelengths is calculated and a curve is plotted between $\Delta\mu$ and λ to give the dispersion of birefringence. This is given in Figure III.3. Table III.2 presents the birefringence values of KDP at different wavelengths in the visible region.

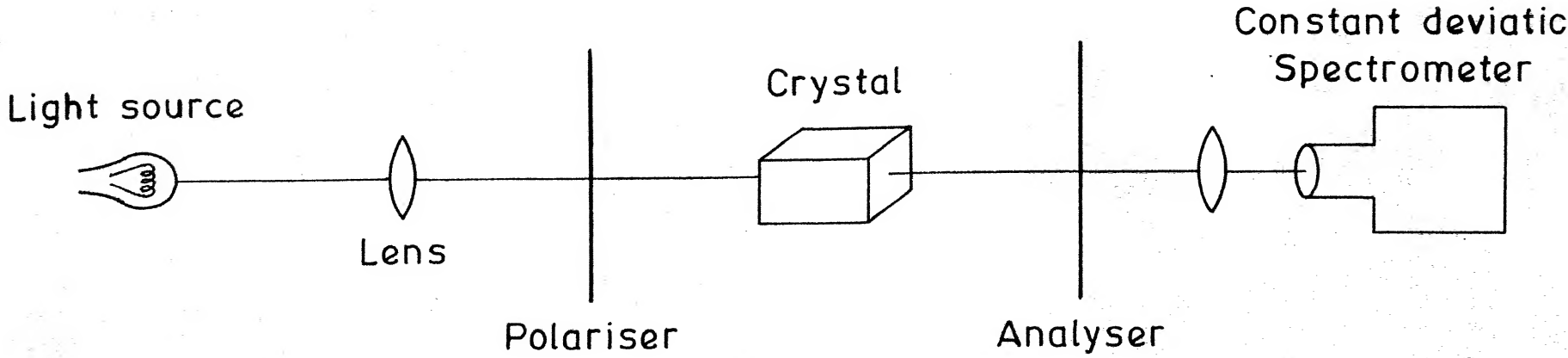

Fig. III.2- Schematic for birefringence measurement.

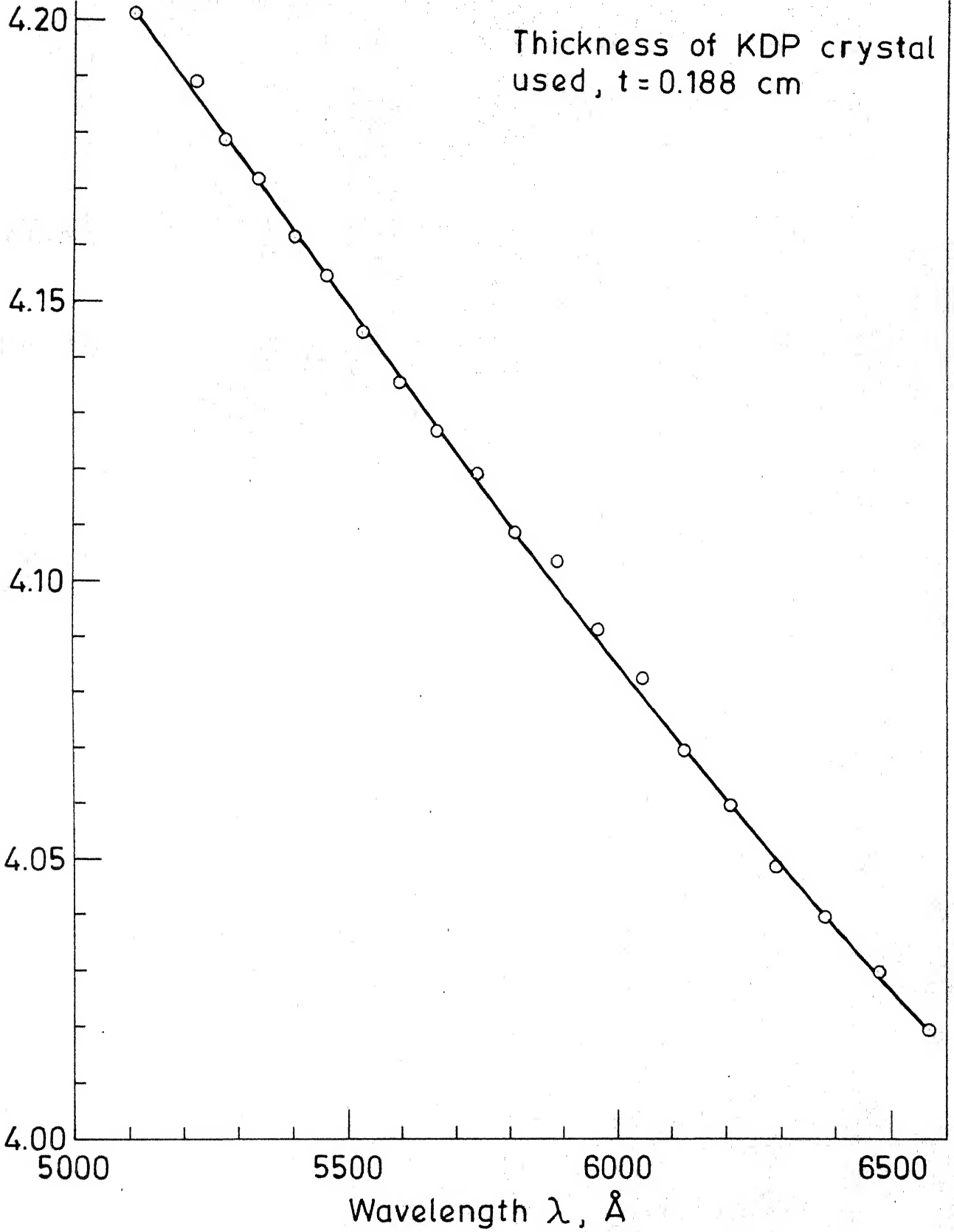

Fig. III.3 - Dispersion of birefringence with wavelength for KDP.

Table III.2. Birefringence Dispersion for KDP as Determined by Banded Spectrum Method

Experimental			Values from References (25)	
Order of band	Wavelength corresesponding to each band λ Å	($\Delta\mu = n\lambda/t$) Birefringence, $\Delta\mu \times 10^{-2}$	Wavelength λ Å	Birefringence, $\Delta\mu \times 10^{-2}$
n-16	6570	4.019		
n-14	6476	4.030		
n-12	6382	4.040		
n-10	6291	4.049	6328	4.05
n-8	6206	4.060	6234	4.07
n-6	6122	4.070		
n-4	6044	4.083		
n-2	5964	4.092		
n	5890	4.100	5893	4.11
n+2	5808	4.109		
n+4	5737	4.120	5770	4.12
n+6	5664	4.127		
n+8	5594	4.136		
n+10	5526	4.145	5560	4.16
n+12	5462	4.155	5461	4.17
n+14	5396	4.162		
n+16	5336	4.172		
n+18	5273	4.179		
n+20	5216	4.189		
n+22	5159	4.199		
n+24	5106	4.210	4358	4.34

Thickness of KDP crystal used

$$t = 0.188 \text{ cm}$$

III.2.2.3. Determination of Half-wave Voltage and Electro-optic Coefficient r_{63}:

III.2.2.3.1. Theory: In the absence of electric field E, KDP crystals remain uniaxial. Therefore light parallel to Z-axis, which is also the optic axis for KDP crystal, will not suffer birefringence. This is because a plane perpendicular to the Z-axis intersects a circular cross-section of radius n_o on the index ellipsoid while a plane in any other direction corresponding to non-Z-axis rays intersects an elliptical cross-section on the ellipsoid.

When a d.c. electric field is applied along the Z-axis of the KDP crystal, the crystal becomes biaxial. The index ellipsoid changes shape (see Figure III.4); the circle contracts along Y' axis which is -45° inclined to the Y-axis in the X-Y plane and expands along the X' axis which is +45° inclined to the X-axis. This results in the birefringence of the crystal to the Z-axis light waves. The refractive indices along the new axes X' and Y' become

$$n'_x = n_o - \frac{1}{2} n_o^3 \, r_{63} \, E_Z \qquad \ldots \text{(III.6)}$$

$$n'_y = n_o + \frac{1}{2} n_o^3 \, r_{63} \, E_Z \qquad \ldots \text{(III.7)}$$

where n_o is the refractive index along X or Y axis in the absence of electric field, r_{63} is the electro-optic coefficient and E_Z is the applied field. The schematic diagram for the determination of half wave voltage in the transmission mode is shown in Figure III.5. The crystal is electroded on both

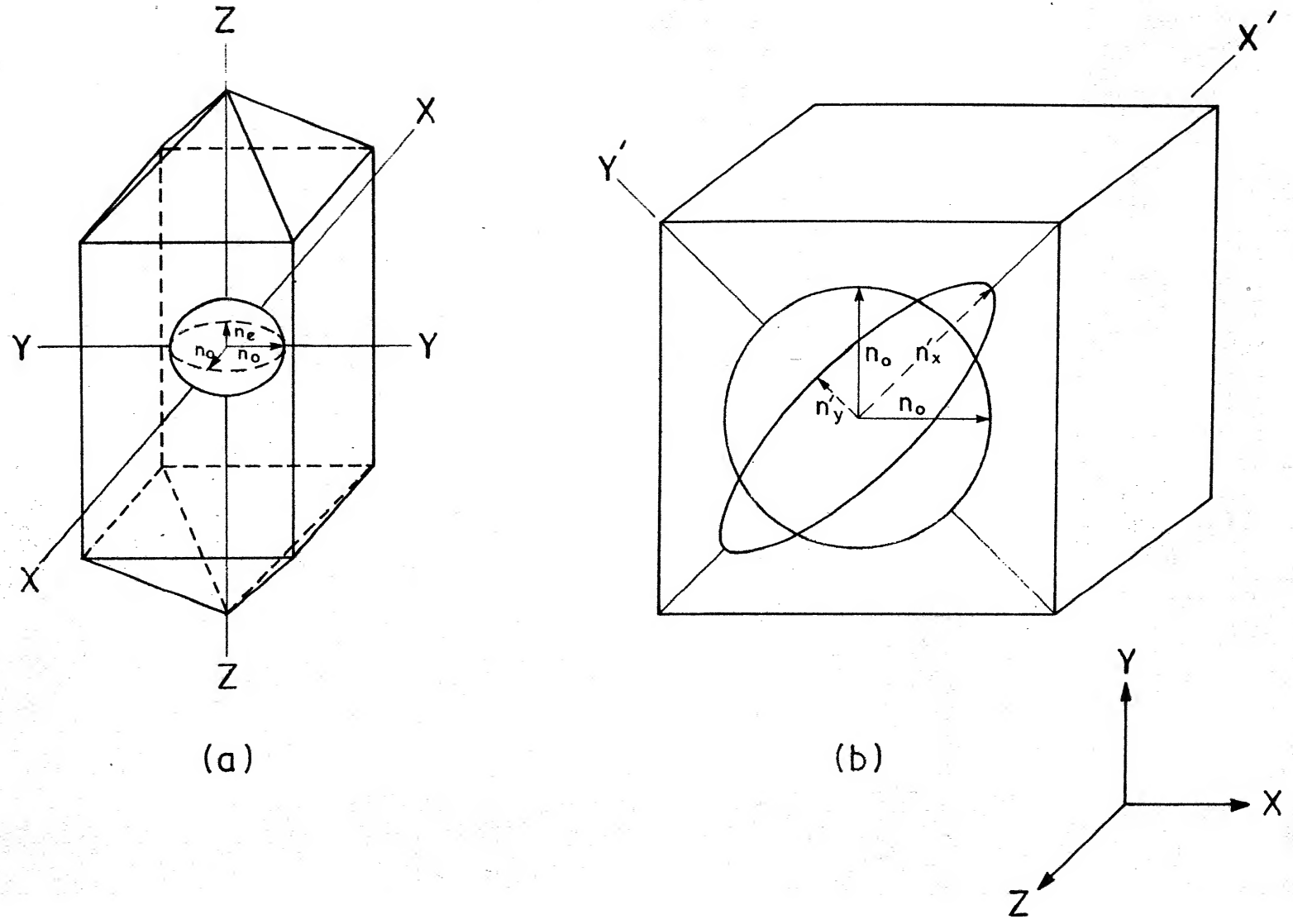

Fig. III.4 - Indicatrix for KDP (a) without field and (b) with field.

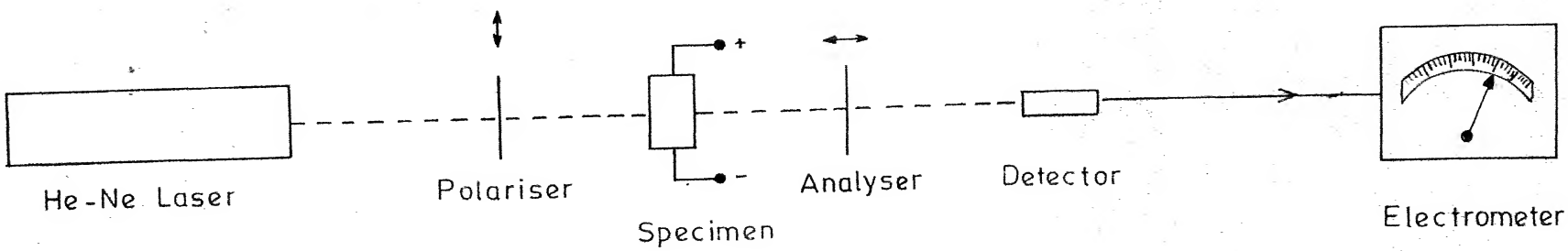

Fig. III.5 - Schematic for half-wave voltage determination.

faces perpendicular to Z-axis with a central aperture for the light beam to pass through. At zero voltage across the electroded faces, the light passes through the crystal unchanged in polarisation but is blocked from reaching the detector by the orthogonally oriented analyser. When an electric potential V is applied across the crystal faces, a field E_Z is produced which leads to the change in the ellipsoid shape. The incident plane polarised light within the crystal can be resolved into two component orthogonal waves in X' and Y' directions. Due to the different refractive indices under E_Z, the two component waves traverse the crystal with different velocities, thereby introducing a phase retardation δ given by

$$\delta = \frac{2\pi}{\lambda}(n'_Y - n'_X)L \qquad \ldots \quad (III.8)$$

where L is the crystal length and λ the wavelength of the incident laser beam.

The two component waves recombine on emergence from the crystal with an elliptical polarisation (due to the phase retardation) as opposed to the original Y-oriented linear polarisation. A component of the elliptically polarised light is in the X-orientation of the analyser and passes onto the detector. Substituting equations (III.6) and (III.7) in equation (III.8) the phase retardation becomes

$$\delta = \frac{2\pi}{\lambda} n_o^3 \gamma_{63} V_Z \qquad \ldots \quad (III.9)$$

where V_Z corresponds to the voltage applied to the crystal along the Z-axis. The voltage required to produce a retardation

of π or half wave is called the 'half wave retardation voltage' ($V_{\lambda/2}$) and is given by

$$V_{\lambda/2} = \frac{\lambda}{2n_o^3 r_{63}} \qquad \ldots \quad (III.10)$$

$V_{\lambda/2}$ is the technically important electro-optic figure of merit since it is a direct measure of the electro-optic property of the material. The value of $V_{\lambda/2}$ can be halved in the reflex configuration where the rear surface of the modulator is electroded with a metallic mirror (the retardation being one-fourth of λ on each pass through the crystal) and the analyser and the detector are also placed in front of the crystal. If the intensity of the incident beam is I_o, the intensity of the emergent beam I is given by

$$I = I_o \sin^2 \delta/2 \qquad \ldots \quad (III.11)$$

In practice, I neither reduces to zero when $\delta = 0$ nor equal to I_o when $\delta = \pi$, due to residual strains and the non-uniformity of the electric field inside the crystal. Consequently a factor called voltage contrast ratio (VCR) defined as the ratio of the output intensity at $V_{\lambda/2}$ to that at zero voltage and given by

$$VCR = \frac{I(V_Z = V_{\lambda/2})}{I(V_Z = 0)} \qquad \ldots \quad (III.12)$$

is measured for assessing the modulator.

III.2.2.3.2.Experimental Details: The schematic diagram for the experimental set up is shown in Figure III.5. The output of a He-Ne laser (2 mW) is passed through the Z-cut crystal of KDP. The specimen is electroded with gold by evaporation leaving a central aperture for the laser beam to pass through so that the electric field can be applied along the direction of propagation of the laser beam. This would give the longitudinal configuration. The beam is then allowed to fall on a photocell whose output is fed to a Keithley electrometer. As the voltage on the crystal is increased, the deflection of electrometer increases and at a particular voltage the deflection starts decreasing. The voltage corresponding to peak deflection gives the half-wave voltage for the He-Ne wavelength. Since it is longitudinal configuration it is independent of the crystal dimensions. Substituting the value of $V_{\lambda/2}$ obtained in equation (III.10), the value for the electro-optic coefficient r_{63} is calculated.

The specimen is placed in a crystal-holder made of perspex. The crystal is held in it by tefflon screws and is filled with silicone oil of suitable grade to avoid any sparking. Copper wires are soldered to either side of the crystal with silver paint. The high voltage source is connected to these copper leads taking care to have proper insulation. A high voltage DC supply (Model 20-1-6, Del Electronic Corporation, N.Y.) which can continuously give any voltage from 0 to 20 kV is employed.

The results obtained for the half-wave voltage and the electro-optic coefficient r_{63} are discussed in Section III.3.4.

III.2.3. Modulator Fabrication and Characterisation:

To fabricate a modulator in the longitudinal mode configuration, a small portion of the grown crystal is cut with its end faces perpendicular to the Z-axis and polished carefully. Rectangular end plate geometry employs a crystal in the form of a rectangular parallelopiped. Gold electrodes are deposited on the faces perpendicular to the optic axis leaving a small clean aperture at the centre for the laser light to pass through. Voltage to the crystal is applied by means of contact wires fired by silver paint to the gold electrodes. A high voltage D.C. supply (Model 20-1-6, Del Electronic Corporation, N.Y.) capable of giving continuous voltage from 0 to 20 kV is used for applying the voltage to the crystal. The crystal is mounted inside perspex casing having glass windows, whose design is shown in Figure III.6. The crystal is immersed in silicone oil which provides good electrical insulation and whose refractive index matches that of glass and the crystal. The oil also improves the transparency of the crystal. O-rings are provided in order to prevent oil leakage.

To determine $V_{\lambda/2}$ and VCR, the modulator is placed between crossed polarisers and laser light from a He-Ne laser is passed through it. The direction of propagation is aligned along the Z-axis of the crystal. This is achieved by adjusting the position of the modulator in such a way that a circular

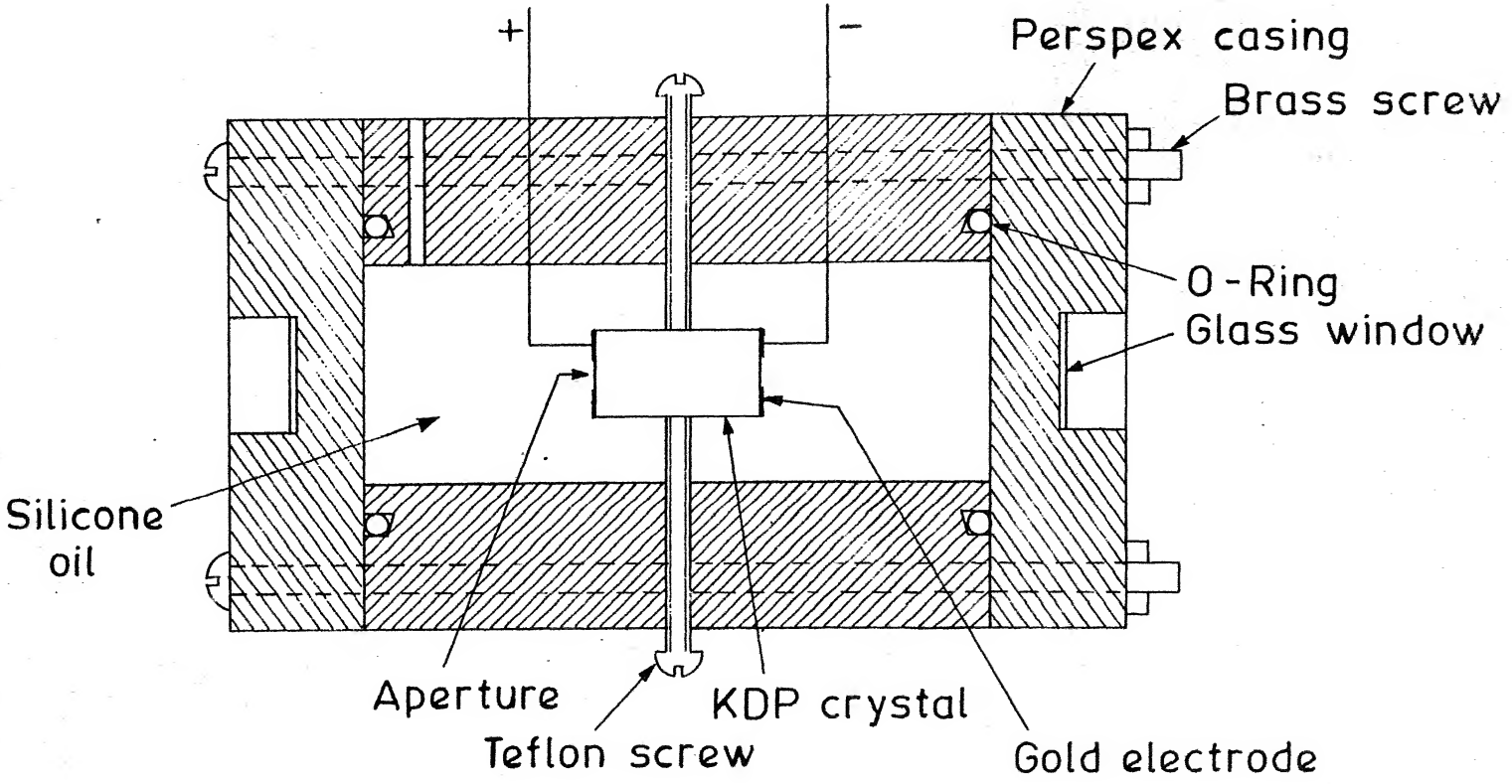

Fig. III.6 - Schematic diagram of KDP electro-optic modulator.

fringe pattern with a black cross at the centre, called the optic figure, is obtained on a white paper screen held behind the modulator at a suitable distance. The direction of propagation is then so adjusted that it coincides with the centre of the cross. The screen is removed after aligning the beam and is replaced by a photo-transistor detector. The emergent light from the modulator is focussed on the detector by inserting a convex lens between the analyser and the detector. The experimental arrangement is shown in Figure III.5. For inclining the polarisation vector of the incident beam at 45° X' or Y' axis of the crystal a small d.c. voltage of, say, 500 V is applied to the modulator and the crossed polarisers are rotated simultaneously at the same rate in the same direction till the detector output as shown in the electrometer deflection becomes maximum. Similar data are taken by reversing the voltage applied to the crystal. The voltage at which the output intensity is maximum gives $V_{\lambda/2}$ and the ratio of the maximum intensity to the minimum gives VCR. The half-wave voltage determined for the modulator made was 9.5 kV and the voltage contrast ratio about 25. The electro-optic coefficient r_{63} is calculated from equation (III.10). The standard $\sin^2$ curves are drawn for different orientations by choosing different half-wave voltages and amplitudes and computerising for $\sin^2$ fitting. The standard curve is shown in dotted lines in Figure III.7 along with the experimental I/I_o intensity vs. voltage curve. The experiments were carried out at 25°C. The results obtained for the modulator characteristics are discussed in the Section III.3.5.

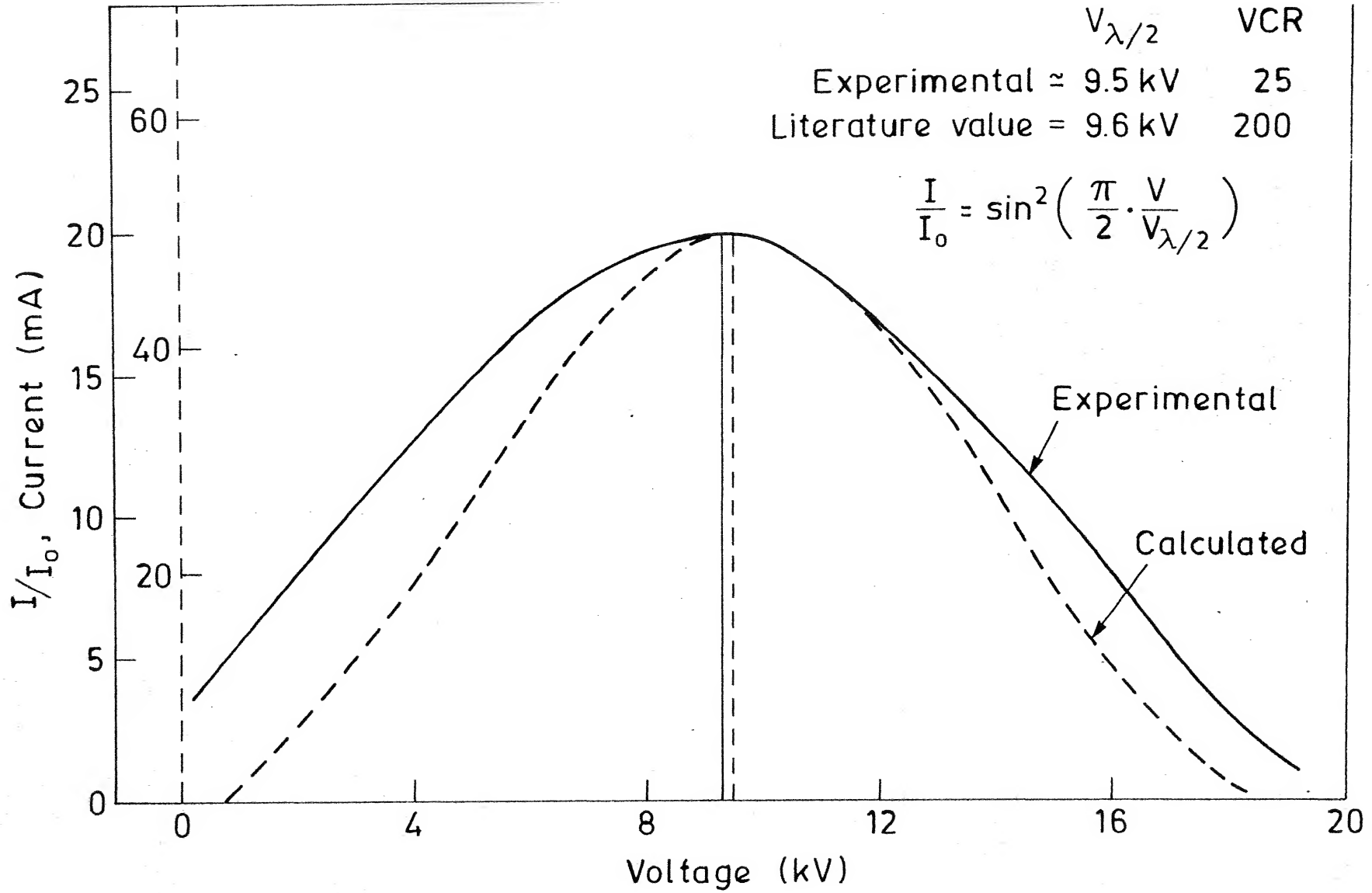

Fig. III.7 - Modulation characteristics of KDP modulator.

III.3. Results and Discussion:

III.3.1. KDP Crystal Growth:

A simple method has been devised to grow single crystals of KDP and other crystals of the same system. The principle of the method is to maintain the saturated solution at a constant temperature by circulating hot water at the proposed growth temperature and to rotate the seed holder at a constant speed. By this method it was possible to grow crystals of size 25 mm x 12 mm x 12 mm in about 48 hours at 50°C.

KDP crystals were also grown by the slow evaporation method. The size of the crystals obtained by this method was necessarily small. These small crystals were used as seed crystals for growing big crystals through the slow cooling method.

For solution growth of crystals, the most important parameters which merit attention are namely (a) the starting temperature at which growth is intended to be carried out (b) the state of saturation of the solution (c) the pH of the solution (d) impurities and dopants, and (e) cooling rate.

(a) Higher the temperature at which the growth takes place, the more likely it is to produce microcracks in the large seed crystals due to the temperature differentials. Hence this would lead to lower quality of grown crystals. The crystals grown in our laboratory at 50°C were of sufficiently good quality for any optical investigation but the quality of the crystals can be improved by growing at relatively lower temperatures.

(b) The state of saturation of the solution should be exact since too much supersaturation would result in too rapid a growth rate to yield a single crystal while a slight undersaturation, on the other hand, would lead to dissolution of the seed crystal. Egli and Thomson[1] rightly point out that a precisely saturated solution can never be made simply by combining the necessary amount of water and salts as determined by solubility curves firstly because astonishingly large amount of published solubility data is not accurate and secondly because evaporation during heating to complete dissolution introduces gross errors.

The technique developed in our laboratory as described in Section III.2.1 is found to be best suited for making a saturated solution at any particular temperature. But during growth there can be sudden changes in supersaturation on the fast growing faces. This results in striations parallel to the prismatic faces as reported by Sabharwal et al.[24] This can be prevented by suitable stirring and maintaining the solution temperature constant or reducing the cooling rate.

(c) The pH of the solution in the present experiments was maintained at 4.07 (as measured by the digital pH Meter, ELICO, Hyderabad) at the growth temperature. The effect of pH on the growth habit of KDP is not as significant as that in ADP but nevertheless noticeable. Solutions with lower pH values result in crystals elongated along the optic axis.

(d) The presence of impurities like iron, manganese etc. in the solution was found to cause a steep tapering of the KDP

crystals along the optic axis. This was observed by intentionally doping the solution with Cr, Mn and Fe in the order of 100 ppm level. The magnitude of the tapering effect was observed to progressively increase in the same order. This morphology change is worth investigating as it could help in eliminating the machining of the crystal for electro-optic characterisation and related studies. It was reported by Sabharwal et al.[24] that the tapering effect is more pronounced when growth is carried out at relatively lower temperatures. The crystals which are tapered during growth are reported to possess residual stress birefringence. So maximum care has to be taken to ensure the absence of impurities in the growing solution.

(e) The cooling rate is also an important factor affecting the crystal perfection. The crystals grown in our laboratory were grown under a rate of cooling of the solution of 0.4°C per day. Higher cooling rates are reported to cause the trapping of mother liquor within the crystals which are strained. Hence in order to grow strain free crystals with no defects as low a cooling rate as is compatible with a reasonable growth rate, has to be employed.

III.3.2. Refractive Index:

Table III.1 shows the experimental values obtained for the ordinary and extra-ordinary refractive indices n_o and n_e for KDP at 25°C using the index matching liquids. The values have a tolerance of ± 0.002. Literature[23] values

for the indices of refraction at sodium wavelength (5893 Å) are given alongside for comparison. Good agreement is seen between the two sets of values.

The dispersion of refractive index with wavelength can be studied by this technique by determining the refractive index using monochromatic wavelength sources. When white light is used, the values obtained for the refractive indices are taken as the average values for the wavelength, most generally taken around 5800 Å. For high precision, it is however advisable to use monochromatic wavelength sources for matching of the refractive index of the crystal with suitable liquids.

Determination of the refractive index of crystals by the use of index matching liquids has been an old and tested method and has been popular in geological studies since a long time. The main advantage of the method is that there is no need to cut the crystal in the shape of a prism. Other merits include that it is very simple and fast to perform and even very small crystallites are sufficient for refractive index determinations.

III.3.3. Birefringence:

Table III.2 presents the birefringence dispersion data for KDP as determined by the banded spectrum method at a temperature of 25°C. Figure III.3 gives the birefringence dispersion curve with wavelength for data given in Table III.2. Literature[25] values for birefringence are also given in Table III.2 for a few chosen wavelengths, so that a comparison is possible.

Such a comparison reveals a general congruity between the two sets of values. The experimental values obtained for birefringence depend heavily on the previous history and the growth conditions of the sample under study. The growth conditions that should be ensured in order to obtain defect-free, strain-free crystals have been discussed in Section III.3.1. The history of the specimen relates to any thermal and mechanical treatment to which it has been subjected. Hence, to obtain the value of natural birefringence of a crystal, the preparation of the crystal, involving cutting and polishing operations, should be done with utmost care so as not to introduce any strain in the crystal.

From the experimental values obtained for refractive indices of KDP crystal at 5890 Å determined by the use of index matching liquids at 25°C, the birefringence value is found (Table III.1). Using this value, the dispersion of birefringence at other wavelengths has been determined by the banded spectrum method.

The banded spectrum method is simple and direct because unlike the prism method, here the value of birefringence for different wavelengths is obtained directly, once we know the values of the two refractive indices of the crystal at a particular wavelength. Using a calibrated constant deviation spectrometer, the different wavelengths corresponding to each dark band of the spectrum are obtained to an accuracy of $\pm$ 1 Å. The determination of birefringence dispersion for a range of wavelengths as allowed by the ends of the spectrum in the

visible region, is thus possible in a single experiment. Moreover this method can be easily employed even for crystals of very small size.

III.3.4. Half-wave Voltage and Electro-optic Coefficient r_{63}:

Table III.3 presents the data I/I_o vs. applied voltage. The value for half-wave voltage obtained for the KDP crystals grown in our laboratory is 9.5 kV which compares very well with the literature[28] value viz. 9.6 kV for He-Ne laser wavelength (6328 Å). Using equation (III.10) the value of the e.o. coefficient r_{63} is calculated, substituting for the $V_{\lambda/2}$, as determined above. The value thus obtained for r_{63} is 9.7×10^{-12} m/V. The literature value[25] for r_{63} for KDP at 6330 Å is 9.3×10^{-12} m/V. The agreement is seen to be good. The measurements were carried out at 25°C.

The experimental set up can be used to determine the wavelength dispersion of the half-wave voltage by carrying out the experiment using different wavelength light sources. The electro-optic coefficient r_{63} is inversely proportional to the half-wave voltage. Therefore, the lower the value of the half-wave voltage, the easier the design and operation of the electro-optic modulator. For the electro-optic modulator device fabricated in the laboratory, the half-wave voltage can be reduced by (i) increasing the homogeneity of the field applied to the crystal by using cylindrical ring electrode (CRE) geometry or alternatively by providing transparent conducting coating for crystal electrodes, (ii) perfect orientation of the modulator with respect to the incident light beam, so

Table III.3. Intensity Ratio vs. Applied Voltage

Applied voltage in kV	I/I_o in mA
0	0.8
1	5.2
2	8.0
3	10.0
4	13.0
5	15.2
6	17.1
7	18.0
8	19.2
9	20.0
10	19.5
11	18.5
12	16.5
13	15.0
14	12.5

$$V_{\lambda/2} = 9.5 \text{ kV}$$

$$\text{VCR} = \frac{I/I_o \text{ (at } V = V_{\lambda/2})}{I/I_o \text{ (at } V = 0 \text{ kV)}} = 25 .$$

that the light beam travels along the optic axis direction of the crystal and (iii) by using the reflex configuration, where the rear face of the modulator is coated with a reflective coating. The value of $V_{\lambda/2}$ is halved in the reflex mode configuration, the retardation being one-fourth of λ on each pass through the crystal.

III.3.5. Modulator Characteristics:

Figure III.5 illustrates the modulation characteristics of the e.o. modulator fabricated using KDP crystal. Longitudinal configuration in the transmission mode is employed. In the present case the intensity of transmitted light is given by

$$\frac{I}{I_o} = \sin^2 \left(\frac{\pi}{2} \cdot \frac{V}{V_{\lambda/2}}\right) \qquad \ldots \quad (III.13)$$

It is quite interesting to see if the curve obtained experimentally follows the theoretical curve for the modulation of intensity. Comparing the standard curves with the experimentally obtained curves, it is possible to get an idea about misorientation of the modulator crystal and the inhomogeneity of the field applied to the crystal. It can be seen from Figure III.5 that the experimentally observed curve follows the theoretical curve for the modulation of intensity fairly well. When perfect homogeneity of the field is ensured by using transparent conducting coating for the crystal electrodes or by going in for the cylindrical ring electrode geometry, the experimental curve is expected to coincide with the standard $\sin^2$ curve. While there is a fairly good agreement

between the experimental and the literature values for the electro-optic parameters $V_{\lambda/2}$ and r_{63}, the value experimentally obtained for the VCR viz. 25 is substantially low compared to the value quoted by Sabharwal et al.[24] which is around 200. The factors contributing to such a reduction in the VCR value can be examined under two categories: (a) those that are intrinsic with respect to the crystal used and the experimental accessories that are employed, whence the value of VCR is fixed by their quality and (b) those that are extrinsic, which thereby allow a scope for immediate tackling and improvement in the VCR. These would include the geometry of the modulator and the orientation of the crystal.

(a) Factors intrinsic with the experimental conditions:

(i) Quality of the crystal used: The presence of strains in the crystal and the optical losses due to scattering within the bulk of the crystal drastically reduce the VCR thereby affecting the performance of the modulator. The presence of an uniform strain throughout the crystal introduces an additional static birefringence which lowers the VCR. The effect of random strains, due to large variations in the growth rates, would be more severe and would partially destroy the spatial coherence of a plane wave travelling through the media. Proper growth conditions and absence of impurities from the growing solution should be ensured to grow strain-free crystals. The machining and polishing operations should be done with utmost care so as not to introduce any strain in the crystal. Growth at relatively lower temperatures at slower growth rates

improves the quality of the crystals considerably leading to higher voltage contrast ratios.

(ii) The quality of the polarisers used and the sensitivity of the detector photo-cell effectively limit the VCR. When the detector has an excellent photo-sensitivity and the polarisers have a high extinction ratio, the VCR is appreciably enhanced.

(b) Extrinsic factors:

(i) The voltage non-uniformity across the effective aperture results in a reduced VCR. This can be overcome by using ring electrodes or alternatively by using transparent conducting coating for the electrodes.

(ii) Any misalignment of the crystal with respect to the incident light beam also contributes to the reduction in VCR value. Perfect orientation of the crystal, ensuring light travel along the optic axis direction of the crystal eliminates this value-limiting factor for VCR.

REFERENCES

(1) Egli, P.H. and Johnson, L.R. in The Art and Science of Growing Crystals (Ed. Gilman, J.J.), John Wiley & Sons, Inc., N.Y. (1963).

(2) Ascoli, A.S. and Drosi, M., Energia Nucleare, 17 (1970) 545.

(3) J.W. Mullin, A. Amatavivadhana and M. Chakraborty, Crystal habit modification studies with ADP and KDP, J. Appl. Chem., 20 (1970) 153.

(4) Janssen, Van, R. et al., The influence of the hydrodynamic environment in the growth and the formation of liquid inclusions in large KDP crystals, Krist. and Tech. (Ger.), 13 (1978) 17.

(5) Zernicka, F. Jr., Refractive indices of ADP and KDP between 2000 A° and 1.5 microns, J. Opt. Soc. Am., 54 (1964) 1215.

(6) Phillips, R.A., Temperature variation of the index of refraction of ADP, KDP and deuterated KDP, J. Opt. Soc. Am., 56 (1966) 629.

(7) Yamazaki, M. and Ogawa, T., Temperature dependences of the refractive indices of ADP, KDP and partially deuterated KDP, J. Opt. Soc. Am., 56 (1966) 1407.

(8) Vishnevskii, V.N. and Stefanskii, I.V., Temperature dependence of the dispersion of the refractivity of ADP and KDP single crystals, Opt. and Spect., 20 (1966) 195.

(9) Zwicker, B. and Scherrer, P., Electro-optical properties of the ferroelectric crystals KH_2PO_4 (in German), Helv. Phys. Acta, 17 (1944) 346.

(10) Shamburov, V.A. and Kucherova, I.V., Variation in anomalous birefringence in crystals of KH_2PO_4, Sov. Phys. Crystal., 10 (1966) 558.

(11) Carpenter, R.O., The electro-optic effect in uniaxial crystals of the dihydrogen phosphate type. III. Measurement of coefficients, J. Opt. Soc. Am., 40 (1950) 225.

(12) Rosner, R.D., Turner, E.H. and Kaminow, I.P., Clamped electro-optic coefficients of KDP and quartz, Appl. Opt., 6 (1967) 778.

(13) Sonin, A.D., Vasilevskaya, A.S. and Strukov, B.A., Electro-optic properties of KDP and deuterated KDP crystals in the region of their phase transitions, Sov. Phys. Sol. State, 8 (1967) 2758.

(14) Perfilova, V.E. and Sonin, A.D., The quadratic electro-optic effect in KDP group crystals, Acad. of Sci. USSR, Bull. Phys. Ser., 31 (1967) 1154.

(15) Perfilova, V.E., Sirotin, Yu. I. and Sonin, A.D., Kristalografiya, 14 (1969) 157.

(16) Vlokh, B.G., Lutsiv-Shumskii, L.F. and Pylypyshin, B.P., Kristallografiya, 16 (1971) 828.

(17) Veerabhadra Rao, K. and Narasimhamurty, T.S., Linear electro-optic dispersion in KDP, J. Phys. C: Solid State, 11 (1978) 2343.

(18) Pisarevskii, Yu. V., Tregubov, G.A. and Shaldin, Yu. V., Electro-optical properties of ADP, KDP and $N_4(CH_2)_6$ Crystals in UHF fields, Sov. Phys. Sol. State, 7 (1965) 530.

(19) Pyle, J.R., Laser modulation using linear electro-optic crystals, Tech. Note PAD 125, Dec. 1966, 35 p., NASA N67-27128.

(20) Ott, J.H. and Sliker, T.R., Linear electro-optic effects in KH_2PO_4 and its isomorphs, J. Opt. Soc. Am., 54 (1964) 1442.

(21) Onako, R. and Ito, H., Electro-optical effect and vacuum UV absorption in KDP and ADP, Acad. of Sci. USSR, Bull. Phys. Ser., 41 (1977) 59.

(22) Onako, R. and Ito, H., Pockels effect in KDP and ADP in UV region, J. Phys. Soc. Japan, 41 (1976) 1303.

(23) J.T. Milek and M. Neuberger, Linear electro-optic modular materials, IFI, Plenum, N.Y. (1972).

(24) S.C. Sabharwal, Malathi Ghosh, B. Ghosh and R.Y. Deshpande, Growth of ADP crystals, Proc. Symp. on Quantum and optoelectronics, BARC, India, 25/28 (1974) 479.

(25) Landolt-Bornstein Tables, 11, Gr. III, Springer Verlag, N.Y., 1979.

IV. CONCLUSIONS

The present thesis deals with $LiNbO_3$ and KDP crystals which are two important materials for electro-optic applications. Following an exhaustive and upto-date literature survey of $LiNbO_3$ covering the crystal growth aspects and the optical behavior, a crystal growth apparatus for growing these crystals has been set up. Satisfactory crystals of small size could be grown. The problem areas in growing large size, good optical quality crystals are identified and analysed with possible solutions for overcoming them.

A substantially more elaborate apparatus, for growth of large $LiNbO_3$ crystals, with a suitably designed furnace to provide a precise and stable temperature gradient at the melt-seed interface is felt essential. Also, the incorporation of a crystal-viewing facility for observing the crystal during growth would help monitor the growth of crystal. In addition, a sealed growth environment, where circulation of oxidising gas is possible, is felt desirable in order to improve the experimental conditions.

For growing KDP crystals, a standard technique has been set up for growth from solution. Crystals of KDP were grown by slow cooling and slow evaporation methods.

KDP crystals of good optical quality and large size were grown by the slow cooling method and characterised for

optical and electro-optical properties. The parameters studied include the refractive index, birefringence, half-wave voltage and electro-optic coefficient r_{63}. The values obtained for these parameters are in good agreement with the published values. Encouraged by this, the fabrication of an electro-optic modulator based on KDP was undertaken. The modulator was designed, fabricated and tested for the longitudinal mode of modulation. The voltage contrast ratio, used as the figure of merit to assess the performance of the modulator, was determined to be 25 which is rather low compared with the published value of 200. Minor changes in the geometry of the modulator are suggested to improve the VCR characteristics. Also improvements in the quality of the experimental equipment accessories and the quality of the crystal used (by employing slower growth rates) are identified to be the solutions for considerable enhancement of the VCR and hence, the modulator performance.

SP-1901-M-SWA-GRO